STRUCTURAL AND METABOLIC MRI TO CHARACTERIZE THE RESPONSE TO SURGERY IN TRIGEMINAL NEURALGIA

by

Hayden J. Danyluk

A thesis submitted in partial fulfillment of the requirements for the degree of

Doctor of Philosophy

in

Experimental Surgery

Department of Surgery

University of Alberta

Abstract

Trigeminal Neuralgia (TN) is a chronic, neuropathic, facial pain condition characterized by severe unilateral pain attacks, electric shock-like or shooting in character, confined to regions of the face innervated by the trigeminal nerve (the fifth cranial nerve, CNV). TN is commonly associated with neurovascular compression of CNV, but may also be idiopathic or occur secondary to other diseases. While the underlying pathophysiology of TN is incompletely understood, it is widely believed that CNV microstructure (specifically myelination) is affected in patients with this condition. TN is treated initially with medications used for neuropathic pain, but many TN patients become medically refractory, at which point various CNV-directed surgical options may be offered. Even with the most effective surgical treatment, a considerable proportion of TN patients are initial non-responders or experience early pain recurrence. Currently, surgical treatment resistance in TN is poorly understood.

In order to better understand surgical treatment resistance in TN, we proposed the use of magnetic resonance imaging (MRI) to perform an in-depth analysis of both CNV and brain features in patients with TN. The main aims of this thesis were: 1) to develop a novel, nerve-specific MRI acquisition protocol permitting more accurate characterization of CNV microstructure in TN; 2) to identify, using MRI, preoperative structural and metabolic CNV and brain abnormalities in TN patients, and to characterize changes in these features occurring longitudinally following surgical treatment; and 3) to examine the differences between *responders* and *non-responders* to surgical treatment for TN using imaging-based CNV and brain features.

Our newly developed nerve-specific MRI protocol more accurately characterized CNV microstructure than others used previously. In contrast to previously published studies, we did not detect clear preoperative CNV microstructural abnormalities in patients with TN, although contralateral thalamus volume was increased. There were also no preoperative differences in CNV microstructure between surgical responders and non-responders, although, contralateral CNV volume was increased. Furthermore, the hippocampus was comparatively enlarged and thalamus shape was different in non-responders. In the early postoperative period (<1-week), divergent changes in thalamic metabolism were observed between responders and non-responders even though CNV microstructure was not appreciably different.

In summary, this thesis provides novel evidence that brain and nerve structural features may distinguish responders to TN surgery from non-responders preoperatively. Additionally, while CNV microstructural changes occur following surgery, our data suggest that these are less able to explain differences in surgical response, which instead may relate to variable metabolic effects of surgery between responders and non-responders. Thus, perioperative assessment utilizing multimodal MRI may provide insight into the underlying pathophysiology of TN as well as therapeutic mechanisms of surgical treatment.

Preface

This thesis, which was part of a larger collaborative effort of various coauthors, is an original work by Hayden James Danyluk. Ethical approval for all projects contained within this thesis was obtained through the Health Research Ethics Board of the University of Alberta.

Chapter 3 of this thesis has been modified with permission from: Danyluk H, Sankar T, Beaulieu C. High spatial resolution nerve-specific DTI protocol outperforms whole-brain DTI protocol for imaging the trigeminal nerve in healthy individuals. NMR Biomed. 2021;34(2):e4427. H. Danyluk was responsible for study design, methods development, subject recruitment, data collection, data processing, manuscript composition and figure generation, and manuscript revision. T. Sankar was a supervisory author and contributed to study design, manuscript generation, and manuscript revision. C. Beaulieu was also a supervisory author and contributed to study design, methods development, manuscript composition and figure generation, and manuscript revision.

Chapter 4 of this thesis has not been published previously. H. Danyluk was responsible for study design, methods development, subject recruitment, data collection, data processing, chapter composition and figure generation. R. Broad contributed to subject recruitment, data collection, and performed surgical treatment on study participants. B.M. Wheatley contributed to subject recruitment, data collection, and performed surgical treatment on study participants. T. Sankar was the supervisory author for this chapter and contributed to study design, data collection, chapter revision, and performed surgical treatment on study participants.

Chapter 5 of this thesis has been modified with permission from: Danyluk H, Andrews J, Kesarwani R, Seres P, Broad R, Wheatley BM, Sankar T. The thalamus in trigeminal

neuralgia : structural and metabolic abnormalities, and influence on surgical response. BMC Neurol [Internet]. 2021;21(290):1–14. Available from: https://doi.org/10.1186/s12883-021-02323-4. H. Danyluk was responsible for study design, methods development, subject recruitment, data collection, data processing, manuscript composition and figure generation, and manuscript revision. J. Andrews contributed to data processing and figure generation. R. Kesarwani contributed to methods development, data collection, data procession, and figure generation. P. Seres contributed to methods development, data collection, and data processing. R. Broad contributed to subject recruitment, data collection, and performed surgical treatment on study participants. B.M. Wheatley contributed to subject recruitment, data collection, and performed surgical treatment on study participants. T. Sankar was the supervisory author and contributed to study design, data collection, manuscript generation, manuscript revision, and performed surgical treatment on study participants.

Chapter 6 of this thesis has been modified with permission from: Danyluk H, Lee EK, Wong S, Sajida S, Broad R, Wheatley BM, and Sankar T. Hippocampal and trigeminal nerve volume predict outcome of surgical treatment for trigeminal neuralgia. Cephalalgia. 2020;40(6):586–96. H. Danyluk was responsible for study design, methods development, subject recruitment, data collection, data processing, manuscript composition and figure generation, and manuscript revision. E. Lee contributed to data collection and processing, as well as figure generation. S. Wong contributed to data collection and processing, as well as figure generation. S. Sajida contributed to data collection and figure generation. R. Broad contributed to data collection and performed surgical treatment on study participants. B.M. Wheatley contributed to data collection and performed surgical treatment on study participants. T. Sankar was the

supervisory author and contributed to study design, data collection, manuscript generation, and manuscript revision, and performed surgical treatment on study participants.

Copyright permissions for all the above listed previously published manuscripts, as well as for use of the other original figures and tables (as specifically mentioned throughout the thesis), have been obtained by H. Danyluk.

Dedication

This thesis is dedicated to my wife, Frances.

Acknowledgements

This thesis was made possible by many incredible people at the University of Alberta. I would like to acknowledge the superb guidance and encouragement provided to me by my PhD supervisor and mentor, Dr. Tejas Sankar. I have benefited greatly from the exposure he has provided me in both academic and clinical realms. Our relationship began at a time when I was in need of direction and guidance, and as such, has been one of the most meaningful in my life. I cannot thank him enough. I would also like to thank Dr. Matt Wheatley who served on my supervisory committee. Dr. Wheatley's guidance and academic contribution to my thesis work was invaluable, however, his influence on my path extends far beyond that which was provided though a supervisory role. I first met Dr. Wheatley while I was working as a flooring installer half a year before I began graduate studies. The encouragement he offered me in that meeting was a key motivator that drove me to pursue research, and ultimately, enroll into the MD/PhD program. I would like to thank Dr. Christian Beaulieu who also served on my supervisory committee. Dr. Beaulieu is an incredible scientist with unmatched research prowess. The intensity with which he approaches scientific truth and discovery is something to be marveled. It has been a privilege to learn from, and work alongside him. Dr. Thomas Churchill is another person who had a profound impact on my path. In early 2016, I approached him out of the blue—I was working at a nearby site and was on a lunch break—and asked him if there was room for me in the Department of Surgery Graduate program. Rather than turning me away, Dr. Churchill to become one of my advocates, and ultimately set up my first meeting with Dr. Sankar. I cannot thank Dr. Churchill enough. I would also like to thank the great people at the Peter S. Allen MR Research Centre for their expertise and support. To Peter Seres specifically,

this work could not have been done without you. I would also like to thank Cam Elliott for being an excellent role model for an aspiring clinician-scientist, and for putting up with me for four years in the shared office space.

I am grateful to my family for their support, encouragement, love, and the motivation they have provided me through this long process. Specifically, to my wife Frances, thank you for reeling me in when I'm up, and holding me up when I'm down. Specifically, to my parents Linda and Brad, and my sister Katelyn, thank you for always being there and being proud.

Table of Contents

List of Tables

List of Figures

List of Abbreviations

ACC: anterior cingulate cortex

AD: axial diffusivity

ADC: apparent diffusion coefficient

ANCOVA: analysis of covariance

ANOVA: analysis of variance

BC: percutaneous balloon compression

BNI: Barrow Neurological Institute

Cho: choline

CNV: fifth cranial—or trigeminal—nerve

Cr: creatine

CSA: cross-sectional area

CSF: cerebrospinal fluid

DTI: diffusion tensor image

DWI: diffusion weighted image

FA: fractional anisotropy

FDR: false discovery rate

FLAIR: fluid-attenuated inversion-recovery

FOV: field of view

FWER: family-wise error rate

GKRS: Gamma Knife radiosurgery

HC: healthy control

ICC: intraclass correlation coefficients

ICHD-3: International Classification of Headache Disorders III

ICV: intracranial volume

IN: internal neurolysis

IQR: inter-quartile range

LINAC: linear accelerator

M: net sum of magnetic moments

MANCOVA: multivariate analysis of covariance

MD: mean diffusivity

MNI: Montreal Neurological Institute

MPRAGE: magnetization-prepared rapid acquisition gradient echo

MRI: magnetic resonance imaging

MRS: magnetic resonance spectroscopy

MS: multiple sclerosis

MVD: microvascular decompression

NAA: N-acetylaspartate

NR: non-responder

NS: nerve specific

NS-FL: nerve-specific FLAIR

NVC: neurovascular compression

PACS: Picture Archiving and Communication System

PR: percutaneous rhizotomy

PRESS: point-resolved spectroscopy

R: responder

RD: radial diffusivity

REZ: root entry zone

RF: radiofrequency

RFT: radiofrequency thermocoagulation

ROC: receiver-operator characteristic curve

ROI: region of interest

SNR: signal-to-noise ratio

SRS: stereotactic radiosurgery

T: applied magnetic field

TBSS: tract-based spatial statistics

TDP: trigeminal deafferentation pain

TE: echo-time

TI: inversion time

TN: trigeminal neuralgia

TN1: trigeminal neuralgia type 1

TN2: trigeminal neuralgia type 2

TNP: trigeminal neuropathic pain

TR: repetition time

V1: ophthalmic branch of CNV

V2: maxillary branch of CNV

V3: mandibular branch of CNV

VAS: visual analogue scale

VBM: voxel-based morphometry

VPM: ventral posteromedial nucleus

WBa: whole-brain anisotropic

Wbi: whole-brain isotropic

CHAPTER 1: Background & Literature Review

1.1 What is TN?

According to the International Classification of Headache Disorders III (ICHD-3), trigeminal neuralgia (TN) is a chronic neuropathic facial pain condition characterized by paroxysmal, electric shock-like pain attacks radiating through the trigeminal nerve distribution (**Figure 1.1**) (1). **Table 1.1** outlines the specific ICHD-3 criteria required to confirm a TN diagnosis. (1). TN is a relatively rare disease, with reported incidences ranging from 4 – 27/100,000 per year (2–4). TN often first appears in the fifth decade and affects women nearly twice as often as men (2). Pain attacks are typically triggered by innocuous stimuli in patient-specific regions of the facial dermatome known as trigger zones (1). During an attack, the pain is very severe, though dull concomitant pain between attacks may also be described (1). TN is a unilateral disease in the vast majority of cases, affecting the right side of the face more frequently than the left for reasons unknown (58% right, 42% left) (5). Bilateral TN—occurring in fewer than 5% of cases—is a very rare condition in which pain attacks can affect both sides of the face, but not simultaneously, and is usually associated with underlying comorbidity such as multiple sclerosis (MS) (4,6). In fact, approximately 6.3% of patients with MS eventually develop TN, representing the highest prevalence of secondary TN in any single patient group (7).

The extreme severity of pain and unpredictable paroxysmal nature of TN dramatically reduces quality of life for TN patients. In fact, TN was historically associated with a high rate of suicide and used to be called the “suicide disease” prior to the development of effective medical and

surgical therapies (8,9). Despite the array of medical and surgical strategies available today, many patients live in a constant state of anxiety and fear over triggering the next pain attack; indeed, there is an elevated risk of mental health and psychological disorders in TN compared to the general population (10).

Table 1.1: ICHD-3 Diagnostic Criteria for Trigeminal Neuralgia (1):

A) Recurrent paroxysms of unilateral facial pain in the distribution(s) of one or more divisions of the trigeminal nerve, with no radiation beyond, and fulfilling criteria **B** and **C**
B) Pain has all of the following characteristics: 1. Lasting from a fraction of a second to two minutes 2. Severe intensity 3. Electric shock-like, shooting, stabbing or sharp in quality
C) Precipitated by innocuous stimuli within the affected trigeminal distribution
D) Not better accounted for by another ICHD-3 diagnosis.

1.2 Classification of Facial Pain and TN:

TN was traditionally classified based on a characteristic set of symptoms. Over time, the most frequent or stereotypical symptom presentation—lancinating and paroxysmal unilateral pain attacks of the face—became known as 'typical' or 'classic' TN (5). This type of TN was observed to be more responsive to treatment, and therefore, was more apt to be treated with escalating doses of medication or surgery (11). Conversely, many patients presented with dull-aching or burning pain exclusively, or in addition to, the 'typical' presentation. These 'atypical'

or ‘non-classic’ facial pain patients were not as responsive to conventional treatments as their ‘typical’ TN counterparts, and as such, would be less likely to be offered surgery in particular, and occasionally had attempts at clinical management abandoned altogether (12).

Categorization of TN patients as ‘typical’ or ‘atypical’ is straightforward for extreme cases. However, the clinical presentation of many TN patients lies somewhere in between, ultimately exposing the challenges associated with facial pain classifications solely based on clinical presentation (11–13). Alternatively, two dominant classification schemes have since emerged which incorporate underlying putative pathophysiology in addition to patient symptomology: 1) *Burchiel classification of facial pain* (12); and 2) *ICHD-3* (1).

1.2.1 Burchiel Classification of Facial Pain:

In addition to clinical presentation, Burchiel’s facial pain classification system also makes use of known or hypothesized underlying pathophysiology as a key determinant for categorization (**Table 1.2**) (12). Burchiel describes two idiopathic forms of TN (unknown cause). The first of these, Trigeminal Neuralgia Type 1 (TN1), is the subtype previously described as ‘classic’ or ‘typical’ TN. This form is characterized by a high frequency of paroxysmal sharp pain attacks—greater than 50%—compared to dull background or concomitant pain (12). Conversely, Trigeminal Neuralgia Type 2 (TN2), formerly known ‘non-classic’ or ‘atypical’ TN, is characterized by the presence of persistent concomitant pain, with paroxysmal sharp pain attacks making up less than 50% of total facial pain experienced (12). Interestingly, neurovascular compression (NVC) of the trigeminal nerve (cranial nerve five—CNV) is not mentioned in Burchiel’s facial pain classification despite being strongly associated with TN and being the direct target of neurosurgical treatments (more on this in subsequent sections).

Not all forms of facial pain localized to the trigeminal distribution are summarized by the idiopathic subtypes TN1 and TN2, as direct injury to the trigeminal system may also be a cause. Patients with injury-derived neuropathic facial pain can be divided into two groups: 1) unintentional damage to the trigeminal system (Trigeminal Neuropathic Pain—TNP); or 2) intentional damage (i.e., following a surgical procedure) to the trigeminal system (Trigeminal Deafferentation pain—TDP) (12). Facial pain of the trigeminal distribution may also occur in patients with other comorbidities: Symptomatic Trigeminal Neuralgia occurs in conjunction with MS; and Postherpetic Neuralgia occurs following Trigeminal *Herpes zoster* outbreak(12). Finally, Atypical Facial Pain describes severe facial pain with no apparent physical cause, which cannot be diagnosed through patient history alone; psychological evaluation is required, as it is believed that this type of facial pain has a psychological origin and can be considered a type of somatoform pain disorder (12).

By defining different types of facial pain based upon their putative etiologies, Burchiel's classification is able to distinguish different forms of 'atypical' facial pain which would have otherwise been lumped together under a single umbrella because of overlapping features: TN2, TNP, TDP, and post-herpetic neuralgia are now easily distinguishable, with different proposed pathophysiology and treatment approaches. However, despite the greater precision afforded by Burchiel's classification of facial pain, it largely remains a scheme used by neurosurgeons and tends to be less widely accepted among clinicians treating facial pain in general. This is in part because of certain shortcomings. For example, Burchiel's classification distinguishes between facial pain resulting from damage to the trigeminal system that was either intentional or accidental (TDP and TNP respectively). While this distinction may be interesting from a neurosurgical point of view, it may be unnecessary considering both TDP and TNP often

present with similar pain profiles and are presumably the result of similar underlying pathophysiological mechanisms. Furthermore, Burchiel's category of symptomatic TN focuses solely on TN associated with MS, disregarding other well-known causes of lesional secondary TN such tumor or arteriovenous malformation (1,7).

Table 1.2: Burchiel Classification of Facial Pain (12):

Diagnosis	History
	Spontaneous onset
Trigeminal neuralgia, Type 1	*> 50% episodic pain*
Trigeminal neuralgia, Type 2	*> 50% constant pain*
	Trigeminal Injury
Trigeminal neuropathic pain	*Unintentional, incidental trauma*
Trigeminal deafferentation pain	*Intentional deafferentation*
Symptomatic trigeminal neuralgia	Multiple sclerosis
Postherpetic neuralgia	Trigeminal *Herpes zoster* outbreak
Atypical facial pain [a]	Somatoform pain disorder

[a] Cannot be diagnosed by history alone

1.2.2 The International Classification of Headache Disorders 3rd Edition (ICHD-3) Classification of Facial Pain Disorders:

The most widely used classification of facial pain is described in the 3rd version of the International Classification of Headache Disorders (1). The ICHD-3 breaks down facial pain into two categories: TN (**Table 1.3**) and painful trigeminal neuropathy (**Table 1.4**). Both TN

and painful trigeminal neuropathy are sub-divided according to underlying pathology, and then may be further classified according to symptom presentation and clinical observations.

1.2.2.1 Trigeminal Neuralgia:

The ICHD-3 classification of TN was previously described in detail in section 1.1. TN is further subdivided into: 1) classical TN; 2) secondary TN; and 3) idiopathic TN. *Classical TN* is that which "develops without apparent cause other than neurovascular compression" of the ipsilateral CNV confirmed during surgery or using preoperative imaging, that causes "morphological changes in the trigeminal nerve root" (**Figure 1.2C** and **D**) (1). The specific pain character of classical TN may be described as *purely paroxysmal*—"patients are completely pain free between pain attacks"—or *concomitant continuous pain*—"continuous or near-continuous pain between attacks in the affected distribution" (1). It is important to note, however, that sensory deficits are present and may be detected in the affected distributions of the face in *purely paroxysmal* TN patients using specific sensory testing methods (14). *Secondary TN* is "caused by an underlying disease" that is known "to be able to cause, and explain, the neuralgia". Secondary TN is further sub-divided by the disease which is causing TN: *trigeminal neuralgia attributed to multiple sclerosis* (caused by MS); *trigeminal neuralgia attributed to space-occupying lesion* (caused by posterior fossa tumor); and *trigeminal neuralgia attributed to other cause* (caused by something other than MS or tumor, most commonly arteriovenous malformation) (1). *Idiopathic TN* is that in which "neither classical or secondary trigeminal neuralgia has been confirmed by adequate investigation including electrophysiological testing or MRI". It is important to note that ipsilateral NVC without morphological changes at the nerve root fall under this classification (**Figure 1.2B**). The

specific pain character of idiopathic TN may also be described as *purely paroxysmal* or *concomitant continuous pain* (1).

Table 1.3: ICHD-3 Classifications of Trigeminal Neuralgia (1):

1) **Classical trigeminal neuralgia**: Trigeminal neuralgia developing without apparent cause other than neurovascular compression.

   Diagnostic criteria:

   A. Recurrent Paroxysms of unilateral facial pain fulfilling Table 1 criteria for *Trigeminal neuralgia*
   B. Demonstration on MRI or during surgery of neurovascular compression (not simply contact), with morphological changes in the trigeminal nerve root.

2) **Secondary trigeminal neuralgia**: Trigeminal neuralgia caused by an underlying disease. Clinical examination shows sensory changes in a significant proportion of these patients.

   Diagnostic criteria:

   A. Recurrent Paroxysms of unilateral facial pain fulfilling Table 1 criteria for *Trigeminal neuralgia*, either purely paroxysmal or associated with concomitant of near-continuous pain
   B. An underlying disease has been demonstrated known that is known to be able to cause, and explaining, the neuralgia
   C. Not better accounted for by another ICHD-3 diagnosis.

3) **Idiopathic trigeminal neuralgia**: Trigeminal neuralgia with neither electrophysiological tests nor MRI showing significant abnormalities.

   Diagnostic criteria:

   A. Recurrent Paroxysms of unilateral facial pain fulfilling Table 1 criteria for *Trigeminal neuralgia*, either purely paroxysmal or associated with concomitant or near-continuous pain
   B. Neither *Classical trigeminal neuralgia* nor *Secondary trigeminal neuralgia* has been confirmed by adequate investigation including electrophysiological tests and MRI
   C. Not better accounted for by another ICHD-3 diagnosis.

1.2.2.2 Painful Trigeminal Neuropathy:

ICHD-3 defines painful trigeminal neuropathy as facial pain in one or more branches of CNV caused by another disorder indicative of neural damage. The primary pain is usually continuous or near continuous, and is commonly described as burning or squeezing, or likened to pins and needles. Brief pain paroxysms may also occur; however, these are not the predominant pain type. Furthermore, there are "clinically detectable sensory deficits within the trigeminal distribution, and mechanical allodynia and cold hyperalgesia are common", though, it is worthwhile to note that the "allodynic areas are much larger than the trigger zones present in TN" (1).

There are five types of painful trigeminal neuropathy defined by ICHD-3: 1) painful trigeminal neuropathy attributed to herpes zoster; 2) trigeminal post-herpetic neuralgia; 3) painful post-traumatic trigeminal neuropathy; 4) painful trigeminal neuropathy attributed to other disorder; and 5) idiopathic painful trigeminal neuropathy. *Painful trigeminal neuropathy attributed to herpes zoster* is defined as "unilateral facial pain less than three months' duration in one or more distributions of the trigeminal nerve, caused by, and associated with, other symptoms and/or clinical signs of acute herpes zoster" such as herpetic cutaneous eruption in the same trigeminal distribution as facial pain or varicella-zoster virus detected in the cerebrospinal fluid (CSF) (1). *Trigeminal post-herpetic neuralgia* is defined as "unilateral facial pain persisting or recurring for at least three months in the distribution(s) of one or more branches of the trigeminal nerve, with variable sensory changes" that developed in "temporal relation" to herpes zoster infection (1). *Painful post-traumatic trigeminal neuropathy* is defined as

Table 1.4: ICHD-3 Classifications of Painful Trigeminal Neuropathy (1):

---

1) **Painful trigeminal neuropathy attributed to herpes zoster**: Unilateral facial pain of less than three months' duration in the distribution(s) of one or more branches of the trigeminal nerve, causes by and associated with other symptoms and/or clinical signs of acute herpes zoster.

   Diagnostic criteria:*

   A. Unilateral facial pain in the distribution(s) of a trigeminal nerve branch or branches, lasting < 3-months
   B. One or more of the following:
      1. Herpetic eruption has occurred in the same trigeminal distribution
      2. Varicella-zoster virus (VZV) has been detected in the cerebrospinal fluid by polymerase chain reaction (PCR)
      3. Direct immunofluorescence assay for VSV antigen or PCR assay for VZV DNA is positive in cells obtained from the base of lesions.

2) **Trigeminal post-herpetic neuralgia**: Unilateral facial pain persisting or recurring for at least three months in the distribution(s) of one or more branches of the trigeminal nerve, with variable sensory changes, caused by herpes zoster.

   Diagnostic criteria:*

   A. Unilateral facial pain in the distribution(s) of a trigeminal nerve branch or branches, persisting or recurring for > 3-months and fulfilling criterion C
   B. Herpes zoster has affected the same trigeminal nerve branch or branches
   C. Pain developed in temporal relation to the herpes zoster infection

3) **Painful post-traumatic trigeminal neuropathy**: unilateral or bilateral facial or oral pain following and caused by trauma to the trigeminal nerve(s), with other symptoms and/or clinical signs of trigeminal nerve dysfunction.

   Diagnostic criteria:*

   A. Facial ad/or oral pain in the distribution(s) of one or both trigeminal nerve(s) and fulfilling criterion C
   B. History of an identifiable traumatic even to the trigeminal nerve(s), with clinically evident positive (hyperalgesia, allodynia) and/or negative (hypaesthesia, hypalgesia) signs of trigeminal nerve dysfunction
   C. Evidence of causation demonstrated by both of the following:
      1. Pain is localized to the distribution(s) of the trigeminal nerve(s) affected by the traumatic event
      2. Pain has developed <6-months after the traumatic event

4) **Painful trigeminal neuropathy attributed to other disorder**: unilateral or bilateral facial or oral pain in the distribution(s) of one or more branches of the trigeminal nerve, caused by a disorder other than those described above, with other symptoms and/or clinical signs of trigeminal nerve dysfunction.

Diagnostic criteria:*

A. Unilateral or bilateral facial pain in the distribution(s) of one or both trigeminal nerve(s) and fulfilling criterion C
B. A disorder, other than those described above but known to be able to cause painful trigeminal neuropathy with clinically evident positive (hyperalgesia, allodynia) and/or negative (hypaesthesia, hypalgesia) signs of trigeminal nerve dysfunction, and affecting one or both trigeminal nerves, has been diagnosed
C. Evidence of causation demonstrated by both of the following:
    1. Pain is localized to the distribution(s) of the trigeminal nerve(s) affected by the disorder
    2. Pain developed after onset of the disorder, or let to its discovery.

5) **Idiopathic painful trigeminal neuropathy**: unilateral or bilateral pain in the distribution of one or more branches of the trigeminal nerve (s), indicative of neural damage by of unknown aetiology.

Diagnostic criteria:*

A. Unilateral or bilateral facial pain in the distribution(s) of one or both trigeminal nerve(s) and fulfilling criterion B
B. Clinically evident positive (hyperalgesia, allodynia) and/or negative (hypaesthesia, hypalgesia) signs of trigeminal nerve dysfunction
C. No cause has been identified

* Not better accounted for by another ICHD-3 diagnosis.

"unilateral or bilateral facial or oral pain following, and caused by, trauma to the trigeminal nerve(s), with other symptoms and/or clinical signs of trigeminal nerve dysfunction". It is important to note that clinical signs of nerve dysfunction may be positive or negative, pain must be localized to the distribution of the trigeminal nerve affected by the traumatic event, and that pain must have developed less than 6-months after the traumatic event (1). *Painful trigeminal*

neuropathy attributed to other disorder characterized as "unilateral or bilateral facial or oral pain caused by a disorder other than those described above" that is known to be able to cause painful trigeminal neuropathy with clinically evident positive (hyperalgesia, allodynia) and/or negative (hypaesthesia, hypoalgesia) signs of trigeminal nerve dysfunction. Additionally, pain is localized to the nerve affected by the disorder, and the pain developed after the onset of the disorder or led to its discovery (1). Finally, *Idiopathic painful trigeminal neuropathy* is defined as unilateral or bilateral pain in the distribution of one or more branches of the trigeminal nerve(s), with positive or negative signs indicative of neural damage, but with an unknown aetiology (i.e., same as above but without an identifiable cause) (1).

In this thesis, patients with painful trigeminal neuropathy have explicitly been excluded from all studies, which instead include only patients with classical or idiopathic TN.

1.3 The Trigeminal System:

In order to appreciate TN's underlying pathophysiology, the motivation behind various surgical approaches, and to understand surgical treatment resistance in TN, it is important to understand the core architecture devoted to conveying sensory information from the face. The following section is devoted to outlining in detail the various components (and their functions) of the trigeminal system.

1.3.1 Anatomy of the Trigeminal Nerve:

Collectively, the trigeminal system supplies all sensory information from the facial region. All left-sided information is supplied by the left CNV, and all right-sided information is supplied

by the right CNV. CNV has three primary divisions: Ophthalmic (V1), Maxillary (V2), and Mandibular (V3) (**Figure 1.1**) (15). V1 is the smallest trigeminal division and is purely sensory in function. The V1 division provides sensory information through its distal branches from the whole eyeball, forehead, upper eyelids, bridge and tip of the nose, lacrimal gland/sac, lacrimal caruncle, and frontal sinuses (15,16). Of notable importance is corneal sensation. This protective function alerts us to foreign objects in the eye, preventing corneal damage and potential blindness as a result. As finer distal branches leave their respective sensory territories, they converge to form the larger V1 nerve which then enters the skull through the superior orbital fissure. The V2 division is also purely sensory, though it is substantially larger than V1 in terms of mean number of nerve fibers (17). V2 carries sensation from the skin of the cheek, part of the temporal region, the lower eyelid, upper lip, side of the nose, a portion of the mucous membrane of the nose, the teeth of the upper jaw, nasopharynx, maxillary sinus, soft palate, tonsil, and roof of the mouth, and enters the skull through the foramen rotundum (15,16). The final division of the trigeminal system, and the largest of the three, is V3 (17). The V3 division has both sensory and motor functions. The principal motor function of V3 is controlling muscles of mastication including the masseter, temporalis, lateral pterygoid, and medial pterygoid, as well as the tensor tympani muscle of the inner ear and tensor veli palatini of the soft palate (15). The primary sensory function of V3 is to convey sensation from the skin and mucous membranes of the cheek, skin of the chin, skin of the lower lip and gums, tongue, upper part of the lateral surface of the ear, tympanic membrane, parotid gland, and scalp (15). Sensory and motor components of V3 converge to form a single nerve and then enter the skull-base through the foramen ovale (15).

All three divisions of the trigeminal nerve converge in a cavernous space known as Meckel's cave, which is bordered above by the inferior-medial surface of the temporal lobe of the brain and below by the sphenoid bone of the middle cranial fossa. This structural feature connects the cavernous sinus to the prepontine cistern of the posterior fossa (16). Housed within Meckel's cave is the collection of all the individual neural cell bodies of the collective trigeminal nerve known as the trigeminal (aka Gasserian or semilunar) ganglion (15,16). The trigeminal ganglion is somatotopically organized, meaning that the cell bodies of each of each nerve branch are arranged to occupy a specific region of the ganglion (18). The V1 division forms the antero-supero-medial region of the trigeminal ganglion. The V3 division lays diagonally opposite to V1, making up the postero-inferior-lateral portion of the trigeminal ganglion. Finally, the V2 division occupies the space in between V1 and V3 (18). Some evidence suggests that the aforementioned somatotopic organization of the trigeminal ganglion is at least somewhat preserved within more proximal locations along CNV also, with the V1 and V3 divisions projecting through ventral-medial and dorso-lateral nerve sections respectively immediately prior to entering the pons (15,17–20). After departing from their cell bodies in the trigeminal ganglion, afferent sensory axons move through the trigeminal nerve root to enter the brainstem via the lateral pons (15). Sensory afferents immediately follow a dorsomedial trajectory, approaching second-order trigeminal cell bodies arranged in an approximately vertical column. Recent application of ultra-high-field magnetic resonance imaging (MRI) and histochemical staining methods suggest that pontine trigeminal afferents may actually bifurcate into the historically described dorsomedial trajectory, as well as a newly observed ventromedial trajectory (21), though follow-up studies are needed to confirm, and assess the relevance of, these findings. Within the brainstem, trigeminal afferents segregate by

fiber type (by extension, sensory modality), ultimately synapsing at one of three different brainstem nuclei arranged in a rostro-caudally oriented column: mesencephalic, principal, and spinal trigeminal nuclei (22,23).

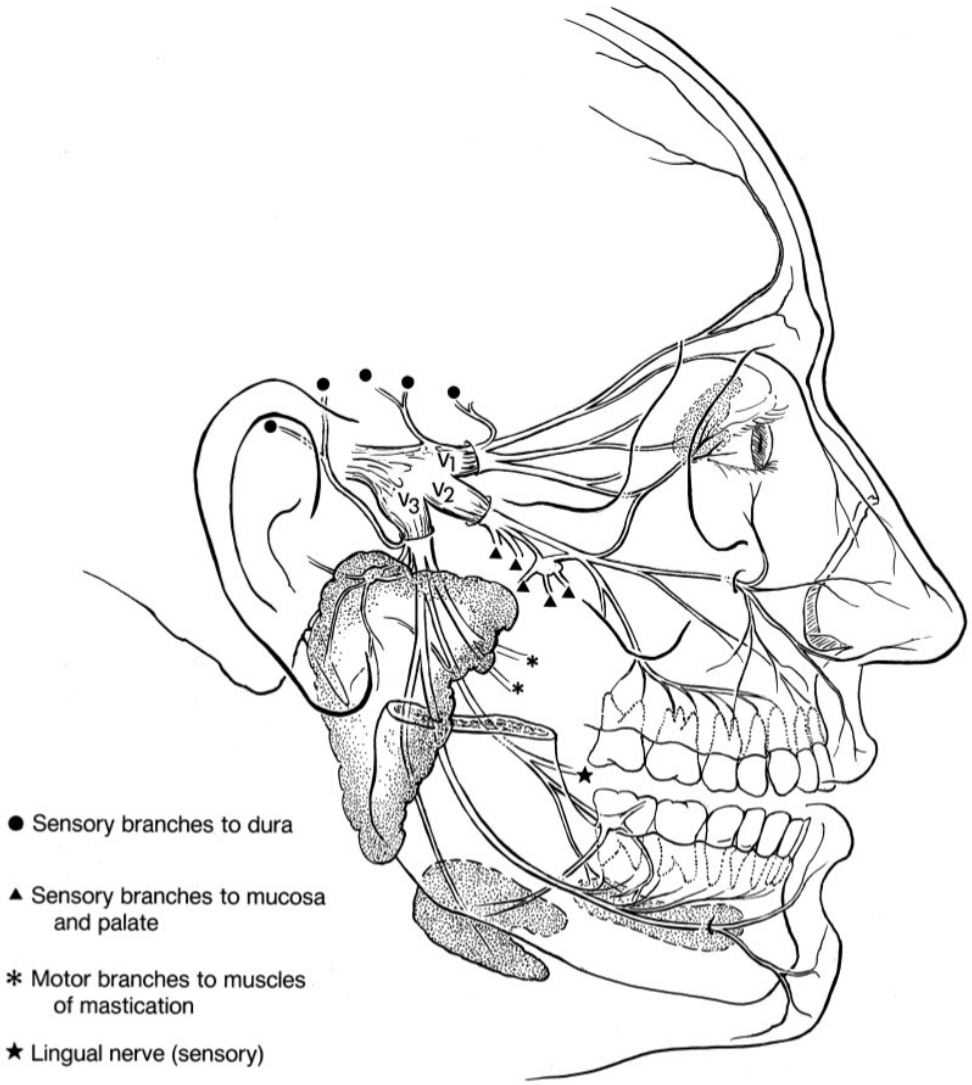

Figure 1.1: Major branches of the trigeminal nerve. V1 denotes the Ophthalmic branch. V2 denotes the Maxillary branch. V3 denotes the Mandibular branch. This figure was produced from (15).

1.3.2 Ascending Ponto-Thalamo-Cortical Projections:

The *trigeminal mesencephalic nucleus* is not technically a nucleus; rather, it more closely resembles a sensory ganglion given that it is primarily made up of unipolar primary afferent cells derived from the neural crest (22,24). This collection of neuron cell bodies extends upward from the pons to the superior colliculus of the midbrain. Most nerve fibers synapsing with this structure are aα-type (proprioceptive), conveying stretch information from muscles of mastication, though mechanoreceptor fibers of the teeth and other supportive dental tissues are also present to a lesser degree (25,26).

The *trigeminal principal (chief) nucleus* lies below the mesencephalic nucleus, occupying the middle portion of the trigeminal nuclear complex and sitting at the same rostral level as CNV (15,23). This nucleus receives facial touch-pressure sensation via heavily myelinated large diameter aβ-type fibers. The principal nucleus represents a tactile map of the face, and is somatotopically organized in the ventro-caudal direction with the lips, nose, forehead, and cheek afferents projecting to the ventral region, and corneal afferents projecting caudally (23).

The *spinal trigeminal nucleus* lies caudal to the principal trigeminal nucleus and extends caudally within the medulla of the brainstem terminating at the level of the second or third cervical intervertebral disc. The spinal trigeminal nucleus receives small diameter lightly myelinated aδ and unmyelinated c-type fibers, and thus primarily transmits pain and temperature sensation from the face and other mucous membranes in the head and neck (27). There are three subdivisions of the spinal trigeminal nucleus in mammals: nucleus oralis; nucleus interpolaris; and nucleus caudalis (28). Each subdivision receives afferents from all three trigeminal divisions and is somatotopically organized generally in a ventral (mandibular

division) to caudal (ophthalmic division) fashion (15). However, it is important to note that somatotopic variation does exist, particularly within the nucleus caudalis. In this spinal trigeminal subdivision, afferents arising from peripheral regions of the face synapse caudally, while those originating from more central perioral regions synapse rostrally, giving rise to an *onion skin* organization of the face for pain (22).

Second order afferents departing the trigeminal nuclei may project to brainstem sensory or motor nuclei—of the trigeminal nerve itself or other cranial nerves—or the cerebellum (29). Other neurons departing all levels of the spinal trigeminal (pain-temperature) and principal nuclei (touch-pressure) decussate within the brainstem and then ascend up to, and synapse with, the contralateral ventral posteromedial (VPM) nucleus of the thalamus via the ventral trigeminothalamic tract (15). An ipsilateral projection of touch-pressure neurons from the principal nucleus to the VPM thalamus is also present, ascending via the dorsal trigeminothalamic tract (15). It is worthwhile noting that an ipsilateral pain-temperature pathway has recently been proposed, suggesting that pain-temperature information may also have a bilateral representation (30).

Outgoing touch-pressure and pain-temperature impulses carried along axon from the third-order neurons of the VPM thalamus project primarily to the cerebral cortex, though, intrathalamic connections or projections to the basal ganglia also exist (15). Temperature-pain and touch-pressure thalamocortical connections depart the VPM thalamus and project to the 'face' location of the primary sensory cortex in the post-central gyrus via the internal capsule to inform spatial awareness/sensation of our face (31). Temperature-pain information also projects from the VPM thalamus to other cortical regions including the cingulum and insula, and may contribute to feelings related to the 'unpleasantness' of pain and directing conscious

attention toward it (32,33). Disruption anywhere along the trigeminal pathway or supporting brain structures that are involved in the sensation or characterization of pain in face could, in theory, be involved in the development and maintenance of TN or other facial pain disorders.

1.4 What Causes TN?

1.4.1 Classical TN:

Coined *Tic Douloureux* by Nicholas Andre in 1765, TN was then described fully by John Fothergill in a 1773 article reporting clinical observations in 14 patients (11,34,35). However, it was not until 1829 that this pain syndrome was localized to the trigeminal nerve by Charles Bell, after which it was called trigeminal neuralgia (36). Based on Bell's work, it was accepted that TN was the result of CNV dysfunction, and thus, neurosurgeons began treating patients with TN by employing surgical techniques targeting CNV directly (11). While performing retrogasserian trigeminal neurotomies, in 1934 Walter Dandy observed that CNV appeared to be compressed by one or more aberrant blood vessels in many patients with TN (37), and the theory that TN is caused by NVC was born. The development of new surgical approaches aiming to relieve NVC and restore the normal anatomy of CNV ensued, and the remarkable early success of these procedures in relieving TN pain seemed to confirm the theory that NVC is indeed a clear cause of TN (38–40). TN associated with NVC of CNV is known today as *Classical TN*, and is the most commonly observed, making up approximately two-thirds of TN cases (1,41).

1.4.1.1 Theory of neurovascular compression:

The theory of NVC states that at least one point of physical contact between an offending blood vessel (or vessels) and CNV must be present—which may vary in severity depending on degree and angle of contact—in order to develop classical TN (**Figure 1.2**)(4,42). It has long been postulated that NVC observed in patients with TN may be causing damage to CNV, resulting in abnormal nerve function (37). Despite NVC along cranial nerves occurring commonly in healthy individuals, it appears that compression specifically at the nerve root is implicated in TN pathophysiology (4,43–46). A 2-6mm long proximal subsection of the nerve root known as the root entry zone (REZ) located where the nerve emerges from the pons appears to be particularly important in the pathophysiology of classical TN. The REZ is a myelination watershed or Obersteiner-Redlich line, representing a transition point between central (i.e., oligodendrocyte) and peripheral nervous system (i.e., Schwann cell) mediated myelination, and likely having a diminished remyelination capacity (47–49). Therefore, proximal vascular compression situated at the REZ may be more pathogenic and may be associated with TN and disorders of other cranial nerves as well (50). Microscopic and histologic methods have indeed observed demyelination, dysmyelination, and neuron loss at sites of CNV vascular compression in patients with TN, establishing a strong link between NVC and pathophysiological CNV change in TN (51,52). More recently, MRI has been used to observe physical alterations—such as atrophy at the site of compression, and potential demyelination—at the REZ of the affected CNV in TN patients *in situ* (53–64). Exactly how the physical changes to CNV observed in relation to NVC may lead to the characteristic pain of TN is explained by The *Ignition Hypothesis*.

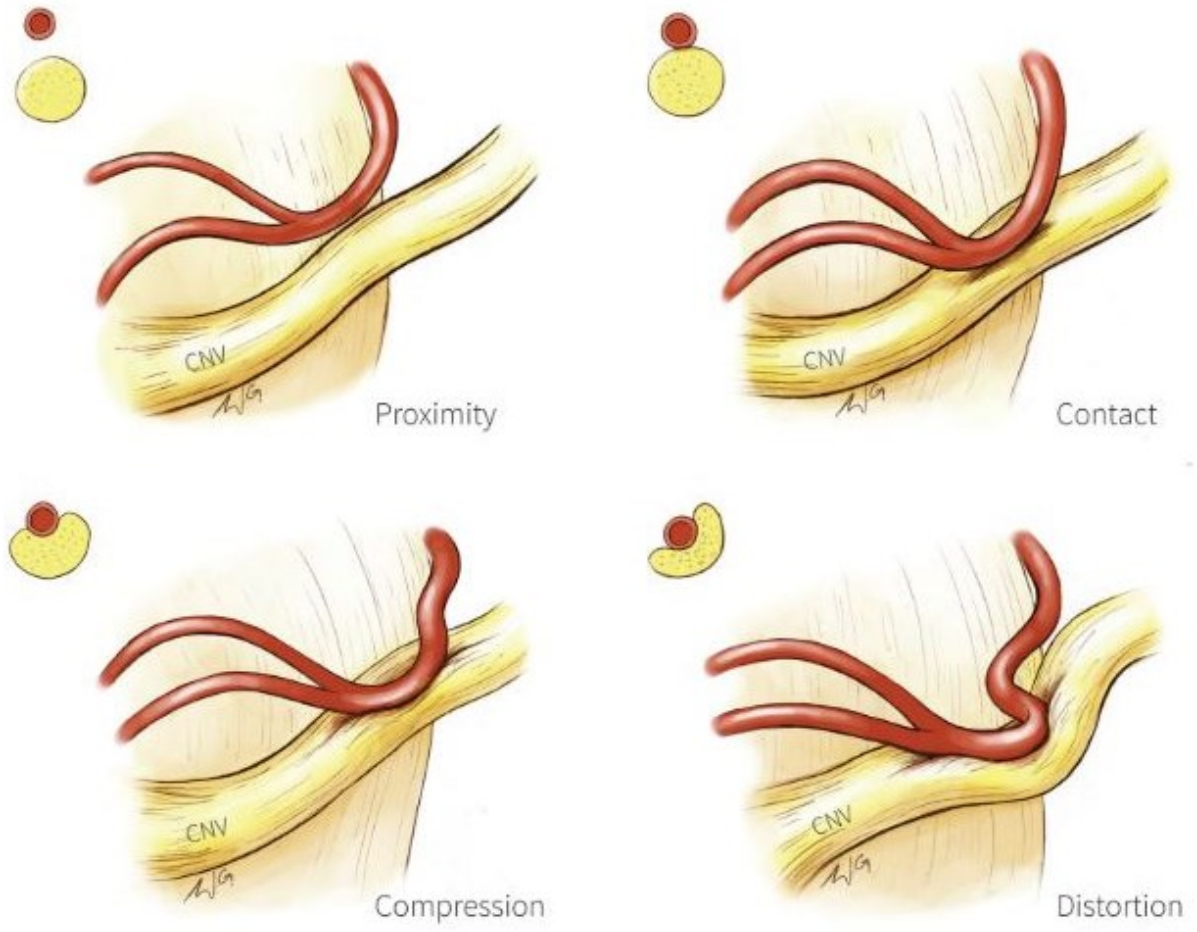

Figure 1.2: Cartoon representation of various severities of vascular compression of the trigeminal nerve. In patients with ICHD-3 idiopathic TN (1) aberrant blood vessel(s) may lie in close proximity to CNV (**A**) or may physically contact CNV (**B**). In classical TN patients, physical contact of sufficient severity is present to compress (**C**) or distort (**D**) CNV. This figure was reproduced from (65) with permission from Frontiers in Neuroanatomy.

1.4.1.2 Ignition Hypothesis:

The pain attacks experienced by patients with TN are best conceptualized through three distinct mechanisms: 1) *Triggering*—a short-lived trigger stimulus generating a painful response which outlasts itself by seconds or minutes; 2) *Amplification*—the tendency of non-painful stimuli to evoke a wide-spread nociceptive response greatly exceeding the tissue area initially stimulated;

and 3) *Termination*—despite the self-perpetuating nature of the pain attack, eventually the pain does cease. These three unique features and distinct mechanisms of TN pain are characterized in detail by the *Ignition Theory* (66).

Triggering:

Though many TN patients report spontaneous pain attacks, the majority occur following some sort of sensory trigger, commonly touch, wind, eating, talking, or brushing one's teeth (67). Interestingly, pain attacks persist for a period of time many orders of magnitude longer in duration than the triggering stimuli itself, and long after the triggering stimuli has ceased. In patients with TN, there appears to be an acquired hyper-excitability of trigeminal nerve sensory fibers at sensitized locations called *ectopic pacemaker sites* (66,68). A process known as *afterdischarge* may occur at these locations, where action potentials may be self-generated, explaining patient accounts of spontaneous pain attacks. While a definitive mechanistic understanding of afterdischarge is still lacking, reduced depolarization thresholds of pacemaker sites are believed to be central to this phenomenon (66,69). In addition to self-stimulation, these sites are also more susceptible to adjacent activation from neighboring axons, through a variety of processes described in detail in the following section. Thus, once this process has been initiated, recruitment of additional adjacent sensory nerve fibers permit a positive feedback cascade, resulting in a pain attack outlasting the initial stimulus by seconds or minutes (66). However, the independent firing and adjacent stimulation of sensory fibers should, under normal circumstances, amount to nothing more than a prolonged tingling or tickling sensation within the stimulated region (66,67). The sensory transition from touch to pain within an increasingly large region of the face is described though the process of *Amplification*.

Amplification:

During a TN pain attack, the triggering sensation (touch) rapidly transforms to excruciating pain. Additionally, there is a massive recruitment of nerve fibers resulting in the pain being felt in an area of the face far more extensive than initially triggered. These unusual features specific to TN pain attacks are permitted through processes known as *ephaptic cross-talk* and *crossed after discharge* (66,67).

During a TN pain attack, triggered axons may depolarize adjacent nerve fibers positioned in close proximity through a process known as ephaptic cross-talk (66,67). Such a mechanism should never occur under normal physiologic conditions given that: 1) sensory and nociceptive pathways do not synapse with one another; and 2) myelin specifically insulates aβ- and aδ-type sensory fibers to prevent adjacent activations through across-membrane current leak (47). However, c-type nociceptive nerve fibers are not myelinated, and are thus more susceptible to ephaptic cross-talk at sites of aβ- and aδ-type sensory fiber demyelination (66,67). This unlikely scenario indeed appears to be the case in TN, as cadaveric CNV dissections have confirmed the presence of sensory axonal clusters devoid of myelin sheaths in these patients (68). It is important to keep in mind that TN is also commonly associated with the demyelinating disorder MS in which proximal nerve root demyelination is also present (1,70). The second process leading to adjacent nerve fiber activation is crossed after-discharge. Unlike ephaptic cross-talk, which occurs through electric-coupling, this process is driven though neurotransmitter or ion release through sites of membrane damage. These stimulatory particles readily diffuse through interstitial space along adjacent axon fibers, eventually triggering action potentials at susceptible sites (71).

Ephaptic cross-talk and charged after-discharge represent plausible mechanisms by which activated sensory neurons may subsequently activate adjacent nociceptive afferents resulting in severe pain attacks initially triggered by sensory stimulation (66). These mechanisms also explain how it is that large facial regions become activated over the course of a TN pain attack, even if neighboring nerve fibers do not necessarily innervate neighboring regions of the dermatome.

Termination:

Considering a stimulus is not required to maintain TN pain attacks, why then do pain attacks stop at all? Electrophysiology has shown that after an action potential fires, axon fibers enter a refractory phase lasting much longer in duration than the time required for the action potential to travel the length of an axon. During TN pain attacks, neurons enter this refractory phase rapidly. Therefore, once a large enough proportion of neighboring neurons have fired, the density of ready-to-fire axons becomes too low to maintain and propagate the self-sustaining pain cascade (66). The pain attack then ceases.

The *neurovascular compression hypothesis* and *Ignition theory* cover different aspects of TN: the former explains why TN is thought to occur in the first place, while the later proposes specific mechanistic underpinnings to explain observed pain attack characteristics. Note that both describe TN as being a peripherally-initiated pain disorder centered on potential abnormalities occurring upstream of the arrival of trigeminal afferents into the trigeminal nuclear complex. However, it must be pointed out that in the general population, NVC of CNV is observed in approximately 17% of non-TN individuals, though estimates have been as high as 25-49% (72–74). Furthermore, studies using advanced MRI techniques (more on this in later sections) found that while CNV microstructure is abnormal at the site of NVC in TN patients,

it is unaffected in asymptomatic subjects with NVC of CNV that do not have TN (55,75). Thus, it would appear that NVC of CNV in and of itself is not sufficient to cause TN in people without the disease. Exactly why NVC appears to cause TN in classical TN patients remains unknown, though it may be possible that some other pathology exists that either permits or exacerbates the disease in this population.

1.4.2 Secondary TN:

Described in previous sections, TN also occurs secondary to MS in approximately 6% of cases, and more rarely, posterior fossa pathology including tumors, vascular malformations, angiomas, and aneurysms (1,7). These posterior fossa lesions collectively represent approximately 5% of TN cases, and are thought to cause TN though physical compression of CNV resulting in demyelination (similar to classical TN), as well as chemical irritation by neoplastic factors (76–78). MS-related TN on the other hand is not associated with nerve compression (79). Rather, demyelinating lesions deposited along the trigeminal pathway facilitate the ephaptic transmission of intrapontine trigeminal nerve fibers (70,80). Interestingly, MS plaques located in supratentorial brain structures are also commonly associated with TN, though, the mechanism behind how plaque deposition in higher-order brain regions contributes to the development of TN is unknown (81). Regardless of lesion location, TN secondary to MS results in a similar clinical picture to classical TN, though tends to be more resistant to treatment (79,81–84).

1.4.3 Idiopathic TN:

Idiopathic TN is that in which no vascular compression of CNV, MS lesions, or any other brain pathology that could cause TN is identified at surgery, or through imaging or other methods

(i.e., electrophysiology) (1). This idiopathic form represents approximately 29-32% of all TN cases (1,85). It is important to note that while the underlying pathology of idiopathic TN is unconfirmed, recent studies have identified the presence of single brainstem lesions (i.e., solitary pontine lesions) in subsets of idiopathic TN patients which appear different microstructurally than demyelinating lesions present in patients with TN secondary to MS (86).

1.5 Treatment of TN:

Early identification and treatment of TN are critically important to limit patient suffering and disability (4,87). Given the complex nature of this pain condition, appropriate management by an experienced clinician is necessary (88). Over-the-counter pain medications such as non-steroidal anti-inflammatory drugs or acetaminophen are often used by patients to manage new onset pain due to TN prior to being formally diagnosed with the condition. Unfortunately, these conventional pain medications are not effective at treating neuropathic pain conditions such as TN and may harm gastrointestinal, renal, and hepatic systems with escalating dosages and prolonged use (88). Given that TN pain is most commonly felt in maxillary and mandibular facial regions, the logical next step taken by many frustrated patients—again, usually prior to a formal diagnosis—is to be seen by their dentist (89). TN poses a particular diagnostic challenge for primary care dentists as many common orofacial pain conditions may present similarly to TN (89). Thus, it is not uncommon for TN patients to have been seen by numerous healthcare providers, to have undergone multiple unnecessary dental procedures, or to have presented to emergency departments seeking help to manage their terrible pain (90,91). Fortunately, once a correct diagnosis of TN is made, well described and effective (at least initially) medical treatments exist.

1.5.1 Medical Management of TN:

Antiepileptic medications such as carbamazepine and oxcarbazepine are the first-line medical treatments for TN (88). Clinical trial data shows that 58% - 100% of TN patients achieve complete or near complete pain control with these medications (92). Despite such a robust response, the utility of these drugs is limited by poor tolerability due to a wide set of diverse side effects—slurred speech, drowsiness, incoordination, vertigo, nausea, diplopia, etc., (93)—and pharmacokinetic interactions (88). Limited evidence supports the use of other medications in lieu or in adjunct to carbamazepine or oxcarbazepine should patients become refractory to these first-line drugs. Additional antiepileptics (gabapentin, pregabalin, lamotrigine, phenytoin), a muscle relaxant (baclofen), and an antipsychotic (pimozide), are recommended second-line therapies by the American Academy of Neurology and European Federation of Neurological Societies (87,92). As alluded to above, it should be noted that the use of conventional pain medications including non-steroidal anti-inflammatories, acetaminophen, or opioids for the treatment of TN is not supported by clinical trial data, and thus, is not recommended (87,88,92).

1.5.2 Surgical Treatment for TN:

While first-line medical therapy effective manages TN pain initially, drug tolerance, cognitive side-effects, and pharmacokinetic interactions dramatically reduce long-term efficacy (88,93). Approximately 35% of TN patients are medically-refractory within 2-years after initiating medication trials (94). For these patients, surgical treatment is the next step in TN management provided they are good surgical candidates, and of course, are willing to undergo a procedure (87). There are two general classifications of mainstream surgical treatment available for TN.

The first—*restorative* treatment—aims to relieve NVC of CNV with the purpose of restoring normal anatomy (42). The second—*ablative* or *destructive* treatment—intentionally inflicts localized damage to CNV, aiming to injure nociceptive fibers and impair the transmission of facial pain (6,95,96).

1.5.2.1 Restorative Surgical treatment:

Back in 1934 while performing retrogasserian trigeminal neurotomies, Walter Dandy observed that CNV was compressed by aberrant blood vessels in the majority of TN patients he was treating with surgery (37). Today it is known that significant vascular compression of CNV is present in approximately two-thirds of TN patients (i.e., classical TN) (1,41,45). Thus, clinicians postulated that vascular compression played a critical role in the development and maintenance of classical TN and soon developed surgical procedures directly targeting this abnormality (see 2.4.1.1 above). Microvascular decompression (MVD)—developed and performed simultaneously in the early 1950s by Gardner, Love, and Taarnhøj—is one such surgery that relieves vascular compression to induce pain relief (39,97). Neurosurgeons must gain access to the prepontine cistern whereupon CNV and compressive blood vessels may be visualized and manipulated directly. Suboccipital craniotomy (i.e., posterior fossa) is now preferred over middle fossa approaches given early reports by Taarnhøj of improved outcomes when using the former (40,98,99). Various blood vessels may be physically compressing CNV, with the most commonly observed culprits being the superior cerebellar artery (~75% of cases) or anterior inferior cerebellar artery (~12% of cases) (100). General venous compression occurs in approximately 18% of classical TN cases and it is worthwhile noting that venous compression is less likely to be severe enough to produce adequate nerve indentation and deviation sufficient to cause classical TN (1,100). Exactly which blood vessels require

manipulation or transposition in order to achieve decompression is at the discretion of the surgeon at the time of the operation. Typically, shards of Teflon are inserted between culprit blood vessels and CNV, structurally re-enforcing or buttressing this point of contact such that compressive blood vessels and CNV no longer touch, though in some cases compressive blood vessel will be transposed away from the nerve using a sling or glue (101).

Early outcome reports indicated that MVD was effective at relieving pain in classical TN with approximately 73% of patients achieving complete or partial pain relief immediately following surgery with no detectable sensory deficits (39,40,97). Today, initial outcomes have improved further with ~96% of classical TN patients being pain free immediately after surgery (102). Pain relief is not permanent in many cases though, with pain recurrence occurring in ~25% of patients within the first 2-years after surgery and then at a steady rate of ~4% per year thereafter (98). The reasons for pain recurrence after initially successful MVD remain incompletely understood, and cannot be explained by clinical factors alone (see 1.5.5 below). The established success of MVD strongly supports the theory that NVC of CNV is a pathophysiologic driver underlying classical TN, and hence, why relieving decompression results in pain relief (51,66,67). However, the mechanism of action of MVD remains unclear. Indeed, remyelination of cranial nerves does occur following adequate decompression, but animal models suggest that this process requires weeks to initiate and months to complete; thus, remyelination cannot be responsible for the immediate pain relief achieved with MVD (103).

Prior to the development of advanced imaging techniques, accurate identification and characterization of vascular compression in TN patients prior to surgery was not possible. As a result, a substantial proportion of TN patients would undergo MVD despite no vascular compression being present or identified at the time of surgery (39,45,97). In a cohort of patients

without vascular compression (i.e., idiopathic TN) undergoing MVD, Taarnhøj noted that "all patients were free of pain after the operation" with intact sensation despite the fact that "no real decompression could be performed" (39). He later postulated that pain relief achieved through MVD in these patients was paradoxically the result of manipulation and compression of CNV rather than decompression (39,40). Today, TN patients undergoing MVD in whom vascular compression is not identified by the surgeon will may receive an internal neurolysis procedure whereby the surgeon uses a blunt-tip instrument to divide the cisternal segment of CNV longitudinally into 5-10 bundles from REZ to petrous bone (104). In one clinical series, 96% of idiopathic TN patients experienced immediate pain relief following this procedure (85% were completely pain free) with 58% of patients still pain-free 5-years after surgery (104). However, given that internal neurolysis for idiopathic TN is effectively a destructive procedure, sensory deficits occur at a much higher rate (~96% patients) than with MVD (104).

1.5.2.2 Ablative Surgical Treatments:

Minimally invasive surgical treatments for TN were first developed in the early 20th century decades before invasive open-brain procedures (105). Despite MVD becoming the most efficacious surgical treatment for medically-refractory TN, these minimally invasive approaches may be more suitable for, or are simply preferred by, certain TN patients over open-brain procedures. Idiopathic TN patients as well as patients with TN secondary to MS lack vascular compression of CNV; therefore, MVD is not recommended for either of these TN subtypes (106). Additionally, ~25% classical TN patients who undergo their first MVD procedure fail to respond initially or experience early pain recurrence less than 2-years after surgery (98,102); given that these patients failed to achieve durable pain relief from initial MVD, they are typically not good candidates for repeat MVD attempts (106). Finally,

considering the tendency of TN to appear in middle-aged to elderly populations, many patients also have concurrent medical conditions rendering them suboptimal candidates for open brain surgery (2,106).

Rather than aiming to restore normal nerve anatomy by relieving NVC as in MVD, ablative procedures instead damage CNV selectively, impairing the ability of ectopic pacemaker sites to generate painful stimuli (4,6,67,106). This destructive approach is simpler and requires less time to perform, is less invasive, and does not require the patient to be as heavily anaesthetized as MVD (6). A variety of ablative methods exist to treat TN which can generally be divided into percutaneous rhizotomy (PR) or stereotactic radiosurgery (SRS) procedures.

1.5.2.2.1 Percutaneous Rhizotomy:

PR is a technique in which surgical access to the trigeminal (Gasserian) ganglion is accomplished by passing a needle through the soft tissues of the cheek, and then into the cranial cavity through a small hole in the skull base called the foramen ovale (6). Haertel first described this technique in detail back in 1914—his landmarks and approach are still the preferred method today (6). The target location inside the cranial cavity is known as Meckel's cave, which is a cavernous structure between the skull base and inferior medial surface of the temporal lobe in which the trigeminal ganglion sits (15,16). The trajectory and angle of the needle may be finetuned by the surgeon—exploiting the somatotopic organization of the trigeminal ganglion (described in detail in section 2.3)—specifically targeting the affected facial dermatomes of the current patient, and critically, to avoid disrupting motor function in muscles of mastication and the destruction of the corneal reflex (18). Once in optimal position, various methods may be employed to induce focal damage to CNV.

Harris demonstrated in 1910 that alcohol could be injected into the trigeminal ganglion to produce pain relief in patients with TN (6,105). Today, Haertel's PR technique is used to access Meckel's cave, and then a caustic substance such as glycerol or alcohol is injected into this space to relieve TN pain (6). After a short period of time (approximately 90 seconds) the injected material is drawn out, and then Meckel's cave is flushed with a saline solution. Physical contact between this caustic substance and neuronal cell bodies, even if only temporary, is sufficient to cause injury. Surgical outcomes vary dramatically between studies presumably due to differences in reporting, technique, and experience. Approximately 70% of patients experience sensory deficit including facial numbness. Initial pain relief rates range between 53% - 98%, with approximately 50% of patients experiencing pain recurrence within three years after surgery (4,6).

In the 1950s, Kirschner developed a new technique to selectively damage the trigeminal ganglion utilizing radiofrequency thermocoagulation (RFT) (6). This method uses heat to burn localized distributions of CNV at the ganglion, and is considered the most destructive form of rhizotomy (4). Patients are typically awakened during surgery to allow for sensory and motor testing with electrical stimulation through the lesioning electrode at sub-lesional thresholds, in order to confirm appropriate position of the electrode such that mastication and the corneal reflex are not threatened by surgery. The patient remains partially awake during thermal lesioning, and sensory testing of the face is performed in order to assure that numbness develops in the painful trigeminal dermatomes (6). This process can be quite painful and may be emotionally distressing to the patient, which are significant obstacles to treatment for many (6,105). Initial rates of pain relief and durability are the highest of percutaneous procedures, with most studies reporting complete pain relief in greater than 95% of patients, with between

a 25% - 50% recurrence rate two years postoperatively (4,6). Significant side-effects including masseter weakness and corneal anesthesia are the highest amongst percutaneous procedures ranging between 1% - 20% depending on the study (4,6,105).

Percutaneous balloon compression (BC) was first reported in 1983 by Mullan and Lichtor, and is the most recently developed PR procedure (107). A needle cannula is inserted into Meckel's cave using Haertel's landmarks for guidance, and then a catheter with an inflatable balloon on the tip is inserted. The balloon is then inflated with a radio-opaque saline solution mixture (6,95,108). Given that the volume of Meckel's cave is finite, any balloon expansion and corresponding pressure increase is directly transferred to the trigeminal ganglion—effectively, this is a controlled mechanical compression of the ganglion. Compression appears to spare trigeminal cell bodies, and rather, appears to primarily affect large diameter aβ- and medium diameter aδ-type sensory fibers; thus, initial pain relief is achieved by disrupting sensory pain attack triggers while long-term pain relief is speculated to be the result of trigeminal nerve remyelination (6,95,109). The rate of initial pain relief is high, approaching 100% depending on study parameters (4,105). Durability of this pain relief is amongst the highest of the PR procedures with a 5-year recurrence rate of 19.2% - 29.5% (6,105). Sensory or motor deficits are fairly common, occurring in the majority of patients; these typically resolve in less than 3-months (6,95,109). BC also causes a trigeminal depressor response which is characterized by hypotension and bradycardia. This undesired physiologic reaction may be avoided by utilizing preoperative atropine, but still renders this procedure inappropriate for patients with significant cardiac comorbidity (6,95).

In general, PR tends to provide a shorter duration of pain relief than MVD (4,6,110). Furthermore, these destructive techniques are also more likely to result in postoperative sensory

and motor deficits. That said, these procedures are minimally invasive, have a lower risk of catastrophic events, and are applicable to TN patients without vascular compression pathology. Additionally, PR may be performed many times over the course of a patient's life, and therefore, is an excellent option for MVD non-responders or early recurrence patients. However, scar-tissue formation at the foramen ovale does increase with each attempt, potentially making subsequent surgeries more challenging, therefore, care must be taken to minimize the number PR procedures performed on a patient and to maximize the interval between treatments. Anaesthesia dolorosa (also known as painful post-traumatic trigeminal neuropathy) is a serious complication of destructive TN surgical treatments in which numbness with overlying spontaneous pain occur in response to nerve deafferentation (1,105,111). This complication is exceedingly rare with percutaneous BC surgery, though, it has been reported after approximately 0.8% of RFT surgeries (105,111). All in all, PR procedures are a viable treatment option for medically-refractory TN patients.

1.5.2.2.2 Stereotactic Radiosurgery:

SRS is a minimally invasive surgical intervention using a 3-dimentional coordinate system to deliver radiation accurately to small targets throughout the body in a single treatment session. This technique was first conceptualized back in 1951 by the Swedish neurosurgeon Lars Leksell who treated one of his TN patients using a modified dental x-ray machine (112,113). Since then, technology has advanced significantly, and Gamma Knife Radiosurgery (GKRS), linear accelerator (LINAC) and CyberKnife Radiosurgery systems have been developed. Collectively known as SRS, each of the aforementioned systems delivers a single high-energy focused dose of gamma wavelength radiation to the designated target (i.e., CNV) (114). This is accomplished by hundreds of individual beams of radiation constructively interfering with

one another at target to amplify to the predetermined therapeutic threshold while remaining far below threshold in surrounding regions (4). Unlike PR methods, SRS usually targets a more proximal region of CNV (mid-cisternal segment) rather than the ganglion (112). Unlike PR and MVD, pain relief achieved through SRS is not immediate, and rather comes on following a postoperative delay which is on average 6-12 weeks (115). The rate of initial pain relief after the latency period is also lower for SRS than is observed with PR and MVD (75% pain free < 3-months after surgery), and durability of pain relief is less than MVD with 71%, 47%, and 27% of patients remaining pain free 1-, 5-, and 10-years postoperatively. Approximately 6% - 38% of patients experience postoperative dysaesthesia, which appears to be correlated positively with better pain outcomes (102,116). The mechanism of action of SRS is not understood, and the delayed-onset pain relief may argue against significant mechanistic overlap with other destructive approaches (i.e., PR). SRS is *completely* non-invasive, never requiring an insertion of any surgical instruments into the cranial cavity, though, the application of a stereotactic frame is required, representing an obstacle for some patients (117). All in all, SRS carries the lowest immediate surgical risk of any of the surgical procedures discussed.

Despite a few drawbacks of SRS compared to MVD and PR—notably delayed-onset pain relief, reduced initial rates of pain relief, and poorer durability of pain relief—SRS is an excellent surgical option for many patents. Given that this technique does not target NVC, idiopathic and secondary TN patients may also be candidates for this surgery. It is worthwhile pointing out that classical TN patients also achieve good pain relief with SRS, and some institutions offer both SRS and MVD as first-line surgical options for medically refractory classical TN patients (102). Additionally, this technique does not require general anaesthesia

making it ideal for patients with comorbid factors excluding them open-brain or PR procedures (4,112).

1.5.3 Selection of Surgical Treatments:

Approach to surgical treatment may vary between institutions, given that there is an absence of firm clinical guidelines governing surgical management of TN; thus, it is the responsibility of the treating physician to select the appropriate surgical option and timing for each particular patient (92,106). Generally speaking, MVD is the first-line surgical treatment offered to classical TN patients deemed fit for open brain surgery given that it produces the highest rates of initial pain relief and longest durability (4,106). Classical TN patients who are not medically fit for MVD will typically be offered SRS or PR instead, while idiopathic or secondary TN patients will be offered SRS or PR upfront. Classical TN patients who fail to respond to initial MVD or experience pain recurrence will not typically be offered repeat MVD unless, of course, inadequate vascular decompression was achieved with the first attempt (92). SRS radiosurgery is considered by some to be first line, and may be offered as an alternative to MVD initially even for patients with classical TN, though most institutions will reserve SRS for idiopathic or secondary TN patients, or those who have failed to respond to, or recurred following, MVD (102).

1.5.4 Assessment of TN Pain and Surgical Outcomes:

Accurately assessing the severity of TN is extremely important given that medications may be modified (e.g., escalation of dose, replacement with or addition of a different drug) or surgical treatments may be offered based on the patient's TN-related suffering (4,87,88,106). It is also important to accurately assess the medical and surgical treatment outcomes in both clinical and

research settings. A number of tools have been developed—not necessarily for TN specifically—to quantify the severity or burden of pain, which have become popular in TN research settings (117–119).

The visual analogue scale (VAS) pain score is a continuous measure of self-reported pain severity from 0-100 (**Figure 1.3**) (119). Patients are instructed to mark the severity of their pain on a 100mm long line that ranges from "no pain" (0mm) to the "worst pain imaginable" (100mm). While VAS has been validated across an array of patient demographics, this tool is influenced by patient literacy, education, and extreme age (e.g., children, elderly) (119,120). VAS being a continuous variable is advantageous in that arbitrary categorization cutoffs are not needed, however, special statistical considerations are still required given that pain scores may not be normally distributed in many pain conditions including TN (120). The Wong-Baker scale instead utilizes pictures of 6 distinct points arranged on a scale, each with a numerical score and simple descriptor (i.e., 8/10, "hurts whole lot") and a picture of a corresponding face (**Figure 1.4**)(118). Although this scale was initially developed for and validated in children, it has also been validated in adult populations relying more so on visual cues and for whom VAS may not be appropriate (118,121,122). Between-patient comparisons with either VAS or Wong-Baker may be challenging given that pain severity is highly personal (123). Additionally, both VAS and Wong-Baker define an upper limit which is a problem for those patients in whom the "worst pain imaginable" actually gets worse at a subsequent timepoint—exactly how to reconcile this scenario is not straightforward.

The Barrow Neurological Institute (BNI) pain intensity score was specifically developed to assess pain severity in TN patients undergoing surgical treatment (**Table 1.5**) (117). This scale considers medication use in addition to subjective descriptors of pain severity when quantifying

TN burden. The scale ranges from 1 (no pain, no medication required) to 5 (severe pain or no pain relief with medication), and mitigates many of the pitfalls of VAS and Wong-Baker outlined previously, and so is used in many TN research settings. It must be noted, however, that the BNI score prioritizes medication reduction over pain relief (2 vs. 3 in **Table 1.5**) and it is not clear exactly why this distinction has been made (117).

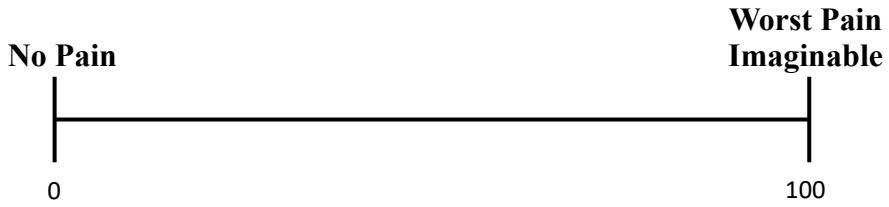

Figure 1.3: Visual analogue scale (VAS). The subject will mark their pain severity on this 100mm long straight line ranging from 0mm ("no pain") to 100mm ("worst pain imaginable"). The distance from 0mm to the patient's mark is measured as their VAS score.

Figure 1.4: Wong-Baker faces pain scale (118)**.** Pain severity is represented by 6 categorical measures ranging from "no hurt" to "hurts worst". The subject will select the face best representing their pain severity. Verbal descriptor for each category may also be read to the subject by the investigator.

Table 1.5: Barrow Neurological Institute Pain Intensity Score (117):

Score	Description
I	No pain, no medication
II	Occasional pain, not requiring medication
III	No pain, completely controlled with medication
IIIa	No pain, continued medication
IIIb	Persistent pain, controlled with medication
IV	Some pain, not adequately controlled with medication
V	Severe pain or no pain relief

1.5.5 Clinical Predictors of Surgical Outcomes:

Over the past century, there has been a large focus on the identification of clinical variables that predict treatment outcomes in patients with TN (11). One of oldest observations is that patients with 'atypical' pain character are more difficult to manage and are less likely to respond to treatment (5,11,124). Female sex is also a negative prognostic factor for MVD, as well as being younger and having TN for a shorter period of time at diagnosis (45,125). Less severe NVC of CNV (or absence) identified at the time of surgery or using preoperative MRI is another negative prognostic factor for MVD (124,125). Additional CNV specific factors that may be detected using preoperative MRI (discussed in detail in later sections) also provide prognostic utility. Predictive scales have been developed using combinations of the prognostic factors outlined above. *Hardaway et al.*'s predictive score assigns points based on TN type, vessel features, and NVC severity (126). Similarly, *Pancykowski et al.*'s predictive score assigns points based on TN type, medication response, and NVC severity (127). Both scoring systems have been validated in TN patients undergoing MVD surgery, though, *Pancykowski et*

al. was shown to be superior in one comparative study (128). It is worthwhile noting that both scales wane in their predictive ability for surgical outcome beyond one year, and the precise influence of different clinical characteristics on durable pain relief remains a matter of debate. One of the motivations for the work in this thesis is the need for more a precise explanation for variability in surgical outcome for TN, ideally based on more objective measures such as neuroimaging.

1.6 Neuroimaging:

In recent decades, non-invasive MRI investigations of CNV and other brain structures in patients with TN have largely replaced post-mortem histological approaches (51,52). The following sections will discuss: 1) general principles of MRI; 2) techniques of MRI acquisition; and 3) image processing and analysis.

1.6.1 General Principles of MRI

MRI exploits magnetic resonance properties of tissue to non-invasively produce accurate and detailed images of body structures of interest (129,130). Given hydrogen's abundance in organic lifeforms, it is by far the most common form of MRI used currently, and therefore, for the entirety of this thesis "MRI" refers to hydrogen-based MRI unless otherwise specified. Hydrogen atoms contain asymmetric charge distribution with a distinct positive and negative region. In the context of MRI, hydrogen atoms may be likened to miniature bar magnets. In the presence of a strong magnetic field—as is used in MRI—individual hydrogen atoms align in parallel (low energy) or antiparallel (high energy) orientations (**Figure 1.5**). A phenomenon

known as precession also occurs, in which hydrogen atoms wobble like a top at Larmor's frequency—dependent on atomic features of the sample and the strength of the surrounding magnetic field (130,131). The system is then energized through the temporary application of a radiofrequency (RF) pulse, forcing synergistic precession (i.e., in-phase) of the hydrogen atoms within the sample (130,132). The sample's synergistic precession produces a measurable alternating electric current as per the Faraday-Lenz law which is detected by a head coil. The magnitude of this electric signal decreases rapidly—order of milliseconds—as the sample de-phases and synergistic precession is lost (T2-decay). The system then slowly—order of seconds—falls back to a lower-energy equilibrium as energy is transferred to surrounding matter (T1-relaxation) (**Figure 1.6**).

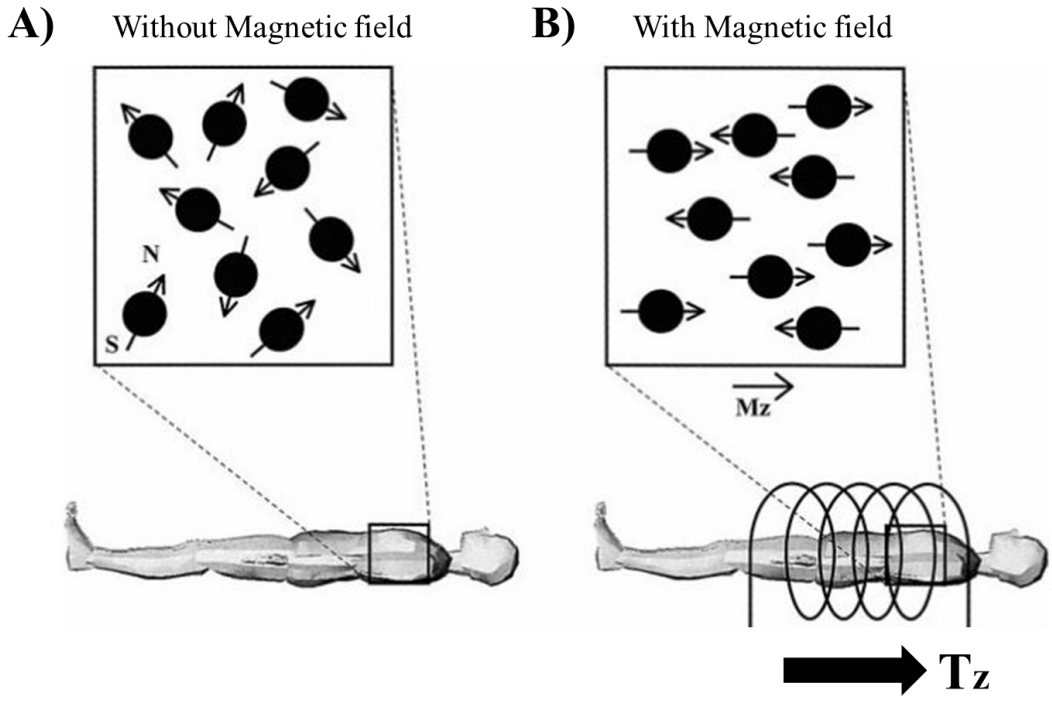

Figure 1.5: Orientation of magnetic moments. (**A**) Without a magnetic field the magnetic moments (arrow) of the nuclei (solid black circle) are distributed at random and thus the net magnetization factor is zero. (**B**) When there is a strong external magnetic field the spinning nuclei align parallel or antiparallel to the external field (Tz) with a few more parallel than antiparallel to produce a net magnetization vector parallel to the external magnetic field. This figure was reproduced from (133) with permission from Copyright Clearance Centre (License: 5460450841524).

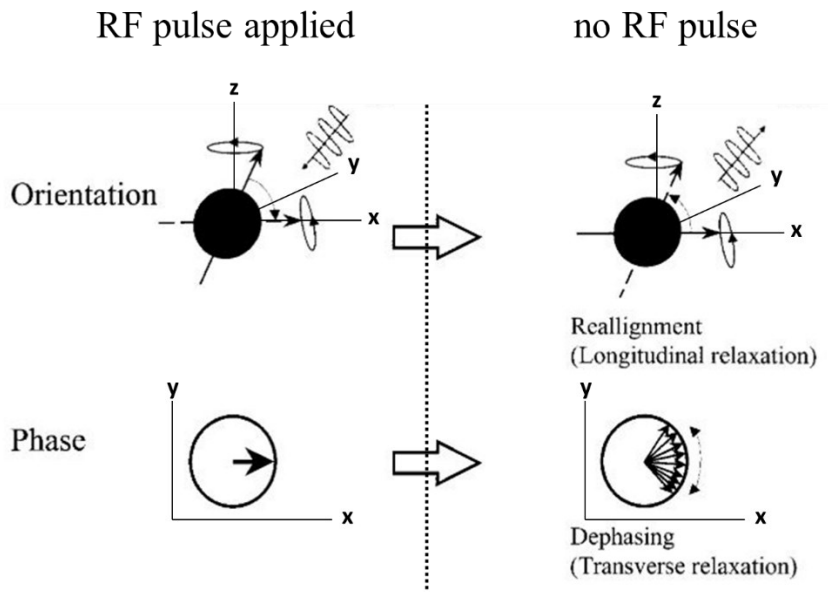

Figure 1.6: Longitudinal (T1) – and transverse (T2) -relaxation process. During relaxation, two processes exist: longitudinal relaxation and transverse relaxation. Longitudinal relaxation (**upper row**) is the realignment of the net magnetization to the external magnetic field. Transverse relaxation is the dephasing of the precessing spins (**lower row**). This figure was reproduced from (133) with permission from Copyright Clearance Centre (License: 5460450841524).

The amount of signal in an MR image depends on the timing of both T1-recovery and T2-decay (**Figure 1.7**). Furthermore, different RF pulse timing and combinations (i.e., pulse sequences) may be designed to maximize contrast between tissues of interest (130,132). Additionally, pulse sequences are designed such that a MR image may be T1- or T2-weighted—more dependent on T1 or T2 properties. A commonly used T1-weighted MR image uses a magnetization-prepared rapid acquired gradient echo (MPRAGE) pulse sequence (**Figure 1.8**) (130,134). MPRAGE images are three-dimensionally acquired and demonstrate very good grey-white matter contrast, making them ideal for anatomical or structural brain analysis (130,134). Another commonly used pulse sequence is Fluid-attenuated inversion recovery (FLAIR). These are designed specifically such that tissues of low interest (i.e., CSF) produce very little or no signal and may be combined with other pulse sequences (130,135).

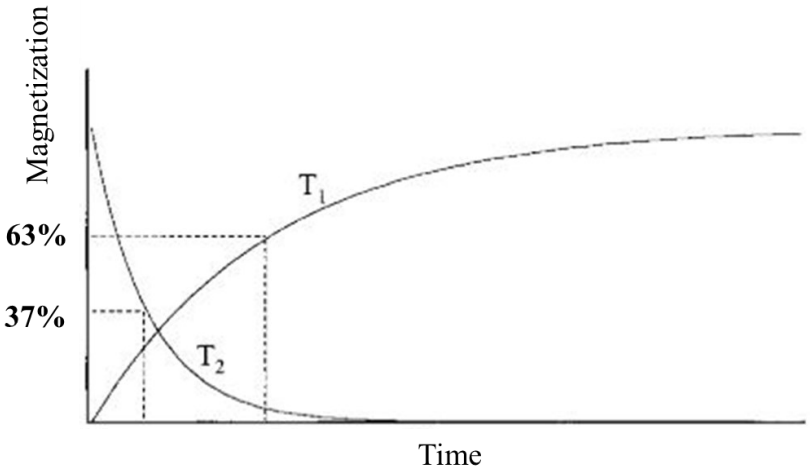

Figure 1.7: Graphical representation of T1- and T2-signal change with time. Longitudinal relaxation is characterized by the T1 relaxation time, which is the time to recover 63% of the original net magnetization vector. Transverse relaxation is characterized by the T2 time, which is the time it takes to decay the signal to 37% of the original signal. This figure was reproduced from (133) with permission from Copyright Clearance Centre (License: 5460450841524).

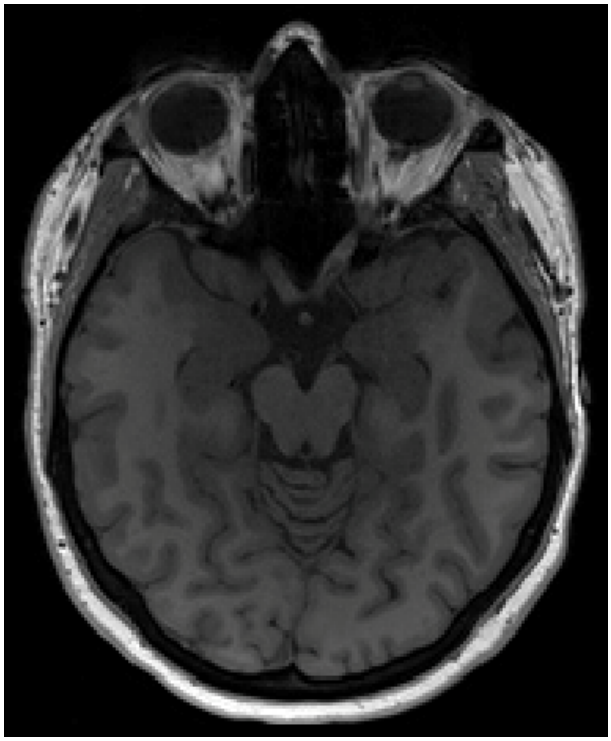

Figure 1.8: Magnetization-prepared rapid acquisition gradient echo (MPRAGE) image. This axial orientation MPRAGE image is T1-weighted and displays superb grey-white matter tissue contrast making it optimal for anatomical brain assessments and volume analysis.

1.6.2 Techniques of MRI acquisition

MRI is a powerful imaging tool that utilizes magnetic properties of hydrogen (typically components of water molecules) to produce signal in the form of electric current. Extensions of this basic MRI process have been developed permitting the analysis of more nuanced tissue properties including water diffusion or chemical composition. These will be discussed in the following section.

1.6.2.1 Diffusion Weighted Imaging:

Diffusion weighted imaging (DWI) is a type of MRI that generates tissue contrast as function of the amount of water diffusion (136–139). DWI pulse sequences can be quite complicated, as additional pulses are required to sensitize the system to motion of water molecules. Following the RF pulse, multiple different magnetic gradients are temporarily applied, each sensitizing the system to motion in a different direction and each producing its own diffusion image (137–139). A minimum of three gradient directions *d* must be used (i.e., d_1 = x-direction; d_2= y-direction; d_3 = z-direction) to accurately characterize the magnitude of water diffusion. Diffusion sensitive images will all be combined to form what is known as a trace image. Signal and contrast in trace images reflect T2*-weighting as well as water diffusion in all directions for which the system was sensitized (i.e., x, y, z) (130,136,139). Trace images may be divided by non-diffusion weighted T2* images (b_0) to remove all T2* contributions (137–140). This produces what is known as an apparent diffusion coefficient (ADC) map for which signal is completely dependent on motion (i.e., water diffusion) where brightness increases with diffusion (129,130,139). Unfortunately, DWI is cannot distinguish ‘types’ of motion (i.e., diffusion vs. head movement), and therefore, is extremely sensitive to any motion artifact (136–

139). DW images are particularly useful clinically to detect ischemic strokes and infarcts, as the resulting edema or inflammation is highly visible with this MR modality (137–139).

1.6.2.1.1 Diffusion Tensor Imaging:

Diffusion Tensor Imaging (DTI) is a more advanced application of DWI in which additional diffusion gradient directions (a minimum of 6) are applied (130,139,140). These additional diffusion gradient directions permit the calculation of three theoretical directional components of water diffusion known as Eigenvectors (ε_1, ε_2, ε_3) (139,140). The scalar component or magnitude of water diffusion of each Eigenvector are known as Eigenvalues (λ_1, λ_2, λ_3). Water diffusion that is equivalent in all directions ($\lambda_1 = \lambda_2 = \lambda_3$) is known as *isotropic* diffusion (139,141). However, this type of diffusion is rare in a biological system given that physical barriers within cells and tissues often restrict water diffusion in at least one direction ($\lambda_1 > \lambda_2 >/= \lambda_3$), resulting in what is known as *anisotropic* diffusion (139,141). In such cases, the direction of the largest magnitude of water diffusion is always defined as ε_1 by convention (also known as $D\parallel$). The magnitudes of perpendicular water diffusion components λ_2 and λ_3 (the average of which is known as $D\perp$) are by necessity lower in magnitude than the primary component (λ_1) (**Figure 1.9**). λ_1, λ_2, and λ_3 may be combined mathematically in different ways to describe various voxel specific characteristics of diffusion asymmetry (i.e., anisotropy) believed to have biological significance. These diffusion characteristics include: fractional anisotropy (FA—a measure of microstructural integrity of white matter); axial diffusivity (AD—maximal component of diffusion thought to be related to axonal health), radial diffusivity (RD—a measure of extracellular space and myelination extent); and mean diffusivity (MD—total water diffusion within voxel) (**Figure 1.10**) (139,140,142,143).

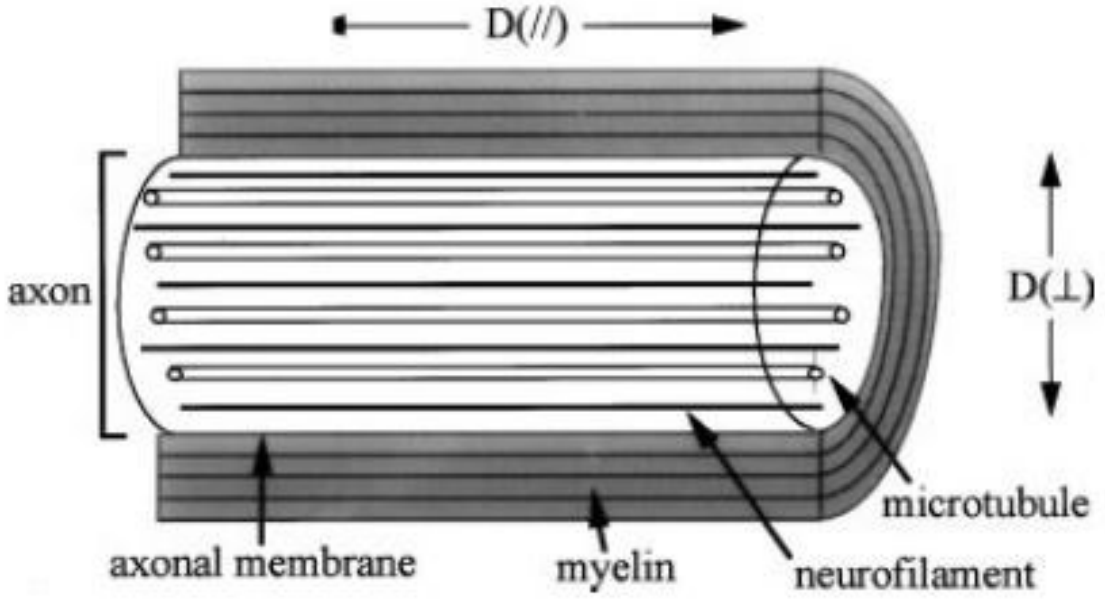

Figure 1.9: Simple Schematic longitudinal view of a myelinated axon and diffusion characteristics. Most superficially, multiple layers of myelin wrap the axonal membrane. Within the neuronal compartment of the axon fiber, microtubules and neurofilaments are oriented longitudinally in the direction of the axon fiber. The largest magnitude of diffusion (axial diffusivity) is in the parallel direction (**D(||)**), while minor components of diffusion (radial diffusivity, **D(⊥)**) are in the perpendicular direction. This figure was reproduced from (141) with permission from Copyright Clearance Centre (License: 5460470309878).

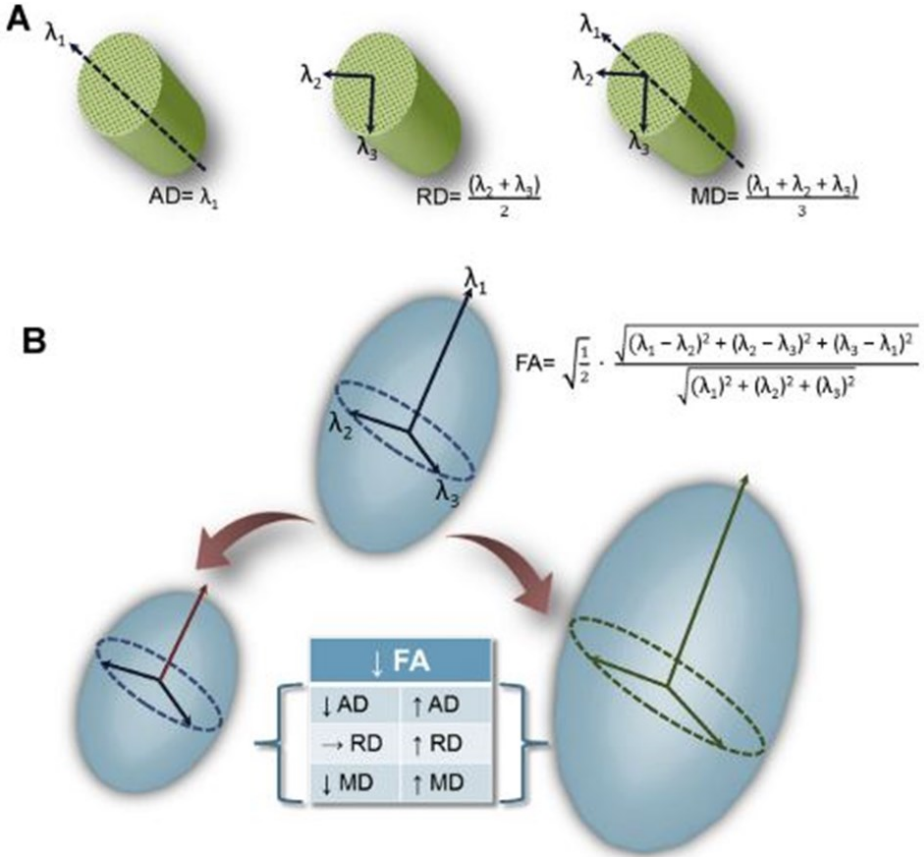

Figure 1.10: Schematic representation of diffusion tensor imaging (DTI)-derived metrics. Visual representations of the derivation of axial diffusivity (AD), radial diffusivity (RD), and mean diffusivity (MD) are displayed (**A**). 3-dimentional representation of fractional anisotropy (FA) is displayed reflecting changing AD, MD, and RD values (**B**). Note that FA change reflects the combination of λ_1, λ_2, and λ_3, and therefore, two systems with reduced FA (for example) may have different AD, RD, and MD. This figure was reproduced from (63) with permission from Copyright Clearance Centre (License: 5460460803848).

1.6.2.1.2 Tractography:

Although the general diffusion metrics provided by DTI (i.e., FA, MD, RD, AD) are useful in their own right, a unique computational opportunity also exists to characterize white matter

macrostructure. That is, relating the diffusion characteristics of one voxel to another (specifically anisotropy or FA) allows bundles of nerve fibers or tracts to be constructed; this technique is known as tractography (**Figure 1.11**) (139,140,144,145).

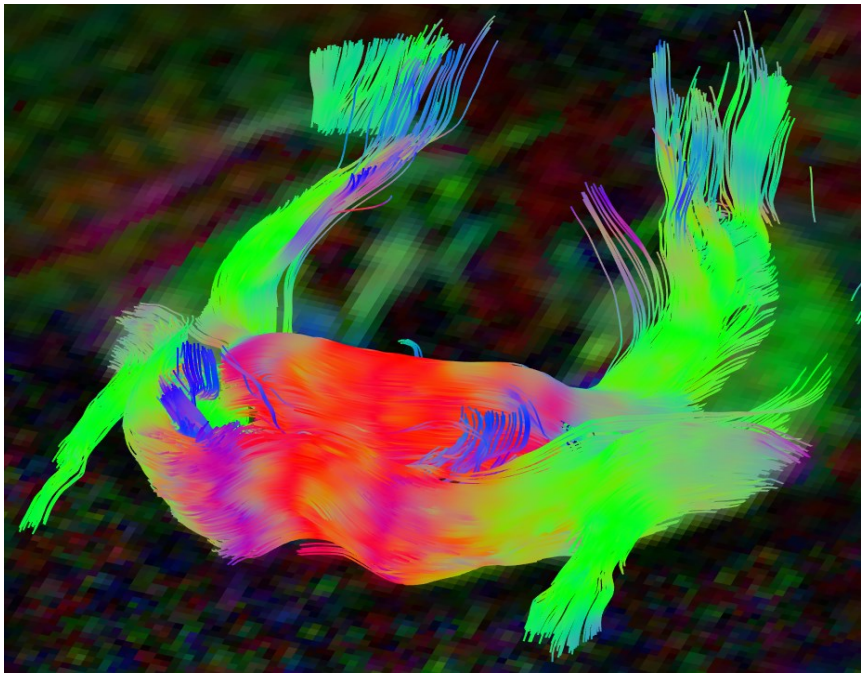

Figure 1.11: Trigeminal nerve and pontine tractography. Visualization of trigeminal nerve and pontine tractography in the oblique orientation allowing for the appreciation of individual streamlines modeling nerve and white mater trajectories. **Green**: anterior-posterior primary diffusion direction; **red**: left-right primary diffusion direction; **blue**: superior-inferior primary diffusion direction.

Different regions of the brain communicate with one another through white-matter connections made up of axon fibers. These fibers are long cylindrical neuronal extensions; thus, water diffusion in the direction parallel to these nerve fibers should be significantly less restricted than diffusion in the perpendicular direction (139,141,144). That is, λ_1 should be much greater than both λ_2 and λ_3 (i.e., large FA) because myelinated cell membranes of axon fibers are relatively impermeable to free diffusing water (47). As a result, the directionality of axon fibers

will be parallel to the direction of anisotropic water diffusion or ε_1 (139,140,144,145). Fiber tracts may be modelled by assuming that neighboring voxels with sufficiently large FA (typically > 0.2) and similar ε_1 orientations (typically < 20º offset) are part of the same white matter bundles.

The exact algorithms used to carry out tractography may be broadly categorized into two classes. *Deterministic tractography* breaks down individual directionality or streamlines of each voxel into a fixed or deterministic direction (139,146). Based on this fixed direction, a decision is made by the algorithm to include neighboring voxels in the same fiber track provided FA and minimum angle thresholds are met. The advantage of this approach is that it is computationally simple, is conducive to user input (e.g., minimum FA, ε_1 offset, streamline length), and generates biologically accurate tracks (146). However, due to deterministic tractography's simplicity, this technique is highly susceptible to false negatives (i.e, fiber track loss or drop out) in the presence of noisy data, motion artifact, or crossing fibers (140). *Probabilistic tractography,* on the other hand, generates a distribution of fiber orientations for each voxel, calculates all possible connections between adjacent locations, and then presents outcomes alongside statistical certainty measures (p-values). The benefit of this approach is that it can 'look past' neighbors, meaning that if a streamline is interrupted by crossing fibers or signal drop out, the fiber track will still continue through the poorly resolved area (146). The drawback of this technique is that it is computationally expensive given that every possible streamline is generated. Furthermore, while the fiber tracks that are generated are statistically the most likely, this does not mean that they actually exist; consequently, false positive errors are common with probabilistic approaches, and therefore, results may not be biologically relevant (136,140,146).

Regardless of whether deterministic or probabilistic tractography is used, brain-wide white matter connectivity may be calculated, from which specific white matter tracts of interest can be investigated thoroughly. Like basic DTI, tractography only requires 6 diffusion directions in order to be performed (139,140,146). However, the accuracy of raw diffusion information does increase substantially if a greater number of diffusion directions is used, although this improvement does not warrant additional scan time requirements in all cases (147). Increasing the number of diffusion directions also permits the use of more sophisticated tractography algorithms, and thus, most studies utilize at least 15 diffusion directions with some using upwards of 200 (146). All in all, tractography is an extremely useful technique to study brain white matter, and is also applicable to the study of large cranial nerves as well (139,148), which is the focus of chapter 3.

1.6.2.2 Magnetic Resonance Spectroscopy:

MRI may also be used to determine the absolute and relative concentration of specific metabolites in brain regions of interest through a process known as Magnetic Resonance Spectroscopy (MRS) (129,130). This technique operates on the same basic MR principles described in previous sections, except that MRS pulse sequences are specifically designed to sensitize the system to shifts in the local magnetic environment resulting from the covalent bond character of close-proximity molecular neighbors. Every hydrogen atom's Larmor frequency will vary depending on the chemical structure of the larger metabolite in which they are contained (130,149). Through this basic principle, metabolic structure may be determined by hydrogen 'chemical shift' signatures plotted on a spectra, and then further, metabolic concentration can be calculated based on the relative strength of this signal in relation to known constants such as water or creatine (**Figure 1.12**) (130,150,151). Two main forms of

spectroscopy exist in practice: single voxel spectroscopy and chemical shift imaging. As the name suggests, *single voxel spectroscopy* obtains metabolic spectra from a single voxel determined *a priori* (149). The benefit of this approach is that very high-quality spectra are produced, permitting more accurate metabolic characterization. However, given that spectral information is obtained from only a small volume of brain tissue, signal amplitude is quite small relative to surrounding noise. Thus, the theoretical advantage of this technique (large discriminatory power between metabolites with similar chemical shifts) may be counteracted in practice by low signal-to-noise ratio (SNR). *Chemical shift imaging*, on the other hand, simultaneously acquires spectral information from multiple voxels in a slab orientation (149).

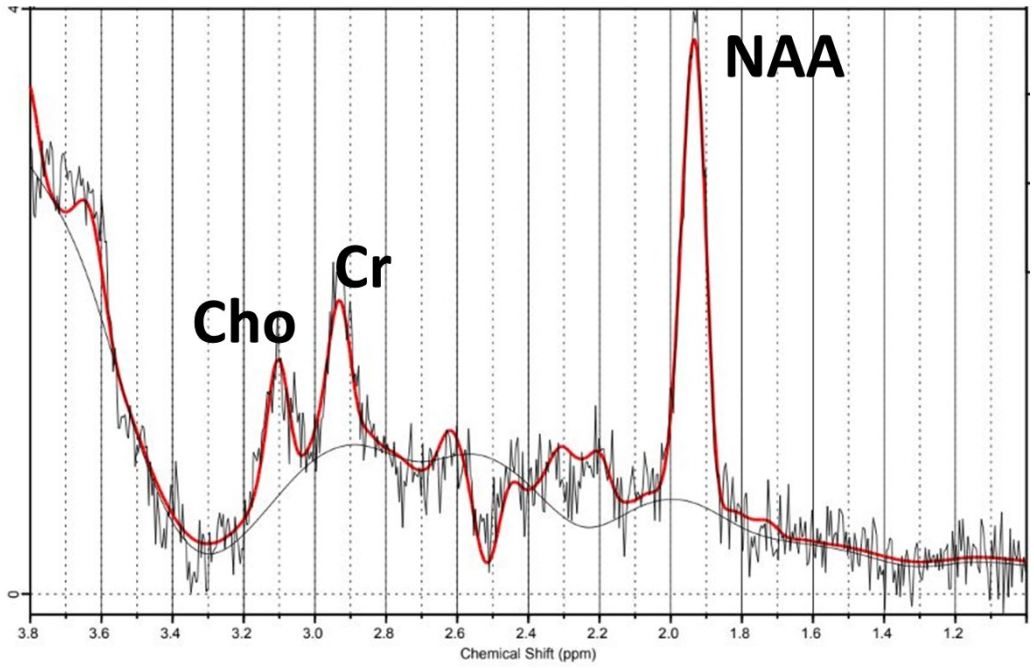

Figure 1.12: Magnetic resonance spectroscopy (MRS) spectra. Labeled MRS spectra from a thalamic region of interest obtained from a chemical shift imaging protocol. **Cho**: Choline; **Cr**: Creatine; **NAA**: N-acetylaspartate; **ppm**: frequency shift in parts per million.

The main advantage of this approach is that one may cover a larger spatial region—producing more signal—and then analyze desired voxel positions post hoc. However, because metabolic identification is dependent on frequency shifts, voxel position within the slab must be determined through phase shifts exclusively unlike in typical MRI. As a direct result, positional accuracy is limited, and voxel 'bleeding' and spatial heterogeneity occur (149).

MRS could in theory identify and describe any chemical compounds of interest (130,149). In practice however, pulse sequences are developed to prioritize key metabolites given their presumed clinical and biological relevance. N-acetylaspartate (NAA) is a compound synthesized in the mitochondria of neurons that is transported along axons (130,152). NAA is found exclusively in the nervous system, and is therefore thought to be a marker of axonal viability and density; decreases in NAA indicate neuronal loss and degradation (130,152). Choline (Cho) represents the sum of all choline and choline-containing compounds (e.g., phosphocholine). Given that choline-containing compounds are typically key components of cell membrane structure, Cho is believed to be a marker of cell membrane turnover, with increases reflecting cellular proliferation and inflammation (153). Glutamate is a key chemical in the brain given that it is the metabolic precursor for GABA, which the primary inhibitory neurotransmitter in an adult brain, and it also acts itself as one of the major brain excitatory neurotransmitters; thus, glutamate has been implicated in many brain disorders (154). Finally, creatine (Cr)-containing compounds include raw creatine and phosphocreatine which are key components of energetic systems and intracellular metabolism and which are well-distributed across the brain; thus, Cr concentrations tend to stay relatively constant throughout the brain (130,150,151).

Although absolute concentrations may be generated for any of the above metabolites, comparisons between people are difficult to interpret given that there is a lack of accepted normal concentration cutoffs. Instead, reporting relative concentrations—obtained by normalizing the concentration of the metabolite of interest to some internal measure that remains constant between people—is the typical practice. A suitable internal standard is Cr, and therefore studies commonly report NAA/Cr, Cho/Cr, or Glu/Cr ratios (150,151).

1.6.3 Approaches to Structural Brain MRI Analysis:

While advancement in MR neuroimaging depends on technical improvements at the level of data (image) collection (155), post-acquisition data processing and analytic techniques are also critically important for research applications of MRI in diseases such as TN. Quantitative brain structural MRI analysis is a focus of the work in this thesis, and a broad overview of relevant approaches is considered in this section, which is divided into techniques related to assessing *grey matter* versus those focused on analyzing *white matter*. Specific details related to individual methods used in each original study in the thesis are covered in the respective associated chapters (i.e., chapters 3-6).

1.6.3.1 Grey Matter:

Grey matter includes both subcortical structures (e.g., hippocampus, thalamus) and the cerebral cortex. Grey matter structural analysis commonly involves the comparison of subcortical structural volumes between populations of interest, which is the approach used in chapters 5 and 6 of this thesis. The calculation of subcortical volumes may be performed using *manual* (volumes generated by a human) or *automated* methods (volumes generated by a computer algorithm).

1.6.3.1.1 Manual Approaches:

The gold-standard of subcortical volumetric assessment is *manual volumetry*, also known as manual segmentation (156). Simply put, this method describes tracing a structure of interest by hand, permitting calculation of the structure's volume. Typically, structures of interest are made almost entirely of grey matter (e.g., thalamus, hippocampus, putamen, caudate nucleus, etc.), but in theory, any brain region can be defined as a structure of interest provided there is an agreed upon definition of its anatomical boundaries. Manual segmentation generated volumes for individual structures are generally very accurate, provided the person performing manual segmentation (often called the "tracer") possesses sufficient anatomical knowledge and employs a consistent approach (157). However, tracing larger or more complicated brain structures can sometimes require hours to perform for even a single structure, which limits the number of structures that can be considered in a given manual segmentation analysis (158). Additionally, unavoidable subjectivity is engrained in this technique given that numerous tracing decisions must be made (e.g., determining structure borders or addressing blurred regions) that may vary between tracers (i.e., inter-rater reliability), or may even vary between the same tracer during different segmentation sessions (i.e., intra-rater reliability) (157–159). Methods do exist to 'objectify' the process, such as employing intensity thresholds to determine inclusion versus exclusion of on-the-cusp border voxels, but in many instances the tracer is forced to rely on their own judgment, increasing the risk of inconsistency and bias.

Manual volumetry may also be used to determine the volume of the ribbon of grey matter on the surface of the cerebral cortex (160). While this approach is subject to many of the same challenges as those outlined for manual volumetry of subcortical structures, due to the

increased structural complexity and extensive folding of the cerebral cortex, cortical ribbon manual volumetry becomes even more labor intensive, and is rarely used in practice (160,161).

1.6.3.1.2 Automated Approaches:

The significant time investment and considerable anatomical knowledge required to perform manual volumetry accurately represent significant hurdles for many neuroimaging groups wanting to do volumetric assessments. Automated segmentation approaches using specialized neuroimaging algorithms circumvent these issues by minimizing the need for end-user input and decision-making, and as such, are becoming more common (157). While there exist several different automated segmentation algorithms implemented in different software packages, in general, these all follow a similar approach (162,163). Even though these packages do not require manual segmentation to be performed by the actual end-user, they do still rely on atlases of brain segmentations performed by expert tracers. As an example, the Montreal Neurological Institute 152 (MNI-152) is a reference atlas—and there are many others—that was created by manual segmentation and averaging together of 152 individual brain MRIs to generate a population-level brain MRI reference. To carry out automated segmentation, algorithms will take an input MRI scan for a subject of interest, and then non-linearly transform it (a process called spatial normalization or co-registration) into MNI-152 template space such that the input images near-perfectly overlap the reference atlas. This permits brain structural boundaries described on the MNI-152 template image to be overlaid onto the input image. Finally, the input image is then transformed back into its original space along with the MNI-152 brain structure boundaries deformed to match the original input image. Volumetric calculations of the brain structures of interest are performed using the MNI-152 template boundaries that have been transformed onto the input image (**Figure 1.13**) (163) . Similar approaches are used by

automated algorithms to determine the volume of cortical ribbon or cortical thickness of brain regions of interest (161).

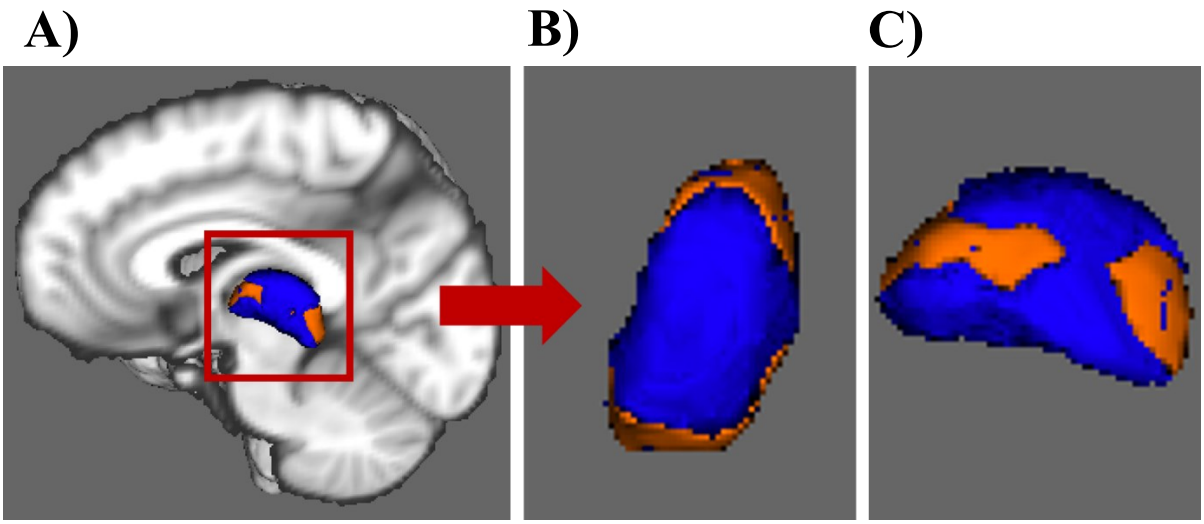

Figure 1.13: Automated segmentation and vertex analysis of the thalamus. Sagittal view of thalamus automated segmentation by FSL-FIRST toolbox overlaid on the MNI-152 template (**A**) (163). Dorsal (**B**) and sagittal (**C**) close-up views thalamus shape change vertex analysis extension of FSL-FIRST toolbox (164). **Orange**: regions of volume increase; **blue**: regions of volume decrease.

Despite automated volumetry avoiding many of manual segmentation's inherent issues (e.g., subjectivity, large time requirement, expert anatomical knowledge), the technique also has shortcomings (157). Unlike manual segmentation, in which slight errors or inconsistencies may occur, automated techniques may fail catastrophically, completely mistracing structures of interest. While the obvious nature of these extreme errors increases the likelihood of their discovery by visual inspection, instances where they go unnoticed may significantly sway the results of an analysis (156). Thus, extensive quality control must be performed by the user in all cases, including verification of the accuracy of MRI-template registrations and individual segmentations, requiring additional time and effort. Additionally, despite automated volumetry

appearing to be an objective alternative to manual segmentation, the user does have significant influence over the analysis in how they may set registration parameters and intensity thresholds for border voxels. Therefore, there is also a real risk of result bias with automated volumetry as well.

A potential advantage of automated methods is that dozens of brain regions of interest or thousands of study subjects may be segmented in a single analysis (156,157). Thus, automated volumetry permits exploratory assessments of volumetric alterations of brain regions previously unimplicated in diseased populations of interest, or may be used to increase the power of studies looking for subtle volumetric variations in a given structure since much larger sample sizes can be accommodated. That being said, blindly 'fishing' for volumetric differences across many brain regions without an *a priori* hypothesis may lead to statistical concerns as false-positives become increasingly likely (see 1.6.2.3 below). Nevertheless, automated volumetry use is becoming increasingly more common given that its benefits outweigh risks in many instances, though caution and a thorough understanding of the underlying anatomy are still recommended when utilizing this approach (157).

This thesis uses manual and automated volumetry approaches to study subcortical structures but did not include any manual or automated assessments of cortical ribbon volume or thickness.

1.6.3.1.3 Voxel-based approaches:

Rather than calculating and comparing the mean volume of a brain region between groups of interest (as is done with both manual and automated volumetry), individual voxels may be compared instead. As an extension of automated volumetry, deformation parameters used to

align subcortical structures of interest to the reference atlas may be compiled and then used to calculate shape differences in relevant brain structures between study groups; this is known as shape or vertex analysis (**Figure 1.13**) (164). Unlike volumetry where raw volume outputs are provided for brain regions of interest, this approach instead generates statistical maps describing the likelihood of directional shape differences between groups of interest for a given subcortical structure (164). This technique is more sensitive to subtle structural change than volumetry since sub-structural volume differences may be detected that could go unnoticed in whole-structure comparisons (i.e., concurrent enlargement and constriction within the same structure). Additionally, when used in conjunction with volumetry, shape analysis allows for sub-regions that may be driving group-level whole-volume differences to be characterized. It is also worthwhile noting that other voxel-based methods exist to perform whole-brain voxel-based between-group comparisons of brain grey and white matter, including voxel-based morphometry (VBM) (165,166) and tract-based spatial statistics (TBSS) (167,168). However, these other methods require large sample sizes and provide results that may be difficult to interpret biologically (168–170); thus, the decision was made not to use other voxel-based methods including VBM and TBSS in this thesis.

1.6.3.2 White Matter:

Similar to manual volumetry in grey matter analysis, white matter may be traced manually by an end-user (**Figure 1.13**). The end user may also define a region-of-interest (ROI) on DWI images within which average diffusion metrics can be calculated and white matter microstructure may be inferred (171). Similar to grey matter volumetry, this approach utilizes slice-by-slice tracing, and therefore is time consuming and susceptible to user bias. Another

option is to perform tractography between ROI endpoints that flank or pass through the structure of interest (148). This approach will only include in the algorithm voxels that are part of a calculated fiber tract while other voxels (that may still lie within the ROI) are eliminated; this technique may be more reflective of functional capacity and also less time-consuming (140). However, given that thresholding values used to determine which voxels are part of the fiber tract must be specified by the user, manual ROI selection augmented by tractography may still produce biased results (165).

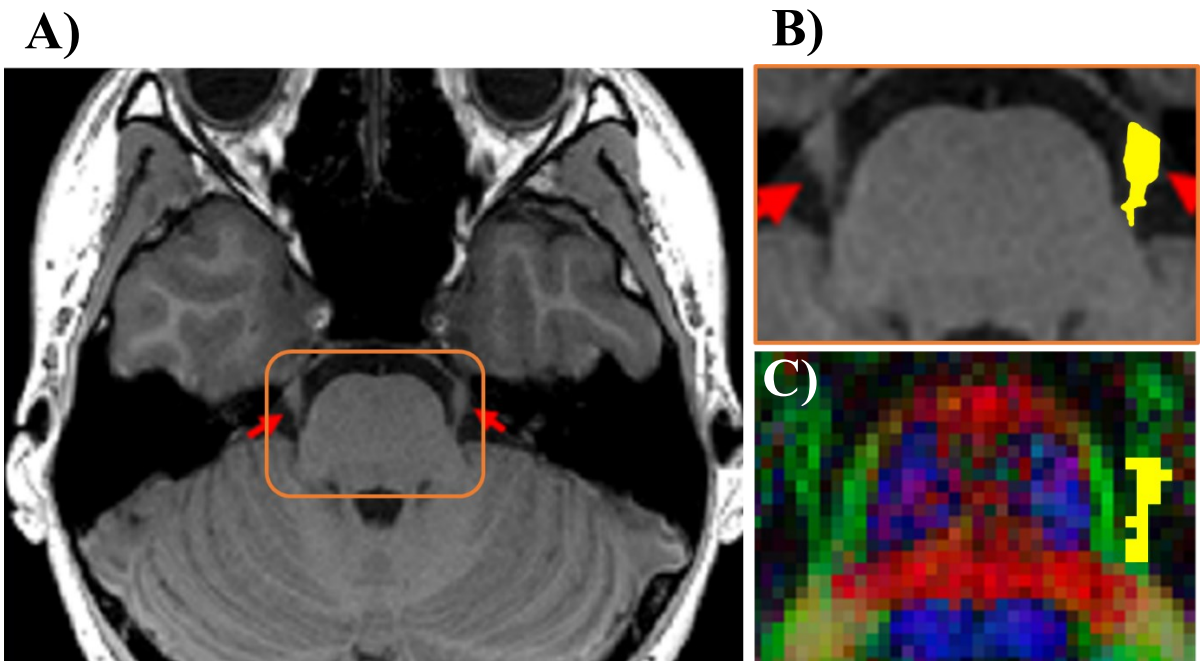

Figure 1.14: Manual segmentation of the trigeminal nerve (CNV). Axial view of a T1-weighted MR image indicating CNV with red arrows (**A**). Enlarged axial view of the brainstem (orange box in panel **A**) on T1-weighted image with the left CNV manually traced (**yellow**) for volumetric analysis (i.e., manual segmentation) (**B**). Enlarged axial view of the brainstem on diffusion tensor image (DTI) with the left CNV manually traced (**yellow**) for average diffusion metric calculation and microstructure analysis (**C**).

1.6.3.3 Statistical Considerations:

In general, a false-positive rate of 1/20 or 5% is considered acceptable for a single comparison of interest in research settings. The false-positive rate depends on the threshold of statistical significance or *alpha* (α) applied to the analysis. However, when the number of comparisons performed increases, so too does the likelihood of false positives increase proportionally—this is known as family-wise error rate (FWER) (172). For example, in an automated segmentation analysis of various brain structure volumes, if one was to evaluate 20 brain structures between groups of interest, then the FWER—chance of identifying at least one false positive—increases from 5% to 100% (172); thus, FWER must be corrected.

The simplest approach to correcting FWER is to adjust the threshold of statistical significance (α) to be more stringent, compensating for additional comparisons. Bonferroni's correction describes increasing the threshold of statistical significance proportionally to match the total number of independent comparisons: for example, if 100 comparisons are performed, then α = 0.05/100 or 0.0005 (172). However, Bonferroni's correction becomes too strict in instances when a large number of comparisons are performed such that true differences will not be identified (i.e, increasing type II error). Additionally, Bonferroni's correction should only be used to correct for independent or unrelated comparisons (172), which may not be the case if brain structures of interest are related functionally or structurally. False-discovery rate (FDR) is a more conservative statistical approach that may also be employed to deal with excess false-positives. However, unlike Bonferroni's method which adjusts α to maintain a p-value of 0.05 (5% chance of a false-positive occurring), instead with FDR α is adjusted such that a q-value of 0.05 is maintained (5% of positive tests observed are actually false) (173). Cluster-based thresholding is another approach to mitigate the statistical challenges of automated quantitative

MRI methods in which larger clusters are considered more likely to be true positives given that noise (i.e., false positives) should be dispersed randomly throughout the image (155,174). However, given that this thesis utilized a hypothesis driven approach yielding only a small number of comparisons

1.6.4 Neuroimaging in TN:

1.6.4.1 CNV Imaging:

As discussed in previous sections, the theory of neurovascular compression (NVC) states that classical TN is linked to physical compression of CNV by a blood vessel (4,42). More specifically, compression occurring at the location where the nerve first exits the pons (i.e., REZ) may be related to increased risk of demyelination since the REZ is a watershed area between centrally- and peripherally-mediated myelination (4,43–45,47–49). Demyelination, dysmyelination, and neuron loss is observed histologically at sites of vascular compression in patients with TN (51,52). Given the potential pathophysiologic involvement of CNV in the development and maintenance of TN, *in situ* MRI evaluation of this structure has been carried out in a number of studies, which focus both on summary volumetric measures of CNV, as well as microstructural nerve features.

1.6.4.1.1 CNV Size:

Atrophy of CNV in TN patients at sites of vascular compression have been noted since the earliest open cranial surgeries were performed to treat TN (37). Nearly a century later, this volume reduction has now been attributed primarily to myelin change and neuron loss (51,52). It has been observed with MRI that volume and cross-sectional area (CSA) of the affected CNV—that is, ipsilateral to the painful side of the face—are reduced when compared to the

unaffected nerve or healthy controls (56,175–179). Furthermore, the volume of the contralateral nerve is no different than healthy controls (56,175–179). The degree of atrophy is positively correlated with the severity of vascular compression, aligning with histological observations and the ignition hypothesis (51,52,66,67,175,179). As mentioned in section 1.5.2.1, MVD aims to alleviate TN pain by targeting NVC directly, with the goal of restoring normal CNV anatomy. In general, better MVD outcome is associated with more severe NVC prior to surgery (175,179). It must be noted, however, that some concerns exist regarding the reliability of MRI to accurately characterize the extent of NVC preoperatively, and assessing nerve volume may be rendered more challenging in the presence of a nearby vessel (180). Available data suggest that outcome after MVD is related to CNV volume in that ipsilateral nerve atrophy is typically associated with a better prognosis (175,176,179), however, there is also a study reporting the opposite relationship (176).

The relationship between surgical outcome of destructive procedures such as PR and SRS and CNV volume is less clear cut (56,181,182). In contrast to MVD, greater nerve atrophy appears to be a predictor of poorer SRS outcomes, though this may be the result of surgical limitations as smaller volume nerves seem to receive disproportionately lower radiation doses (178,183). Additionally, one study evaluating outcomes of RF surgery found no preoperative CNV volume difference between responders and non-responders (184) .

1.6.4.1.2 Diffusion MRI studies of CNV in TN

NVC in classical TN appears to affect CNV through demyelination, dysmyelination, and neuron loss, which in turn leads to hyperactivity and severe pain (51,52). Studies of nerve microstructure conventionally require nerve specimens and histologic wet lab techniques; thus, non-invasive alternative approaches to investigate CNV microstructure in *situ* are of particular

interest. DTI is one such technique that may be used to infer nerve microstructure based on water diffusion restriction. DTI studies of TN are plentiful, and primarily focus on the REZ because of the strong implications of this region in TN pathophysiology.

The most widely examined DTI measure in white matter imaging is FA, in which higher values are considered to be consistent with greater axon microstructural integrity. REZ FA is consistently reduced in the ipsilateral affected CNV compared to the contralateral unaffected CNV and compared to CNV in healthy controls (53–55,57–62,64,86,185,186). MD is also consistently increased in the ipsilateral REZ of TN patients, while abnormalities in AD and RD are identified less reliably (53–55,57–62,64,86,185,186). This reproducible DTI signature of increased FA and decreased MD (and potentially increased AD and RD) is consistent with demyelination and axon loss, and thus, appears to align with histological observations of CNV at the site of NVC. It is worthwhile noting, however, that other microstructural changes to CNV (i.e., edema) may produce a similar diffusion signature. Interestingly, DTI studies have also shown that CNV microstructure appears unaffected at the site of incidental NVC in asymptomatic subjects who do not have TN, suggesting some additional nerve pathology is likely present in TN (55,75). It must be noted, however, that huge variation exists in the quality of acquired DTI scans across studies, as different scanners, head coils and imaging protocols have been used.

Unlike crude measures such as nerve volume and CSA, which appear to relate to surgical outcome, CNV DTI does not reliably correlate with clinical measures or surgical outcome, and results between studies are often conflicting. Only one study to date has reported preoperative CNV diffusivity differences between responders and non-responders to MVD (187). Chen *et al*. observed that while raw CNV diffusivity did not differ between surgical outcome groups,

the percentage difference between ipsilateral and contralateral CNV FA is larger in non-responders (specifically Burchiel TN type 2) (187). Another study found that non-responders to RF surgery preoperatively displayed a larger spread of CNV diffusion metric values, though, raw diffusion metrics also did not differ between surgical response groups (188). No other studies have reported preoperative CNV diffusivity differences between responders and non-responders to surgical treatment for TN (62,184,189–191). Preoperative pain severity does not appear to reliably correlate with CNV diffusion (190,192), though return of CNV diffusion measures to preoperative levels was associated with pain recurrence in a small group of TN patients (n=5) ~6-months following GKRS (191). This same study also found that successful GKRS appeared to reduce CNV FA 6-months postoperatively (191). Another study observed that greater reductions in 6-month postoperative CNV FA was associated with longer-term pain relief following GKRS (189). These findings are not surprising though, considering destructive techniques are thought to induce pain relief by causing local nerve damage (described previously) which should be reflected by a reduction in FA. An opposite relationship was later shown in which CNV diffusion appeared to normalize in surgical responders but not non-responders (62). However, responder and non-responder groups may have been unsuitable for direct comparison given that they were composed of patients primarily undergoing restorative (MVD) versus destructive (GKRS) surgical treatments (62). Interestingly, another study reported that CNV AD and RD normalize (decrease) following RF surgery in responders—in alignment with MVD reports—even though RF is a destructive procedure (184). All in all, reports of CNV diffusivity in relation to clinical measures or surgical outcome have, to date, been inconsistent.

The more or less consistent finding of decreased CNV REZ FA, and increased MD, AD, and RD, suggest that DTI may reproduce histological findings of demyelination and axon loss in TN (51,52). However, the vast majority of studies utilizing nerve DTI in TN make use of lower-resolution whole-brain DTI protocols with large voxel volumes of 2x2x2=8 mm^3 (54,184,186) or 1.9x1.9x3=10.8 mm^3 (63,86,189,193) that are as such, more likely to blur together the diffusion information from CNV with surrounding CSF (194). In fact, two studies utilizing higher-resolution DTI protocols (1.6x1.6x1.2 mm^3 and 1.6x1.6x2.0 mm^3) found that, in contrast to the findings of the rest of the field, ipsilateral FA and MD are not abnormal compared to the contralateral nerve or heathy controls (57,59). Furthermore, the compressive blood vessel(s) itself could be influencing measures of nerve diffusion also. Thus, one must consider the possibility that methodological factors related to DTI acquisition could be influencing nerve DTI results in TN.

Recent investigations have begun evaluating more proximal locations along the trigeminal pathway using DTI, in particular, within the brainstem where CNV axons travel before synapsing in trigeminal nuclei. Indeed, this is a logical next location to evaluate along the trigeminal pathway given that demyelinating MS plaques in this location are associated with TN (1). Brainstem lesions appear to be present in some classical TN patients as well, who may be less likely to respond to conventional surgical treatments (86). Even in classical TN patients in whom brainstem lesions are not visible, abnormal brainstem diffusion metrics have been observed and related to surgical outcomes, potentially implicating this region in classical TN as well (193). Specifically, these brainstem diffusivity abnormalities—like CNV—include reduced FA and increased MD, AD, and RD, suggesting pathological myelin change may be occurring at these sites (86,193).

1.6.4.2 Brain Imaging in TN:

Several grey and white matter brain structures have been implicated in chronic pain generally, and TN specifically. The more commonly appearing structural (grey volumetry or white matter connectivity) and functional abnormalities are typically observed in *somatosensory-salience* and *limbic systems*; these will be discussed in the following sections.

1.6.4.2.1 Somatosensory-Salience System Alterations:

Proceeding rostrally from CNV, the trigeminal sensory system next includes second-order neurons originating from brainstem nuclei. Disruption of these nuclei may contribute to the development of facial pain (1,86,193). Trigeminal brainstem nuclei project to third-order neurons in the contralateral VPM nucleus of the thalamus. Structural and functional alterations to the thalamus are consistently observed in patients with chronic pain (195), and the thalamus appears hyperactive at baseline compared to HCs in both TN and other pain conditions affecting the trigeminal system including migraine (196,197)**.** Interestingly, thalamus hyperactivity correlates positively with pain severity in TN, suggesting that increased sensory load from the face relayed through the thalamus may be a feature of the disease (197). Abnormalities in absolute thalamus volume, however, appear inconsistent across studies, as enlargement, reduction, and no change in volume have all been reported in TN, though, different volumetric methods were used between studies potentially influencing results (62,197,198). Metabolic abnormalities have also been observed in TN patients, with decreased contralateral thalamus NAA/Cr being consistently reported, indicating an association with reduced neuronal integrity (195,198–200). Third-order trigeminal afferents project from the thalamus up to the somatosensory cortex via the internal capsule. In TN patients, FA is reduced and MD is increased in the contralateral thalamus and along these internal capsule projections (201,202).

Facial regions of the primary somatosensory cortex—where trigeminal afferents ultimately terminate—are also enlarged in TN patients, and display increased functional activity that correlates positively with pain severity (62,202,203). Collectively, these findings add support to the notion that abnormalities in sensory-relay architecture along the trigeminal pathway from CNV up to the somatosensory cortex are indeed a robust feature in patients with TN.

Another key structure in the somatosensory-salience system is the insula. Rather than participating directly in the transmission or interpretation of sensory information, the insula instead plays a key role in higher-order functions such as salience and the redirection of attention and focus (204). Specifically, the right insula is involved in directing attention to painful stimuli, and as such has been shown to display increased functional activity in acute pain states (204–206), as well as reduced volume in patients with chronic pain conditions (62,207,208). Similarly in patients with TN, right insular activity is increased and volume is decreased (62,209). Following successful surgical treatment of osteoarthritis of the hip and TN, insular volume increase (or normalization) is observed, suggesting that abnormal insula structure may reflect a consequence rather than a cause of chronic pain and TN (210,211). However, it must also be noted that the insula is one of the more common locations for supratentorial lesions to occur in patients with TN secondary to MS, potentially suggesting that damage to this structure could also contribute to TN development or maintenance (81).

Unsurprisingly given the complementary functions of these structures in somatosensory-relay and salience, strong and direct connectivity between the thalamus and insula is well documented (212). Taken collectively, it appears most likely that the aforementioned findings reflect increased sensory load coming from, and therefore increased focus on, the painful region of the face in TN. It is, however, impossible to say with certainty at this point whether

somatosensory-relay and salience abnormalities are a predisposing cause or an effect of medically-refractory TN.

1.6.4.2.2 Limbic System Findings:

The limbic system defines a circuit of structures first described by Papez in 1937 that is responsible for learning, memory, and emotion (213). Since then, a strong interconnection between emotion/memory and the pain experience has been observed, and therefore evaluating limbic system structure and function in the context of chronic pain conditions and TN is logical (214–216).

The anterior cingulate cortex (ACC) is a central structure of the limbic system with extensive intra- and extra-limbic projections, which serves as a main limbic system hub (215). The ACC is critically involved in negative affect and cognition, and as such, plays a vital role in adaptive control which is a highly cognitive process that determines the optimal course of action when facing uncertainty or danger (215). Given its extensive connectivity, the ACC is well suited for this task, which figures prominently in pain perception. For example, the ACC is reciprocally connected to the right anterior insula, with which it coactivates during painful experience (204). Furthermore, the ACC receives raw incoming sensory information directly from the thalamus via the thalamo-cingulate tract facilitating rapid aversion response (213). It has been well established that ACC activity increases acutely during painful experience (216,217). Furthermore, ACC volume loss is observed in TN and other chronic pain conditions, which has subsequently been shown to normalize following successful surgical treatment for chronic hip pain (62,208,210,218). Interestingly, ACC functional connectivity to other limbic system structures differs between responders and non-responders to surgical treatment for TN preoperatively (219). Furthermore, the success of anterior cingulotomy in achieving pain relief

in patients with intractable pain conditions may suggest that ACC structural and functional abnormalities are actively involved in the generation and maintenance of chronic pain (220).

A key limbic system structure integrally involved in learning and memory is the hippocampus. Learning and memory appear to be involved in pain perception and recollection. For example, hippocampus structure (specifically, shape change) in patients with chronic low back pain is related to pain intensity and recollection accuracy, and furthermore, may be involved in memory triggers of acute pain in chronic pain patients (214,221). Exactly how the process of memory and learning influence pain remains elusive, though, animal model studies strongly suggest hippocampal neurogenesis plays a causal role in pain persistence and severity (222). Furthermore, the hippocampus appears to be one of the most common supratentorial lesion locations in patients with TN secondary to MS, strengthening the notion that the hippocampus may be implicated in TN of all types (81). Though one study observed a hippocampal volume reduction in TN (223), this finding has not yet been widely reproduced. Another important limbic system structure in close proximity to, and sharing strong bi-directional connectivity with the hippocampus is the amygdala, which is primarily involved in fear and anxiety responses (213). Volume reduction in the amygdala has also been observed in TN (207). The amygdala displays increased activity and functional connectivity at baseline in patients with TN, which appears to correlate positively with duration of illness, and may resolve following successful surgical treatment (207).

Interestingly, general limbic system modifications have been observed to occur over time in patients with chronic low back pain (216). Specifically, it was shown that as patients transition from acute to more-difficult-to-treat chronic back pain, there is also a transition from primarily somatosensory-salience to limbic system abnormalities (216). Furthermore, TN patients who

do not respond to surgical treatment display altered preoperative limbic system functional connectivity that also correlates with duration of TN diagnosis (219). These findings raise the intriguing possibility that perhaps time-dependent limbic system changes occur that may lead to surgical treatment resistance. Applying this logic to TN specifically, perhaps surgical intervention must be performed before potentially prohibitive limbic system modifications occur, and furthermore, limbic system modifications identified using MRI before surgery may be used to predict surgical outcome.

CHAPTER 2: Rationale, Specific Aims, and Hypotheses

The overarching purpose of the work presented in this thesis is to improve our understanding of TN and its resistance to surgical treatment in some patients. Broadly, retrospective and prospective MRI-based investigations were performed to assess specific features of CNV structure/microstructure, brain structure, and brain metabolism before and after TN surgery. Responders and non-responders were identified through longitudinal assessment, permitting direct comparison of pre- and postoperative imaging features between surgical outcome groups.

The specific aims of this thesis were:

1. To develop a novel nerve-specific imaging protocol permitting more accurate characterization of CNV microstructure in TN
2. To identify preoperative structural and metabolic CNV and brain abnormalities in TN patients, and characterize alterations of these features occurring longitudinally following surgical treatment
3. To examine the differences between *responders* and *non-responders* to surgical treatment for TN using identified imaging-based CNV and brain features

Study-by-study rationale, aim, and hypothesis are as follows:

Study 1 (Chapter 3): High Spatial-resolution Nerve-specific DTI Protocol Outperforms Whole-brain DTI For Imaging the Trigeminal Nerve in Healthy Individuals

Rationale/Aim: TN is associated with microstructural changes in CNV identified using DTI. Studies of DTI measures of axonal microstructure appear to confirm CNV demyelination in

TN, but also show that DTI metrics in CNV have an uncertain relationship with surgical outcome. These previous studies all utilize lower-resolution protocols that are susceptible to errors from partial volume effects, particularly due to adjacent CSF, which may result in inaccurate nerve microstructure calculations. The purpose of this study was to develop a nerve-specific DTI protocol in healthy subjects that provides more accurate assessment of CNV microstructure than lower-resolution whole-brain protocols that have been used previously.

Hypothesis: Development of a nerve-specific DTI protocol with improved resolution and addition of fluid attenuation will provide superior delineation and improve the accuracy of microstructural characterization of CNV. More accurate characterization of CNV microstructure in TN may better help to understand and predict surgical outcome.

Study 2 (Chapter 4): Trigeminal Nerve Diffusion in Patients Undergoing Surgical Treatment for Trigeminal Neuralgia

Rationale/Aim: Building on study 1, our primary objective was to use our newly developed, nerve-specific DTI protocol to replicate previous CNV DTI findings in TN patients and healthy control subjects, and then to compare pre and early postoperative (1-day, 1-week, 1-month) CNV diffusivity metrics between responders and non-responders to surgical treatment for TN.

Hypothesis: Pre and early postoperative differences in CNV diffusivity metrics exist between responders and non-responders to surgical treatment for TN.

Study 3 (Chapter 5): The Thalamus in Trigeminal Neuralgia: Structural and Metabolic Abnormalities, and Influence on Surgical Response

Rationale/Aim: Despite abnormal CNV structure and function being a characteristic feature of TN (especially classical TN), CNV microstructure may not explain the entire variance of outcome after surgical treatment. More proximal locations along the trigeminal pathway—such as the brainstem and primary sensory cortex (as summarized in 1.6.3.2.1)—are also abnormal in TN and may influence surgical response. The thalamus is another key component of the trigeminal pathway involved in relaying afferent facial pain information; however, the role of the thalamus in TN and its influence on durability of pain relief after TN surgery have been understudied. The purpose of this study was to investigate the role of the thalamus in TN by evaluating its pre and postoperative structure and metabolism, and then further relating these features to the outcome of surgical treatment for TN.

Hypothesis: TN patients display structural and metabolic abnormalities in the thalamus which are associated with surgical outcome in TN.

Study 4 (Chapter 6): Hippocampal and Trigeminal Nerve Volume Predict Outcome of Surgical Treatment for Trigeminal Neuralgia

Rationale/Aim: Limbic system alterations have been observed as patients transition from acute to more-difficult-to-treat chronic pain states. It is not yet well-known whether limbic system modifications also occur in TN patients rendering them more difficult to treat surgically. Our primary objective in this study was to perform a preoperative volumetric analysis of limbic system structures—with specific focus on the hippocampus and amygdala—as well as CNV,

in a large cohort of TN patients undergoing MVD. Preoperative limbic structural and CNV volumes were compared between responders and non-responders.

Hypothesis: TN patients who do not respond adequately to surgical treatment can be distinguished preoperatively using neuroanatomical features, specifically the volume of CNV and limbic system structures.

CHAPTER 3: High Spatial-resolution Nerve-specific DTI Protocol Outperforms Whole-brain DTI For Imaging the Trigeminal Nerve in Healthy Individuals

Modified with permission from (224): Danyluk H, Sankar T, Beaulieu C. High spatial resolution nerve-specific DTI protocol outperforms whole-brain DTI protocol for imaging the trigeminal nerve in healthy individuals. NMR Biomed. 2021;34(2):e4427.

3.1 Introduction:

DTI is widely used for the identification of brain white matter tracts via tractography and permits indirect assessment of axon/myelin micro-structure using quantitative diffusion parameters. Nerves (cranial or peripheral) also have a high degree of anisotropic water diffusion; thus, DTI may provide similar insights in various cranial nerve pathologies and assist neurosurgical guidance (148,225). For example, DTI has shown reduced FA and increased MD in the REZ of CNV in patients with TN (54,61,63,86,186), which is often associated with NVC of the REZ of CNV or multiple sclerosis (1,76,104), though some discrepancy exists as studies have also shown FA and MD of CNV to be normal in TN (57,59). However, DTI of cranial nerves is challenging due to their location near bone/air interfaces which can cause susceptibility-induced image distortions, their small size (2.7 mm diameter for CNV (175)) which limits delineation, and their immediate surroundings of isotropic, rapidly diffusing CSF which may cause inaccuracies in nerve diffusion parameter quantitation because of partial volume effects.

Many previous nerve DTI studies of CNV in TN have employed low-resolution "whole-brain" acquisition protocols with thick slices of 2 mm or greater, yielding large voxel volumes of 2x2x2=8 mm^3 (54,184,186) or 1.9x1.9x3=10.8 mm^3 (63,86,189,193) relative to a

comparatively small structure. The resulting partial volume effect with adjacent CSF will reduce FA and elevate MD erroneously. For example, MD values in the unaffected CNV of TN patients have ranged from 1.2–4.3x10^{-3} mm^2/s (54,57,58,63,184,186,189,193), which is 1.5-5x that expected of adult white matter (~0.8x10^{-3} mm^2/s). However, effects of partial volume and CSF contamination may be reduced by improving spatial-resolution. As such, higher spatial-resolutions have been used for imaging/tracking CNV either through the utilization of thinner slices such as 1.2 mm (x1.6x1.6 mm^2 in-plane) (59) or isotropic voxels (1.25x1.25x1.25 mm^3) (226). Additionally, CSF contamination may be reduced by eliminating fluid signal through the use of FLAIR in combination with DTI (227). FLAIR-DTI has demonstrated improved tracking and quantitative diffusion parameter estimation for small white matter tracts bathed in CSF such as the fornix and the optic nerve (228,229). CSF suppression has previously been used in DTI of CNV, though the advantages of FLAIR were not evaluated and low spatial resolution was used (1.9x1.9x3 = 10.8 mm^3) (61). Further, CNV MD was found to be quite high in healthy controls at 1.7x10^{-3} mm^2/s (61), suggesting resolution improvements are also needed to mitigate persistent partial volume effects.

The purpose of this study was to develop two high-resolution isotropic DTI protocols (1.2x1.2x1.2 = 1.7 mm^3 — 4-7x smaller voxel-size than most previous work in this field) with and without FLAIR CSF suppression to image the proximal section of the human CNV (includes the REZ). Slice coverage was limited in these nerve-specific protocols to enable averaging to enhance signal-to-noise ratio while keeping a reasonable scan-time at 3T. Using healthy young adults, these nerve-specific DTI protocols were compared with two common whole-brain DTI protocols (2 and 3mm thick slices) to determine which approach provides superior delineation of CNV and most accurate nerve diffusion parameter quantification.

3.2 Methods:

3.2.1 Subjects:

This prospective study was approved by our institutional human ethics review board. Written informed consent was obtained by all five healthy subjects (age and sex of participants = 24F, 45F, 22M, 24M, 26M), who had no history of underlying neurological, psychiatric, or chronic pain conditions.

3.2.2 Imaging Protocol:

A 3T Siemens Prisma MRI (Erlangen, Germany) was used with a 64-channel head radiofrequency coil to perform a 22-minute acquisition including a 3D T1-weighted structural (magnetization-prepared rapid acquisition gradient echo), two nerve-specific DTI, and two whole-brain DTI scans. One key point is that the nerve-specific axial-oblique DTI scans were aligned on the 3D T1-weighted structural scan (FOV = 250 x 250 mm^2, 208 slices, 0.85 mm isotropic, TR = 1800 ms, TE = 2.37 ms, TI = 900 ms, 8° flip angle, 3:41 min) along the same plane as CNV (with left-right and anterior-posterior tilt if necessary) to encompass both left and right CNV in the same slice (**Figure 3.1**). This allowed for better visualization of the cisternal region of the nerve while also reducing the number of thin 1.2 mm thick slices to 13, but still maintaining adequate coverage of both left and right nerves with minimized scan-time. Four DTI protocols **(Table 3.1** for details**)** were acquired for every subject: *(i)* **NS**: nerve-specific axial-slab with 13 slices, 182 x 182 acquisition matrix, 1.2 mm isotropic, b_{1000} 20 directions x 3 averages, 10 b_0, anterior-posterior (AP) phase-encode direction, 3:41 min scan; *(ii)* **NS-FL**: nerve-specific axial-slab FLAIR with 13 slices, 182 x 182 acquisition matrix, 1.2

mm isotropic, b_{1000} 20 directions x 5 averages (2 more averages to make up for signal-to-noise ratio loss with FLAIR), 10 b_0, inversion time 2300 ms, AP phase-encode direction, 7:22 min scan; *(iii)* **WBi** (54): whole-brain 2 mm isotropic with 70 axial slices, 122 x 122 acquisition matrix, b_{1000} 30 directions x 1 average, 6 b_0, AP phase-encode direction, 2:29 min scan; and *(iv)* **WBa** (63,230): whole-brain anisotropic 3 mm slice with 50 axial slices (1.9x1.9 mm^2 in-plane), 128 x 128 acquisition matrix, b_{1000} 64 directions x 1 average, 5 b_0, AP phase-encode direction, 3:43 min scan. All four DTI protocols used parallel imaging with GRAPPA R = 2, phase partial Fourier = 6/8, and were interpolated with zero-filling (x2) on the scanner to yield reconstructed images with half the in-axial-plane voxel dimensions.

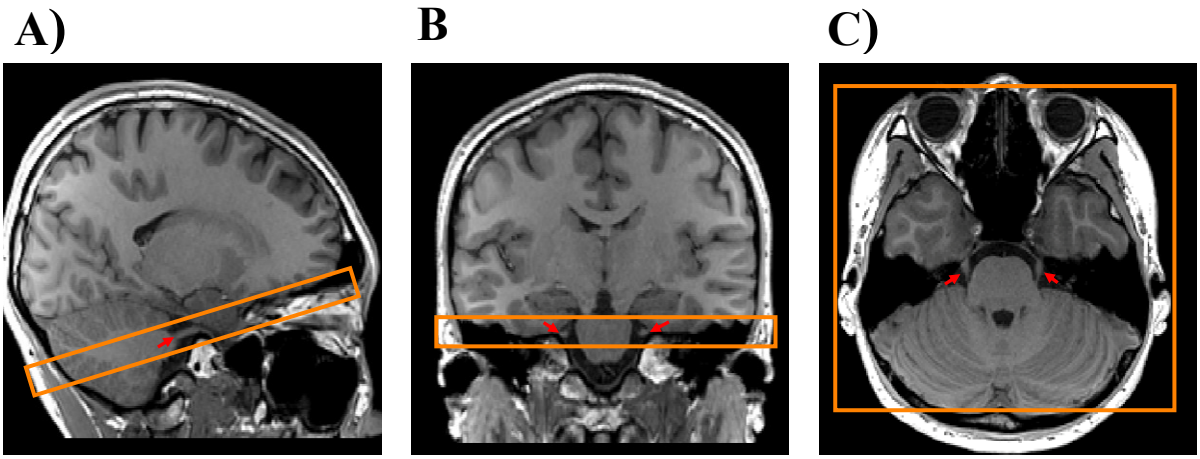

Figure 3.1: Axial-oblique slab placement and orientation of 1.2x1.2x1.2 mm^3 high-resolution nerve-specific diffusion tensor imaging (DTI) protocols. The 13 1.2 mm slices thick axial-oblique slab (orange) is overlaid on T1-weighted MRI structural images in sagittal (**A**), coronal (**B**), and axial (**C**) orientations. The trigeminal nerve is indicated with red arrows. This figure was reproduced from (224) with permission from Wiley Publishing.

Table 3.1: Diffusion tensor imaging (DTI) acquisition parameters for high-resolution nerve-specific protocols with (NS-FL) and without (NS) fluid suppression and isotropic (WBi) and anisotropic voxel (WBa) whole-brain DTI protocols. This table was reproduced from (224) with permission from Wiley Publishing.

Protocol	NS-FL	NS	WBi	WBa
axial-resolution (mm^2)	1.2 x 1.2	1.2 x 1.2	2.0 x 2.0	1.9 x 1.9
slice thickness (mm)	1.2	1.2	2	3
voxel volume (mm^3)	1.7	1.7	8.0	10.8
fluid suppression	yes	no	no	no
axial-interpolation	yes	yes	yes	yes
interpolated resolution (mm^2)	0.6 x 0.6	0.6 x 0.6	1.0 x 1.0	0.94 x 0.94
# of slices	13	13	70	50
FOV (mm)	220	220	244	240
acquisition matrix	182 x 182	182 x 182	122 x 122	128 x 128
TR (ms)	3900	3000	3200	3000
TE (ms)	68.0	65.0	55.8	67.0
TI (ms)	2300	/	/	/
b-value	1000	1000	1000	1000
directions	20	20	30	64
averages	5	3	1	1
# of b_0s	10	10	6	5
multiband factor	0	0	2	2
acquisition time (min)	7:22	3:41	2:29	3:43

FOV: field-of-view; **TR**: repetition-time; **TE**: echo-time; **TI**: inversion-time; directions: number of diffusion directions;

3.2.3 Data Processing:

DTI processing: ExploreDTI was used for signal drift correction, Gibbs ringing, subject motion and eddy current correction between diffusion gradient directions (171). Fiber assignment by continuous tracking deterministic tractography of each CNV was performed with a low starting point FA threshold = 0.1, end FA threshold = 0.2, angle threshold = 30°, seed point resolution = interpolated voxel size, step size = interpolated voxel dimension, and minimum fiber length = 20 mm. In the coronal view, two region-of-interest 'and' gates (a specific type of ROI that restricts streamline generation only to those passing through all 'and' gates that have been placed—two in this specific case) were drawn manually around the outer circumference of each

CNV on native space FA colour map DTI images to generate nerve segments (left and right nerve segments done separately): one proximal region-of-interest on the first slice where CNV could be distinguished from the pons of the brainstem (**Figure 3.2B-E**) and one distal region-of-interest on a slice 5.0-5.6 mm away (**Figure 3.2G-J**). Location of placement of proximal and distal ROIs is displayed on T1-weighted images in the axial orientation (**Figure 3.2A, F**). Each nerve segment yielded an average FA, MD, AD, and RD measure, each representing the average of all streamlines contained within the tractography generated nerve segment.

CNV volume: CNV was manually segmented by a trained observer (co-author HD) on T1-weighted structural images using the ITK-SNAP toolbox (231). In the coronal plane, the nerve was first traced on the proximal-most slice where CNV could be distinguished from the pons of the brainstem. CNV was then traced in each of the next 5 slices, proceeding distally, producing a total nerve segment length of 5.1 mm (6 slices x 0.85 mm voxel size). The volume of left and right CNV were measured separately.

3.2.4 Statistical Analysis:

Within-subject, between-protocol comparisons: Each subject's left and right CNV was analyzed independently, resulting in a total of 10 nerves being available for analysis. A non-parametric repeated-measures ANOVA (Friedman test) was used to compare within-subject diffusion metrics between the four DTI protocols, followed by Wilcoxon signed-rank post-hoc testing. Threshold for statistical significance was set at $p < 0.008$ (two-tailed) following correction for multiple comparisons using Bonferroni's method (0.05 / 6 comparisons per diffusion measure) (GraphPad Prism v7, 2017).

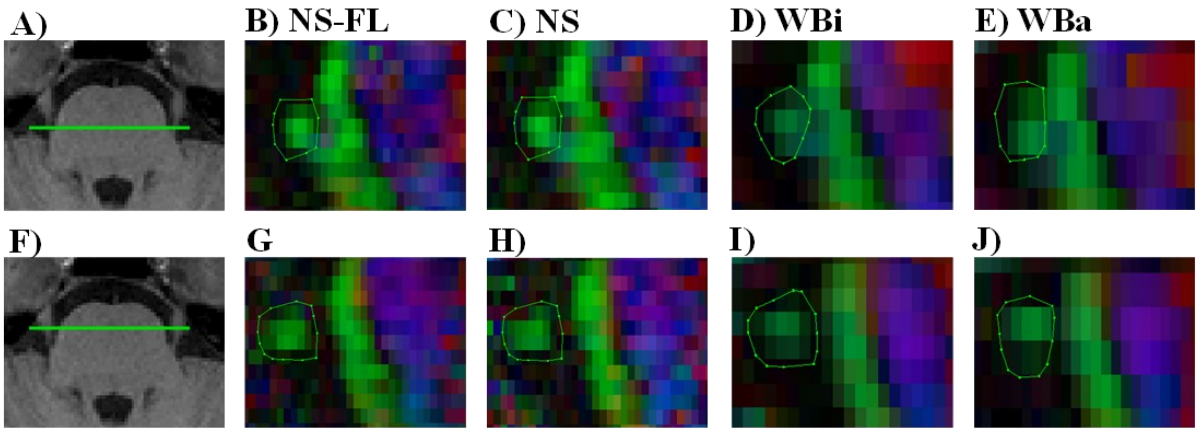

Figure 3.2: Coronal nerve delineation on fractional anisotropy colour maps for all four diffusion tensor image (DTI) protocols within the same subject. With the exception of nerve-specific without fluid suppression (NS) and nerve-specific with fluid suppression (NS-FL) DTI protocols, these coronal-images do not represent identical slices given the different resolutions. Slice locations at the trigeminal nerve's first emergence from the pons of the brainstem (indicated on T1-weighted axial-orientation image with a green line - **A**), where the proximal regions-of-interest (green circles) were placed for tractography nerve segment generation, are displayed in the top row (**B-E**). Cisternal slice locations (indicated on T1-weighted axial-orientation image with a green line - **F**) where distal regions-of-interest were placed for tractography nerve segment generation are displayed in the bottom row (**G-J**). Nerve delineation improves greatly with 1.2x1.2x1.2 mm^3 high-resolution nerve-specific protocols with FLAIR fluid suppression (NS-FL – **B,G**) and without FLAIR fluid suppression (NS – **C,H**) compared to the lower-resolution 2x2x2 mm^3 isotropic (WBi – **D,I**) and 1.9x1.9x3 mm^3 anisotropic (WBa – **E,J**) whole-brain protocols. Note that the all voxels appear anisotropic since these images were 2x zero-fill interpolated in the axial plane. Recall that the colour reflects the direction of the primary eigenvector: green – anterior/posterior; red – left/right, blue – superior/inferior. This figure was reproduced from (224) with permission from Wiley Publishing.

Correlation of T1 nerve volume and DTI metrics: D'Agostino & Pearson Omnibus Normality testing was performed to determine if the distributions of CNV volume or protocol-specific diffusion measures violated normality ($p < 0.05$). For each DTI protocol, correlation was assessed between CNV volume from T1-weighted images and nerve segment average DTI metrics (GraphPad Prism v7, 2017). Spearman correlations were performed for datasets violating normality, while Pearson correlations were performed for datasets approximating Gaussian distributions. Statistical significance was set at $p < 0.013$ (two-tailed) following Bonferroni correction for multiple comparisons (0.05 / 4 correlations per diffusion measure).

3.3 Results:

The two high-resolution 1.2 mm isotropic nerve-specific protocols (NS-FL, NS) were positioned in the same plane as CNV and showed complete depiction of the cisternal section of the nerve in both hemispheres. Although both low-resolution whole-brain protocols (WBi, WBa) were positioned with AC-PC alignment, they ended up with a similar orientation in relation to the nerve as nerve-specific protocols (**Figure 3.3A-D** for mean b0 and **3.3E-H** for mean b1000 axial-oblique images). The lower resolution whole-brain protocols WBi (2x2x2 mm^3) and WBa (1.9x1.9x3 mm^3) yield blurrier b0 and b1000 images, albeit with a smoother 'less grainy' appearance due to higher signal-to-noise ratio. They also displayed greater distortions (i.e., stretching along the anterior/posterior phase-encoding direction in the brainstem) relative to the high-resolution nerve-specific protocols NS-FL and NS. The principal-eigenvector colour-encoded FA maps illustrate a dramatic improvement in the delineation of CNV from adjacent fluid/tissue and brainstem components with the high-resolution 1.2 mm isotropic nerve-specific NS-FL (**Figure 3.3I**) and NS (**Figure 3.3J**) relative to the 2 mm isotropic (**Figure 3.3K**) and 3 mm thick slice (**Figure 3.3L**) lower-resolution whole-brain protocols. Interpolation by zero-filling on the scanner is a common practice in DTI to yield better/sharper looking images/maps that have 4x more voxels in-plane to assist region-of-interest analysis (**Figure 3.3M-P**), but they are still subject to the same partial volume effects as without interpolation. The improved depiction of CNV is also clear in the coronal orientation (**Figure 3.2**). There does not appear to be a qualitative difference between primary eigenvector colour-coded FA maps from the FLAIR (NS-FL) and non-FLAIR (NS) versions of the high-resolution nerve-specific protocol (**Figure 3.2B and G vs. C and H; Figure 3.3** – column 1 versus column 2).

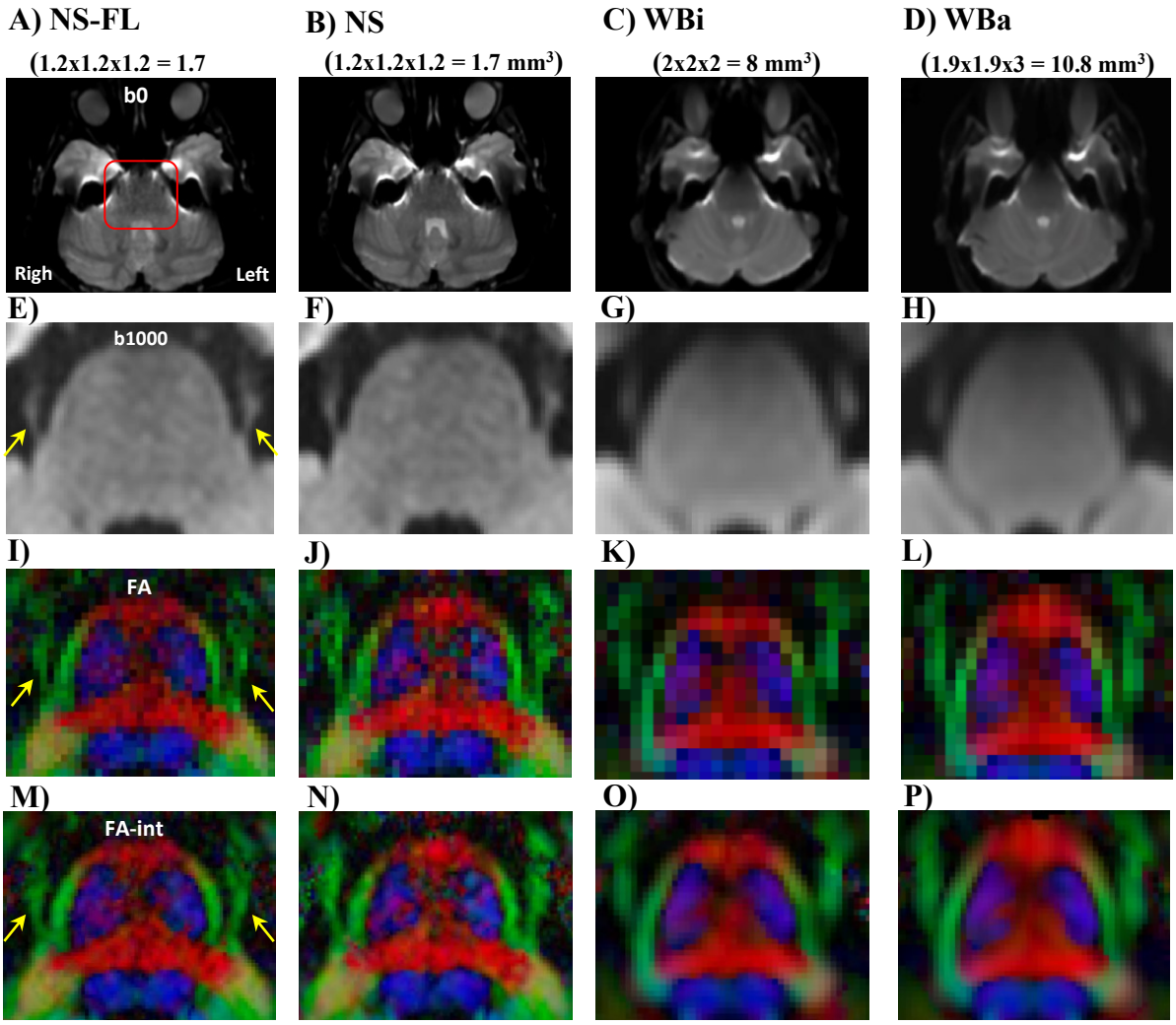

Figure 3.3: Visual comparison of axial images from the four diffusion tensor imaging (DTI) protocols within the same subject. With the exception of nerve-specific without fluid suppression (NS) and nerve-specific with fluid suppression (NS-FL) DTI protocols, these axial-images do not represent identical slices given the different slice thickness. The red box (**A**) overlaid on mean b0 images (**A-D**) indicates the zoomed in region of the other images **(E-P)**. The higher resolution nerve-specific protocols show better depiction of trigeminal nerve (yellow arrows in **E, I, M**) as well as less blurring and distortions on mean b1000 images **(E, F)**, which are evident in the isotropic (WBi—**G**) and anisotropic (WBa—**H**) whole-brain protocols. FA colour maps from the original matrix (**I-L**) and 2x zero-fill interpolated data (**M-P**) highlight the improved nerve (and brainstem) demarcation from NS-FL and NS **(I, M; J, N**) compared to WBi and WBa **(K, O; L, P**). This figure was reproduced from (224) with permission from Wiley Publishing.

Tractography generated nerve segments appear in anatomically correct locations for all DTI protocols, which is confirmed in the axial plane-of-view (**Figure 3.4A-D**). However, visual

depiction of the nerve segments differs dramatically between protocols, with high-resolution nerve-specific protocols NS-FL and NS appearing larger (**Figure 3.4E,F**) than both isotropic (WBi: **Figure 3.4C,G)** and anisotropic (WBa: **Figure 3.4D,H**) lower-resolution whole-brain protocols.

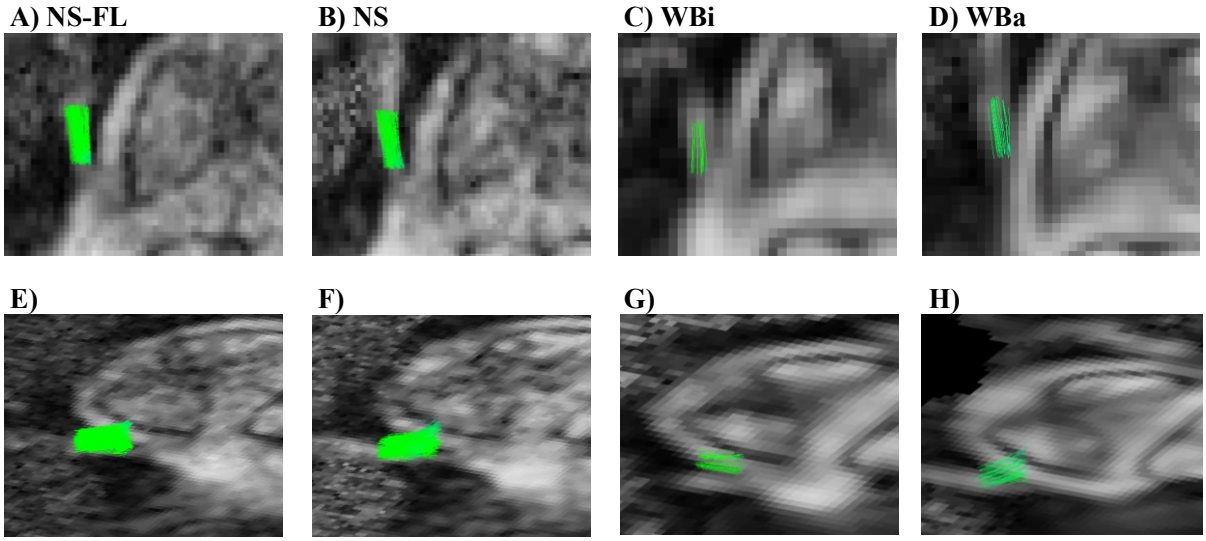

Figure 3.4: Trigeminal nerve segment tractography generated from each diffusion tensor imaging (DTI) protocol in the same subject. Trigeminal nerve segments (green) generated from each DTI protocol (nerve-specific with fluid suppression: NS-FL; nerve-specific without fluid suppression: NS; isotropic whole-brain: WBi; anisotropic whole-brain: WBa) within a single subject are overlaid on respective fractional anisotropy maps in axial (**A-D**) and side-angled (**E-H**) orientations. These nerve segments appear anatomically correct and were used to extract the diffusion metrics. Note that the nerve tractography extends proximally and distally beyond what is displayed, but, streamlines were trimmed by proximal and distal regions-of-interest (same ones used for initial tractography generation – as in Figure 2) to enable quantitative comparison between DTI protocols. This figure was reproduced from (224) with permission from Wiley Publishing.

Over the tractography-derived segment of the nerve, the two lower-resolution whole-brain protocols WBi (2 mm isotropic) and WBa (3 mm thick slices) yielded median FA of 0.34 (0.32-0.35 IQR) and 0.35 (0.33-038 IQR), respectively, and median MD of 1.6 $x10^{-3}$ mm^2/s (1.6-1.7 $x10^{-3}$ mm^2/s IQR) and 1.9 $x10^{-3}$ mm^2/s (1.9-2.0 $x10^{-3}$ mm^2/s IQR), respectively (**Figure 3.5A,**

B). In contrast, the 1.2 mm isotropic high-resolution nerve-specific protocols NS-FL (with FLAIR) and NS (without FLAIR) yielded higher median FA values of 0.48 (0.46-0.48 IQR, p = 0.002) and 0.50 (0.47-0.54 IQR, p = 0.002) respectively, and more reasonable lower MD values of 1.0 $x10^{-3}$ mm^2/s (1.0-1.2 $x10^{-3}$ mm^2/s IQR, p = 0.002) and 1.3 $x10^{-3}$ mm^2/s (1.2-1.3 $x10^{-3}$ mm^2/s IQR p =0 .002), respectively (**Figure 3.5A, B**). Between the two whole-brain DTI protocols, the larger voxel volume WBa (10.8 mm^3) yielded elevated nerve AD of 2.8 $x10^{-3}$ mm^2/s (2.7-2.8 $x10^{-3}$ mm^2/s IQR), RD of 1.5 $x10^{-3}$ mm^2/s (1.5-1.6 $x10^{-3}$ mm^2/s IQR), and MD compared to the lower AD of 2.2 $x10^{-3}$ mm^2/s (2.2-2.3 $x10^{-3}$ mm^2/s IQR, p = 0.002), RD of 1.3 $x10^{-3}$ mm^2/s (1.3-1.4 $x10^{-3}$ mm^2/s IQR, p = 0.002), and MD (p = 0.002) of the smaller voxel volume WBi (8 mm^3). AD and RD were greater (p = 0.002 and p = 0.002 respectively) in both whole-brain protocols compared to each nerve-specific protocol (**Figure 3.5C,D**). Additionally, the FLAIR high-resolution nerve-specific NS-FL protocol yielded lower FA (p = 0.002), MD (p = 0.002), and AD (p = 0.002) compared to its non-FLAIR counterpart NS.

CNV volume and all protocol-specific diffusion metric datasets passed D'Agostino & Pearson Omnibus Normality testing except NS-FL FA ($p < 0.001$) and WBa AD (p = 0.038). Therefore, Pearson correlations were performed for all CNV volume and protocol-specific diffusion measure correlations except NS-FL FA and WBa AD (Spearman used instead). There was a positive correlation between T1-identified CNV volume and FA for the anisotropic whole-brain protocol WBa ($R^2 = 0.59$, p = 0.010), while there were no other correlations between CNV volume and any of the other diffusion metrics, including for all other DTI protocols as well (**Figure 3.6**).

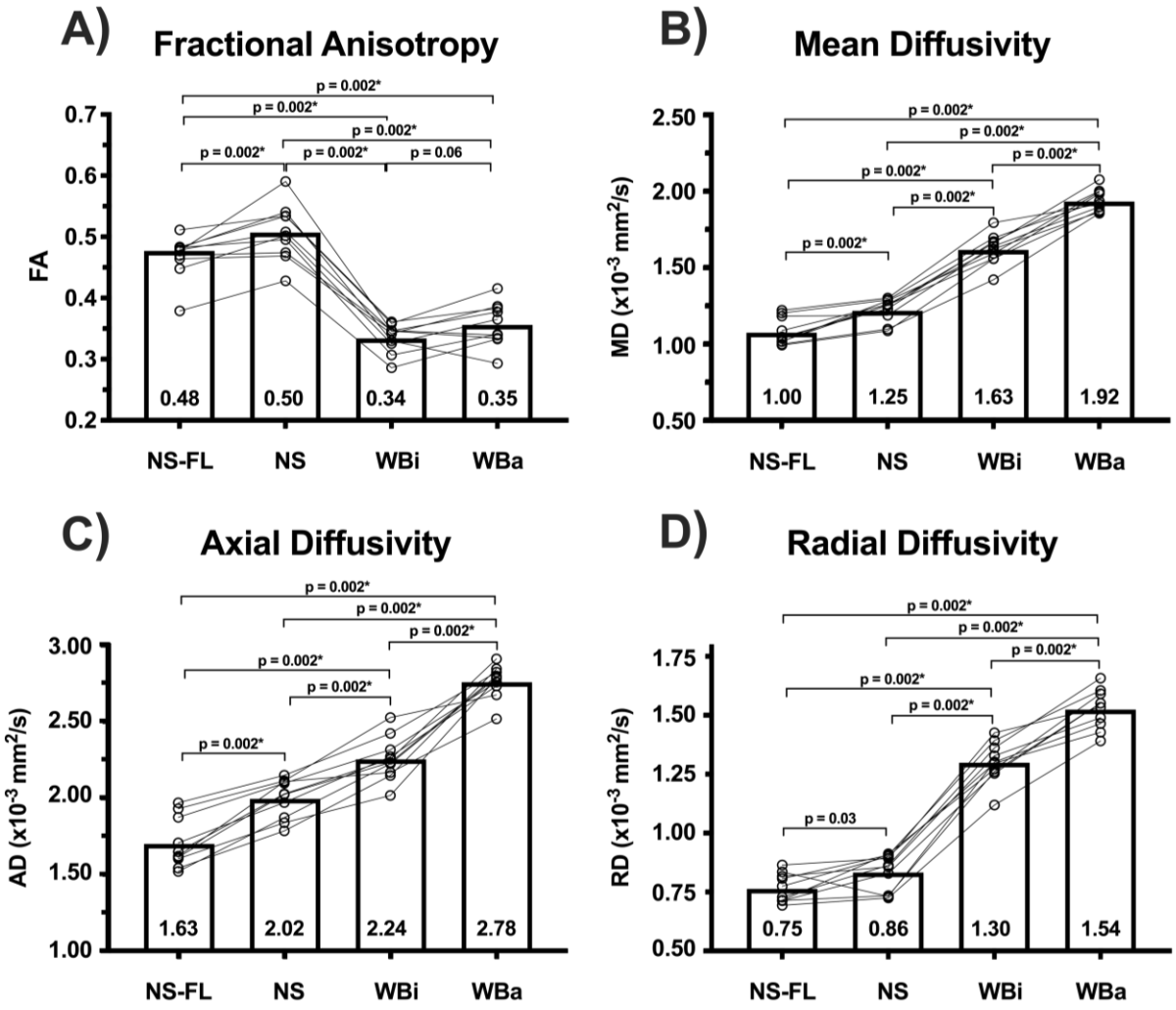

Figure 3.5: Diffusion metrics from the tractography-derived trigeminal nerve segments (n=10) for each of the four diffusion tensor imaging (DTI) protocols within the same 5 subjects. Fractional anisotropy (FA—**A**) is greater in the 1.2x1.2x1.2 mm^3 high-resolution nerve-specific DTI protocols both with FLAIR fluid suppression (NS-FL) and without FLAIR fluid suppression (NS) compared to the lower-resolution 2x2x2 mm^3 isotropic (WBi) and 1.9x1.9x3 mm^3 anisotropic (WBa) whole-brain DTI protocols. NS-FL and NS had lower mean diffusivity (MD—**B**), axial diffusivity (AD—**C**), and radial diffusivity (RD—**D**) than WBi and WBa. MD and AD were lower in NS-FL than NS suggesting less partial volume effects with CSF. MD, AD, and RD were greater in WBa than WBi, further supporting increased partial volume effect with larger voxel volume even between whole-brain protocols. Median average trigeminal nerve segment diffusion measures are presented, and a line connects repeated measures of the same nerve between protocols. Statistical significance ($p < 0.008$) is indicated with *. This figure was reproduced from (224) with permission from Wiley Publishing.

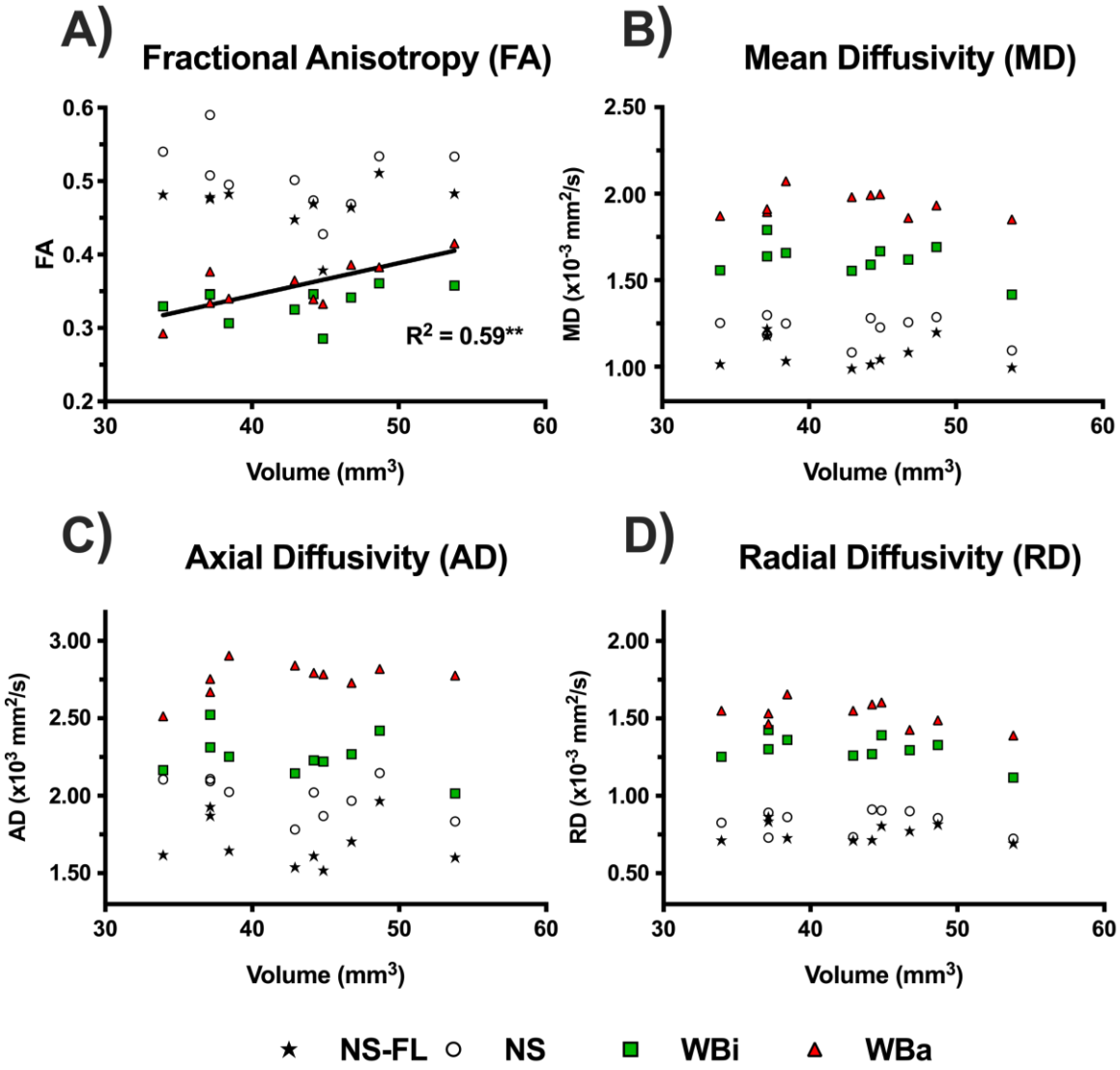

Figure 3.6: Correlation analysis of trigeminal nerve volume from T1-weighted images versus diffusion metrics. There is a positive correlation between fractional anisotropy (FA—**A**) and T1-derived nerve volume for the WBa DTI protocol ($R^2 = 0.59$, $p = 0.010$), while there is no correlation for WBi, NS, or NS-FL DTI protocols. There is also no correlation between T1-derived nerve volume and average mean diffusivity (MD—**B**), axial diffusivity (AD—**C**), and radial diffusivity (RD—**D**) for any of the DTI protocols. Note Pearson or Spearman correlations were performed where appropriate. This figure was reproduced from (224) with permission from Wiley Publishing.

3.4 Discussion:

CNV microstructure is typically studied using low-resolution whole-brain DTI. Given its anatomical location and small size, DTI of CNV is challenging (148,225). In this report, two high-resolution nerve-specific DTI protocols (1.2x1.2x1.2 mm^3) with and without FLAIR fluid-suppression were developed and compared to two whole-brain DTI protocols with commonly used lower-resolutions (2x2x2 mm^3 and 1.9x1.9x3 mm^3) (54,63,230). Within healthy subjects, sharper resolution greatly improved nerve delineation and accuracy of nerve diffusion parameter quantification, while the addition of FLAIR fluid-suppression also provided measurable benefit by reducing partial volume effects with CSF further. Additionally, the lowest resolution whole-brain protocol displayed a positive correlation between CNV FA and volume. Therefore, nerve DTI is influenced by the effects of partial volume and CSF signal contamination, becoming less accurate at lower imaging resolutions and for smaller structures.

In order to improve spatial-resolution while maintaining sufficient signal-to-noise and a reasonable scan-time, averaging was used and coverage was limited to 13 slices in the nerve-specific protocols (229). Spatial-resolution was increased to 1.2 mm isotropic (5-6x smaller voxel volume of 1.7 mm^3 relative to the whole-brain protocol voxel volumes of 8 mm^3 and 10.8 mm^3) with 20 diffusion encoding directions yielding scan-times of 3.5 min without FLAIR or 7.5 min with the extra inversion pulse and delay associated with FLAIR preparation. Greater averages were used for the 1.2 mm isotropic FLAIR protocol (5 averages) compared to the 1.2 mm isotropic non-FLAIR protocol (3 averages) to compensate for signal loss resulting from FLAIR and to equalize signal-to-noise between the two protocols. Higher spatial resolution is less prone to intra-voxel dephasing, and the smaller slab coverage of 15.6 mm leads to better shimming and improved Bo homogeneity that can reduce T2* blurring and artifacts. It is

worthwhile to note that 1.2 mm thick slices have been used to image CNV with DTI before, though, in-plane resolution of this anisotropic voxel protocol was 1.6x1.6 mm^2 and FLAIR was not used (59). Furthermore, interpolation by zero-filling was used to sharpen the appearance of axial-plane resolution for all protocols, as this approach is frequently used by the TN imaging field (62,63,86). We performed a within-protocol comparison of these interpolated images to their non-interpolated counterparts to characterize the effect of zero-filling on measures of nerve diffusion. Importantly, between-protocol nerve diffusivity difference—the key feature of this manuscript—was preserved when performing nerve tractography on non-zero-filled images. However, there is an apparent tendency for zero-filling to produce elevated measures of nerve diffusion, particularly AD which leads to elevated MD and FA since RD does not differ, compared to non-zero-filled images, although this observation varies greatly at the individual-subject level (**Figure 3.7**).

Our high-resolution nerve-specific protocol without FLAIR generates higher CNV FA and markedly lower MD, AD, and RD compared to both lower-resolution whole-brain protocols. Specifically, the highest observed MD, AD, and RD were generated from the largest voxel volume (10.8 mm^3) whole-brain anisotropic protocol, and are ~1.5x, ~1.4x, and ~1.8x greater, respectively, than those generated from the nerve-specific protocols. Specifically, nerve AD generated from this whole-brain protocol was $2.8x10^{-3}$ mm^2/s, approaching free water CSF diffusivity of $3x10^{-3}$ mm^2/s at a body temperature of 37C. Furthermore, delineation and tractography of CNV was also greatly improved with the higher-resolution nerve-specific protocol (1.2 mm isotropic) compared to both lower-resolution whole-brain protocols, in line with findings of the Human Connectome Project whole-brain diffusion protocol with high

spatial resolution (1.25 mm isotropic), but also with higher b-value shells and much longer scan-times (226).

First described by Kwong et al. in 1991, suppression of CSF signal through the use of FLAIR together with DTI is another approach to minimize CSF signal contamination (227). Fluid suppression in combination with cranial nerve DTI has been shown to significantly improve the delineation, identification, and diffusion quantitation of the human optic nerve (cranial nerve II) (229). FLAIR-DTI has only once been used to study CNV, though their lower spatial-resolution protocol (1.9x1.9x3 = 10.8 mm^3) yielded an elevated average MD value of $1.7x10^{-3}$ mm^2/s for CNV in healthy participants (61). In contrast, our nerve-specific higher-resolution FLAIR-DTI protocol yielded significantly lower MD ($1.0x10^{-3}$ mm^2/s) than its non-FLAIR counterpart, approaching the MD expected in healthy adult white matter (~$0.8x10^{-3}$ mm^2/s), in strong agreement with optic nerve MD measures previously obtained with fluid-suppressed DTI ($1.1 x10^{-3}$ mm^2/s) (229). It is important to note that scan-rescan variation could contribute to differences in measures of nerve diffusivity between nerve-specific protocols. However, a within-subject (N=1, 2 nerves) scan-rescan assessment showed that between-nerve-specific-protocol nerve diffusivity differences were 2-8X larger than scan-rescan variation, and that FLAIR appeared to be more consistent than its non-FLAIR counterpart, granted these results are only from a single study subject (**Figure 3.8**). Thus, suppression of CSF signal through the addition of FLAIR to nerve DTI also increases diffusion quantification accuracy, though such improvements may only appear at sufficiently high spatial resolutions.

The primary implication of this study is that DTI accuracy in small structures (i.e., cranial nerves) can be diminished by the effects of partial volume and CSF contamination, and is thus, heavily influenced by acquisition protocol—mainly voxel size and techniques of CSF

suppression. Improved resolution and the addition of fluid suppression to the nerve-specific protocols yielded more accurate CNV diffusion parameters despite using only 20 diffusion encoding directions, while the isotropic and anisotropic voxel whole-brain protocols used 30 and 64 directions, respectively. It is worthwhile noting that increasing the number of diffusion directions to 100 for NS-FL (1 average) yielded nearly identical CNV average diffusion measures as those generated from the current form of NS-FL featured in this manuscript (20 directions, 5 averages) (**Figure 3.9**), which was expected considering increased number of diffusion directions is necessary only for complex modelling and crossing fibers (147). Additionally, the positive correlation observed between CNV volume and FA at lower resolutions (1.9x1.9x3 mm^3) suggests that FA may become a surrogate measure of nerve volume because of partial volume effects (232). Considering the prevalence of nerve atrophy in TN (41,76,175,233), one must be cognizant of this phenomenon when performing FA comparisons between nerves (or any structures with known volume differences). It is worthwhile to note that this same correlation has been observed before in patients with TN (54,59). This is not to say that nerve FA and volume reduction do not occur in unison; rather, higher-resolution DTI protocols are needed to rule out the possibility that partial volume effects may be driving these concurrent observations.

This study is not without limitations. First, within-subject between-protocol comparisons were performed using healthy young adults instead of older or clinical populations which may have smaller nerves (e.g., TN patients with >70% cases occurring at ages >50 years) (2). However, the effects of partial volume between low- and high-resolutions (with FLAIR) ought to be greater and worsen with smaller nerve volumes. Most CNV DTI studies measure diffusion parameters within a manually placed region-of-interest within the nerve boundaries. In this

report, however, tractography was used for delineating the nerve, which by design avoids voxels with FA values below our set thresholds (which could potentially be included in a manual ROI approach). To be consistent with other groups, all findings of this report were reproduced using a manual region-of-interest approach (data not shown). Full-brain coverage protocols are advantageous in that they may be used for both nerve and whole-brain assessments, while this is not possible of nerve-specific protocols. However, this study's findings justify the use of additional scan-time for a nerve-specific DTI in addition to whole-brain DTI if CNV is a key anatomy of interest. In theory, nerve-specific scan-times could potentially be reduced from 3.5 min (non-FLAIR-DTI) and 7.5 min (FLAIR-DTI) with further optimization to the number of directions and averages. It is worthwhile noting that while fluid attenuation did occur with NS-FL, it was not complete (**Figure 3.10**), potentially due to the skull-base location and in-flowing spins (234), in combination with the minimum TR of 3.9 s that was used to minimize scan-time for future clinical application.

3.5 Conclusion:

High-resolution nerve-specific DTI with the addition of fluid suppression (FLAIR) significantly enhances the identification and accurate diffusion quantification of CNV. This approach would be advantageous for studies of CNV in trigeminal neuralgia, and could also be used for DTI of other cranial nerves or small structures.

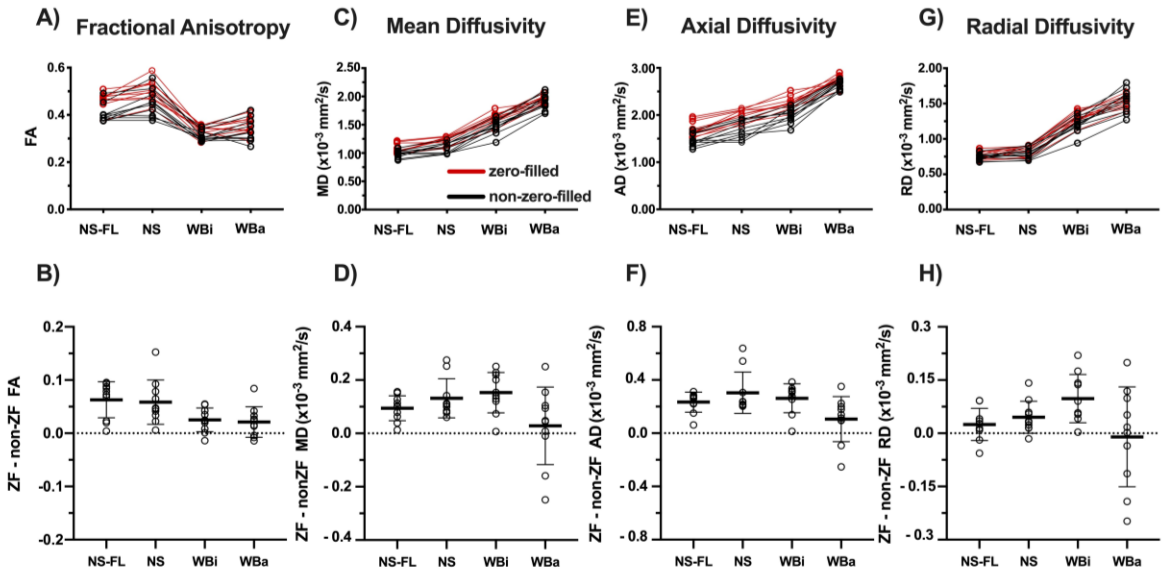

Figure 3.7: Comparison of nerve diffusion parameters from zero-filled (ZF) interpolated and non-zero-filled (non-ZF) interpolated images over 5 subjects (2 nerves each). The between-protocol differences for nerve-specific relative to the whole-brain protocols in fractional anisotropy (FA—**A**), mean diffusivity (MD—**C**), axial diffusivity (AD—**E**), and radial diffusivity (RD—**G**) are the same for the non-ZF images (black) as they are for the ZF data (red) presented in the Results. There are large within-protocol variations in ZF – non-ZF difference of nerve FA (**B**), MD (**D**), AD (**F**), and RD (**H**) for all protocols tested at the individual nerve level. However, AD appears to be consistently higher for ZF which would also cause higher MD and higher FA since RD is unchanged. The mean +/- standard deviation bars of the ZF – non-ZF difference are also shown (**B**, **D**, **F**, **H**). This figure was reproduced from (224) with permission from Wiley Publishing.

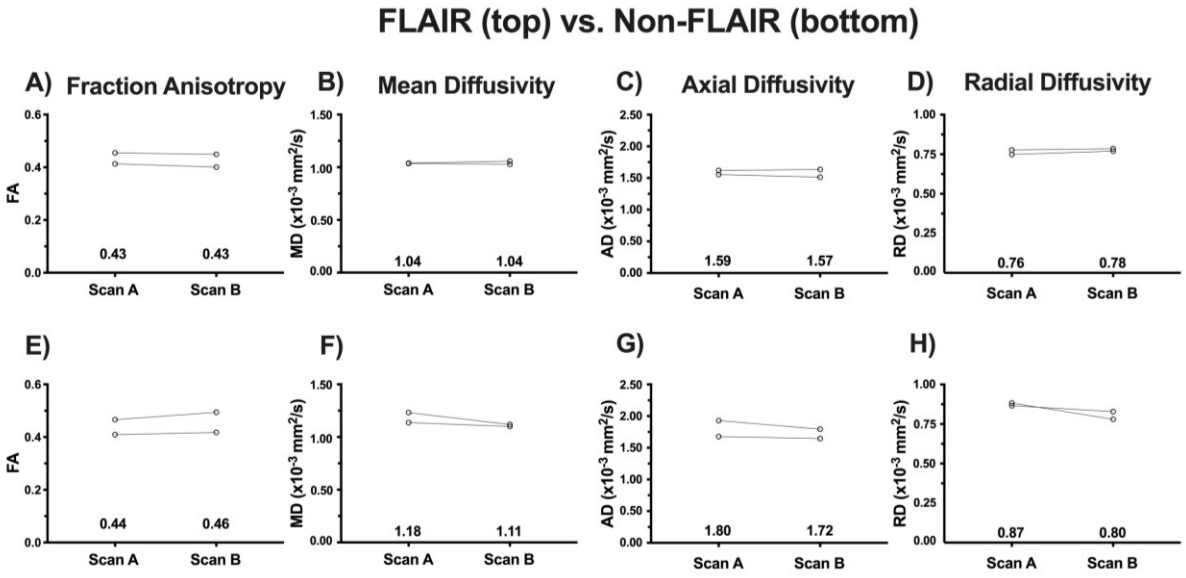

Figure 3.8: **Scan-rescan reliability comparison between FLAIR (top) and non-FLAIR (bottom) nerve-specific protocols for two nerves in one healthy subject.** There is no difference in nerve fractional anisotropy (FA), mean diffusivity (MD), axial diffusivity (AD), or radial diffusivity (RD) between scan A and B for the nerve-specific FLAIR protocol (**A-D**). There are small differences in nerve FA, MD, AD, and RD between scan A and B for the non-FLAIR nerve-specific protocol (**E-F**). This figure was reproduced from (224) with permission from Wiley Publishing.

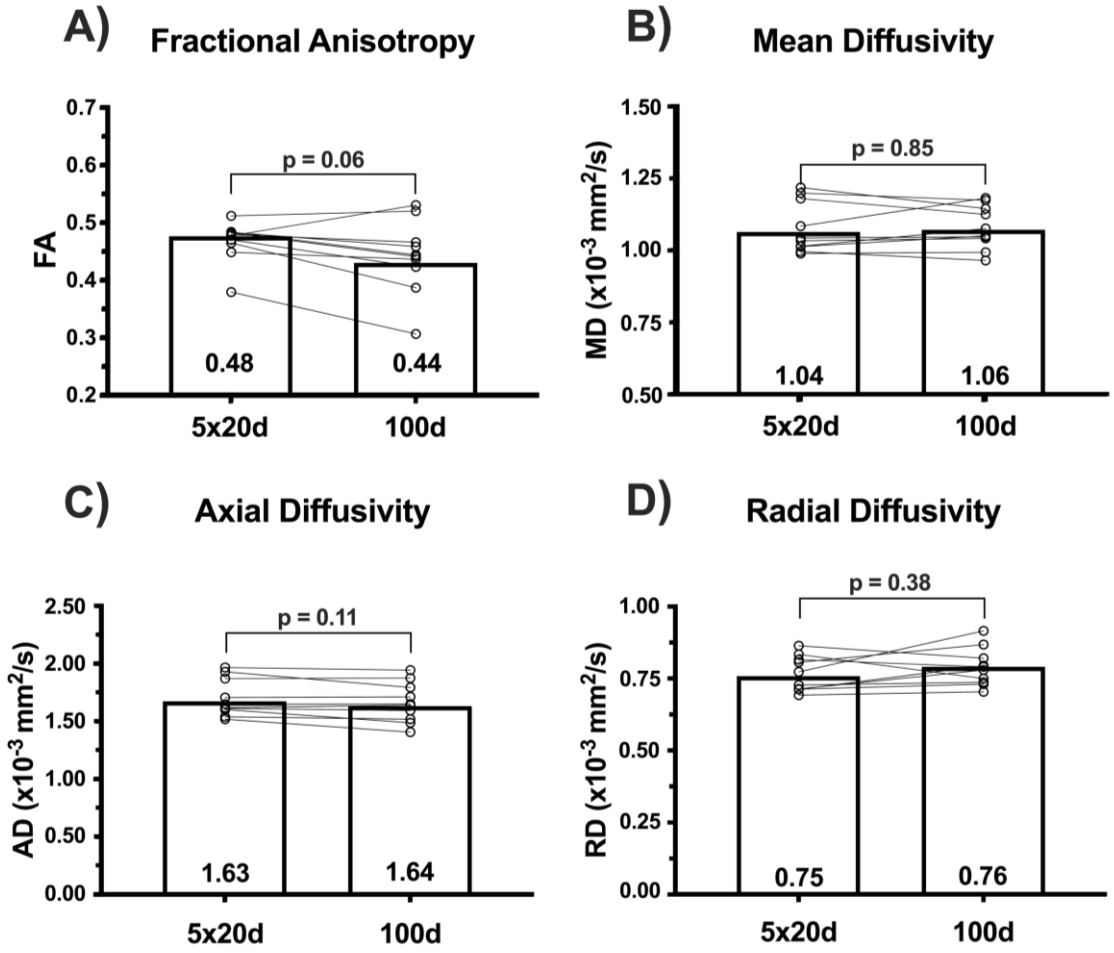

Figure 3.9: Comparison of 20 direction-5 averages and 100 direction-1 average nerve-specific FLAIR protocols in 5 healthy subjects (10 nerves). There are no statistically significant group-level differences between the two protocols for nerve fractional anisotropy (FA—**A**), mean diffusivity (MD—**B**), axial diffusivity (AD—**C**), or radial diffusivity (RD—**D**). Average FA data spread is larger for the 100 direction-1 average protocol, suggesting this protocol is less consistent. Median average trigeminal nerve segment diffusion measures are presented, and a line connects repeated measures of the same nerve between protocols. Non-parametric paired statistics (Wilcoxon sign-rank) were used. Statistical significance ($P < 0.05$). This figure was reproduced from (224) with permission from Wiley Publishing.

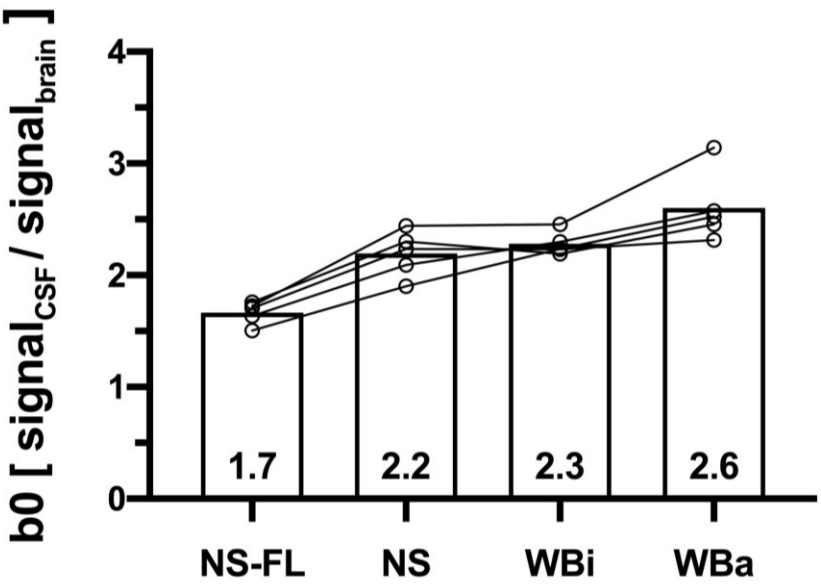

Figure 3.10: Comparison of CSF / brain signal ratios on mean b0 images between diffusion tensor imaging (DTI) protocols in 5 healthy subjects. Brainstem CSF signal is 2.2-2.6x greater than that of the brain for all three non-FLAIR DTI protocols, and is lowest at 1.7 for the nerve-specific FLAIR protocol, suggesting that FLAIR-DTI provides some attenuation of the CSF signal but did not null CSF signal completely. This figure was reproduced from (224) with permission from Wiley Publishing.

CHAPTER 4: Trigeminal Nerve Diffusion in Patients Undergoing Surgical Treatment for Trigeminal Neuralgia

4.1 Introduction:

DTI studies examining CNV in TN are plentiful. The most widely used DTI measure in nerve imaging is FA, for which higher values indicate increased axon microstructural integrity (141). In patients with TN, FA at the REZ (i.e., site of vascular compression in classical TN) is consistently reduced in the ipsilateral affected nerve compared to the contralateral unaffected nerve and CNV in healthy controls (HC) (53–55,57–62,64,86,185,186). MD is also consistently increased in the ipsilateral REZ of TN patients, while AD and RD abnormalities are identified less consistently (53–55,57–62,64,86,185,186). Decreased FA and increased MD are expected with demyelination and axon loss; thus, DTI appears to confirm histological findings in TN, which include demyelination, dysmyelination, and neuronal loss at the REZ, especially in association with NVC (9,59,60).

It has long been hypothesized that preoperative CNV microstructure (indicated by diffusion metrics) may be related to surgical outcome given that surgery targets CNV directly. However, there are mixed data on differences in CNV microstructure between responders and non-responders to surgery at various perioperative time points, and no studies to date have found raw diffusion metrics to differ between surgical response groups before surgery (62,184,187–191). While it is indeed possible that no differences in nerve structure exist between responders

and non-responders, one must also consider the potential that methodological limitations related to DTI acquisition may be hindering the accuracy of nerve DTI. Previously outlined in detail in Chapter 3, ipsilateral CNV has a smaller CSA and volume in patients with TN (56,175–179), and thus, is susceptible to increased effects of partial volume which artificially alters diffusion metrics when sufficiently low-resolution DTI protocols are used (54,59,224).

Recently, we developed a nerve-specific high-resolution FLAIR-DTI protocol to image CNV and compared it head-to-head against other DTI protocols typically used to study TN—described in detail in Chapter 3 (224). The improved resolution (1.2x1.2x1.2 mm^3) in combination with fluid-attenuation dramatically improves the accuracy CNV diffusion metrics acquired using our FLAIR-DTI protocol compared to lower-resolution whole-brain protocols typically used to study TN (2x2x2 mm^3 and 1.9x1.9x3 mm^3) (54,63,230). Additionally, FLAIR-DTI is not susceptible to the same false positive finding as the lower-resolution whole-brain protocols in which FA becomes a surrogate measure for nerve volume (224).

Our central hypothesis was that pre and postoperative differences in CNV diffusion exist between responders and non-responders to surgical treatment for TN. Our primary objective was to replicate previous CNV DTI findings in TN patients and HC subjects using our novel FLAIR-DTI protocol, and to compare pre and early postoperative CNV diffusivity between responders and non-responders to surgical treatment for TN.

4.2 Methods:

4.2.1 Study participants:

This was a prospective, longitudinal study of patients undergoing surgical treatment for TN at the University of Alberta Hospital between 2017 and 2020, approved by the Health Research Ethics Board—Health Panel of the University of Alberta. Potential study patients were identified in clinic by any one of three neurosurgeons and provided informed consent.

Inclusion criteria: medically-refractory classical or idiopathic TN defined using ICHD-III criteria (1); scheduled for surgical treatment by MVD or percutaneous BC.

Exclusion criteria: confirmed multiple sclerosis or other lesional causes of TN; diagnosed psychiatric illness; history of any prior non-TN neurosurgical procedures.

Additionally, 20 HC subjects matched to the TN group in mean age and sex distribution, and without chronic pain or psychiatric conditions, were recruited.

4.2.2 Data Acquisition and Processing:

4.2.2.1 MR Imaging Acquisition:

All MR imaging was performed at the Peter S. Allen MRI Research Centre using a 3T Siemens Prisma MRI (Erlangen, Germany) with a 64-channel head radiofrequency coil. A newly developed nerve-specific FLAIR-DTI protocol was used to image CNV in all HCs and TN patients included in the study. The acquisition parameters of this FLAIR-DTI protocol are described in detail in Chapter 3 (224).

All TN patients underwent MRI scanning within 1-month prior to surgery (*preoperative* time-point), and then were evaluated after surgery within 0-48 hours (*day* postoperative time-point), 5-12 days (*week* postoperative time-point), and 3-6 weeks (*month* postoperative time-point). HC subjects underwent a single MRI scanning session. TN patients also completed a pain questionnaire describing pain attack frequency, location, and severity measured with a 0-100 mm VAS score prior to all scanning time-points. All TN patients were followed for at least 12-months after surgery.

4.2.2.2 Nerve Diffusion Assessment:

All DTI data processing was performed using the ExploreDTI toolbox as outlined in Chapter 3 (171,224). Nerve tractography was performed to generate a 6.3 mm long CNV segment extending out distally from the nerve's first emergence from the pons which included the REZ and presumed site of NVC in cases where it was present. Diffusion metrics FA, MD, AD, and RD were generated and averaged across the entire CNV segment, and then desired comparisons were performed. Nerve segment generation is outlined in detail in Chapter 3 (171,224).

4.2.3 Clinical Characteristics and Outcome Assessment:

The following demographic/clinical data were collected: sex; age; duration of TN since diagnosis; side-of-pain; preoperative pain severity (measured using VAS); branches of CNV affected; number of previous surgical procedures for TN; surgery type (MVD or BC); and current medications used at the time of preoperative imaging. Additionally, we determined NVC severity scores for each patient based on the scoring system of Sindou et al. (0: no neurovascular contact or venous contact alone; 1: arterial contact with no indentation of nerve root; 2: arterial contact with displacement and distortion of nerve root; 3: arterial contact with

marked indentation in nerve root) (235). NVC severity scores were derived by a single observer by examining routine high resolution clinical preoperative T2 weighted MRI scans, and confirmed (in patients undergoing MVD) by intraoperative findings as indicated in operative reports. Note that, at our institution, patients who are found to have no compressive arterial NVC at the time of MVD also undergo internal neurolysis. Study participants were classified as responders or non-responders as follows: *responders* – 1) documented evidence of immediate and persistent pain relief for at least one-year after surgery (Barrow Neurological Institute (BNI) facial pain score IIIa or better) (117); and 2) no offer of or repeat surgical TN treatment; *non-responders* – 1) inadequate initial pain relief from surgery or early pain recurrence within one year of surgery; or 2) offered or underwent repeat surgical treatment within one year.

4.2.4 Statistical Analysis:

Between-group comparisons: CNV diffusion metrics FA, MD, AD and RD were compared between HC and TN groups as well as responder (R) and non-responder (NR) groups using either parametric (Student's T-test) and non-parametric statistical tests (Mann-Whitney U) respectively.

Within-subject comparisons: CNV diffusion metrics FA, MD, AD, and RD were compared within individual subjects between nerves (ipsilateral vs. contralateral) or timepoints (ipsilateral CNV preoperative vs. postoperative) using parametric (paired T-test) and non-parametric (Wilcoxon signed-rank) statistical tests where appropriate.

Threshold for statistical significance for all comparisons was set at $p < 0.05$ (two-tailed) (GraphPad Prism v7, 2017).

4.3 Results:

4.3.1 Study Participants:

Twenty-three TN patients and 20 HC were included in this study between 2017 and 2020 (**Table 4.1**). Thirteen TN patients were included in 1-day postoperative assessments, 18 TN patients were included in 1-week postoperative assessments, and all 23 TN patients were included in 1-month postoperative assessments.

4.3.2 Clinical characteristics and demographics:

All TN: Clinical and demographic features of all 23 TN patients and 20 HCs are presented in **Table 4.1**. TN and HC groups were well matched in age (56.3 $\pm$ 10.4 years and 54.9 $\pm$ 9.4 years respectively, $p = 0.65$) and sex distribution (14F/9M and 11F/9M, $p = 0.70$). Average TN duration was 5.3 $\pm$ 3.9 years, with right-sided TN being more common than left-sided TN (15R/8L). NVC was identified in 17/23 TN patients, and average preoperative VAS was 77.6 $\pm$ 27.3 across the entire TN patient group. This study included first-time surgical procedures for 17/23 TN patients and MVD surgery was the most common (16 MVD, 7 BC). All TN patients were on antiepileptic medication at surgery, including carbamazepine/oxcarbazepine ($n = 21$) and/or gabapentin/pregabalin ($n = 12$). Three TN patients were also on antidepressant/anxiolytic medication, six were on baclofen, one was taking opioids, and two others were taking cannabis oil.

Table 4.1: Comparison of demographic and clinical characteristics between TN patients and healthy controls (HC), as well as within TN patients (responders vs. non-responders). Mann Whitney, and Chi-square or Fisher's-exact tests used where appropriate. Means ± standard deviations are presented.

	Responders	Non-Responders	P-value (2-tailed)	TN	HC	P-value (2-tailed)
Total #	17	6	-	23	20	-
Sex (Female/Male)	8/9	6/0	0.048*	14/9	11/9	0.70
Age (years)	58.6 ± 9.7	47.4 ± 10.3	0.016*	56.3 ± 10.4	54.9 ± 9.4	0.65
Duration of TN (years)	4.6 ± 3.3	8.8 ± 4.7	0.061	5.3 ± 3.9	N/A	-
Side of pain (left/right)	6/11	2/4	>0.99	8/15	N/A	-
Pre-op VAS (mm)	80.7 ± 23.6	72.3 ± 37.2	0.53	78.5 ± 27.0	N/A	-
NVC (yes/no)	14/3	3/3	0.27	17/6	N/A	-
NVC score (0/1/2/3)	3/3/6/5	3/0/2/1	0.64	6/3/8/6	N/A	-
Virgin (yes/no)	14/3	3/3	0.28	17/6	N/A	-
Surgery type (MVD/BC)	13/4	3/3	0.32	16/7	N/A	-
Carbamazepine/ oxcarbazepine (yes/no)	15/2	6/0	>0.99	21/2	N/A	-
Gabapentin/pregabalin (yes/no)	7/10	5/1	0.16	12/11	N/A	-
Other antiepileptics (yes/no)	2/15	1/5	>0.99	3/20	N/A	-
Antidepressant (yes/no)	2/15	1/5	>0.99	3/20	N/A	-
Baclofen (yes/no)	2/15	4/2	0.021*	6/17	N/A	-
Opioid (yes/no)	0/17	1/5	0.26	1/22	N/A	-
Cannabis oil (yes/no)	1/16	1/5	0.46	2/21	N/A	-

NVC (yes/no): neurovascular compression; **NVC score** (0/1/2/3)(235): degree of neurovascular compression; **Virgin** (yes/no): first-time surgical treatment for TN; **MVD**: microvascular decompression; **BC**: balloon compression rhizotomy; **other antiepileptics**: lamotrigine, topiramate; **antidepressant**: amitriptyline, duloxetine. *p<0.05

By response to surgery: In total, there were 17 responders to surgery and 6 non-responders. Non-responders were exclusively female (6F/0M), while responders had a balanced sex distribution (8F/9M). Non-responders were younger than responders (47.4 $\pm$ 10.3 years and 58.6 $\pm$ 9.7 years respectively, $p = 0.016$), and showed a trend toward longer duration of TN compared to responders (8.8 $\pm$ 4.7 years versus 4.6 $\pm$ 3.3 years respectively, $p = 0.061$). NVC severity score was not different between outcome groups ($p = 0.64$, Fisher's exact test), nor was frequency of surgery type ($p = 0.32$, Chi-square test). The proportion of patients taking baclofen was higher in non-responders than responders ($p = 0.021$), with no other differences in medication use. Individual TN patient clinical profiles are presented in **Table 4.2**.

Table 4.2: clinical characteristics of individual TN patients

	Sex	Age (years)	Side	Duration (years)	Pre-op VAS (mm)	Branch	NVC score	SX types	# prev. SX	Medications
Responders:										
1	M	57.5	R	6	66	3	2	MVD	0	carbamazepine
2	M	49.0	R	1	100	1/2/3	2	BC	3	oxcarbazepine, baclofen
3	M	45.1	L	9	98	1	2	MVD	0	carbamazepine, pregabalin
4	F	58.5	R	11	100	2/3	3	MVD	0	carbamazepine
5	M	63.9	R	8	82	1/2/3	2	MVD	0	carbamazepine
6	M	67.5	R	6	71	2/3	1	BC	1	carbamazepine
7	F	74.1	L	3	81	2	3	MVD	0	oxcarbazepine, pregabalin
8	F	65	R	1	93	3	1	MVD	0	gabapentin
9	F	60.3	L	6	36	2/3	3	MVD	1	gabapentin, amitriptyline
10	F	64.9	L	7	100	2/3	3	MVD	0	carbamazepine, gabapentin
11	F	60.4	L	7	86	2/3	2	MVD	0	carbamazepine, oxcarbazepine
12	F	60.4	R	15	80	2/3	0	BC	0	carbamazepine
13	M	41.8	R	2	89	1/2	2	MVD	0	carbamazepine, gabapentin, topiramate
14	F	68.5	L	1	100	3	1	MVD	0	carbamazepine
15	M	61.5	R	2.5	79	3	0	MVD/IN	0	carbamazepine
16	M	63.3	R	2.5	95	2/3	3	MVD	0	oxcarbazepine, lamotrigine, gabapentin
17	M	40.6	R	1	15	2/3	0	BC	0	carbamazepine, baclofen, duloxetine, cannabis oil
Non-Responders:										
18	F	37.3	L	6	63	2/3	0	MVD/IN	0	oxcarbazepine, baclofen
19	F	48.9	L	8	2	1/2/3	2	MVD	0	carbamazepine, gabapentin, baclofen

20	F	56.2	R	13	60	1/2/3	2	BC	1	carbamazepine, gabapentin, lamotrigine, baclofen, hydromorphone
21	F	55.5	R	3	100	1/2/3	0	BC	0	oxcarbazepine, gabapentin
22	F	57.5	R	13	100	1/2/3	0	BC	2	carbamazepine, gabapentin
23	F	36.3	R	3	89	2/3	3	MVD	0	carbamazepine, gabapentin, baclofen, amitriptyline, cannabis oil

Male; **F**: female; **VAS**: visual analogue scale; **Branch**: affected trigeminal nerve branches; **NVC**: neurovascular compression; **SX**: surgical treatment; **MVD**: microvascular decompression; **BC**: balloon compression rhizotomy; **IN**: internal neurolysis.

4.3.3 Surgical Outcomes:

Preoperative TN pain reported using VAS pain scores for the entire TN patient cohort was 77.6/100. There was no preoperative difference in VAS score between responders (80.7 ± 23.6) and non-responders to surgical treatment for TN (72.3 ± 37.2, $p=0.53$). At the 1-month postoperative timepoint, responders displayed a near complete reduction in TN pain (3.53 ± 8.6, $p < 0.001$). In contrast, non-responders did not display a 1-month TN pain score reduction at the group level (39.5 ± 44.8, $p=0.063$). Preoperative and postoperative (1-week and 1-month) VAS scores for the entire TN patient cohort, as well as responders and non-responders are displayed are **Figure 4.1**.

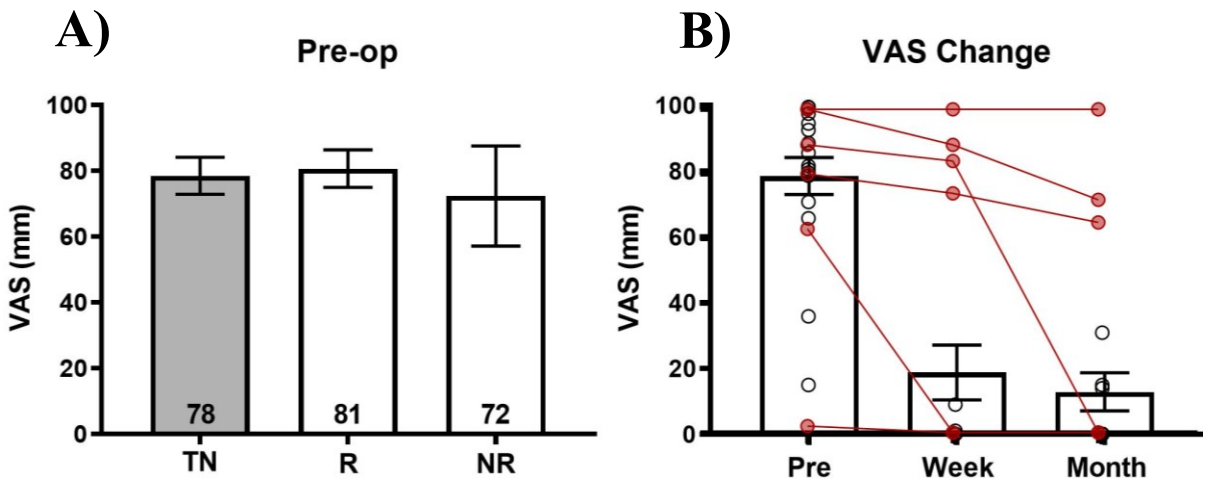

Figure 4.1: Perioperative visual analogue pain score (VAS). Preoperative VAS scores are displayed for the entire TN cohort (grey bar), and responders (R) and non-responders (NR) (**A**). TN group perioperative VAS change (bars) is shown with individual responder (n=17, black circles) and non-responder (n=7, red circles) overlaid (**B**). Repeated measures of the same non-responder subjects are connected with a red line. Note: 3 non-responders are pain-free by 1-month; they are classified as non-responders because they developed pain recurrence by 1 year as defined by criteria in 4.2.3.

4.3.4 Preoperative CNV Diffusivity:

Preoperative CNV diffusivity for HC and TN patients is displayed in **Figure 4.2**. There was no preoperative difference between HC and ipsilateral TN patient CNV FA (**A**—HC = 0.45 $\pm$ 0.05; TN = 0.45 $\pm$ 0.07; p = 0.91), MD (**B**—HC = 1.12 x10^{-3} mm^2/s $\pm$ 0.09 x10^{-3} mm^2/s; TN = 1.16 x10^{-3} mm^2/s $\pm$ 0.11 x10^{-3} mm^2/s; p = 0.19), AD (**C**—HC = 1.75 x10^{-3} mm^2/s $\pm$ 0.17 x10^{-3} mm^2/s; TN = 1.80 x10^{-3} mm^2/s $\pm$ 0.18 x10^{-3} mm^2/s; p = 0.50), or RD (**D**—HC = 0.81 x10^{-3} mm^2/s $\pm$ 0.08 x10^{-3} mm^2/s; TN = 0.83 x10^{-3} mm^2/s $\pm$ 0.10 x10^{-3} mm^2/s; p = 0.89). Additionally, there were no preoperative differences in diffusion within TN patients between ipsilateral and contralateral CNV (FA: ipsi = 0.45 $\pm$ 0.07, contra = 0.47 $\pm$ 0.07, p = 0.13; MD: ipsi = 1.16 x10^{-3} mm^2/s $\pm$ 0.11 x10^{-3} mm^2/s, contra = 1.15 x10^{-3} mm^2/s $\pm$ 0.12 x10^{-3} mm^2/s, p

= 0.67; AD: ipsi = 1.80 x10^{-3} mm^2/s ± 0.18 x10^{-3} mm^2/s, contra = 1.82 x10^{-3} mm^2/s ± 0.19 x10^{-3} mm^2/s, p = 0.57; RD: ipsi = 0.83 x10^{-3} mm^2/s ± 0.10 x10^{-3} mm^2/s, contra = 0.82 x10^{-3} mm^2/s ± 0.13 x10^{-3} mm^2/s, p = 0.89).

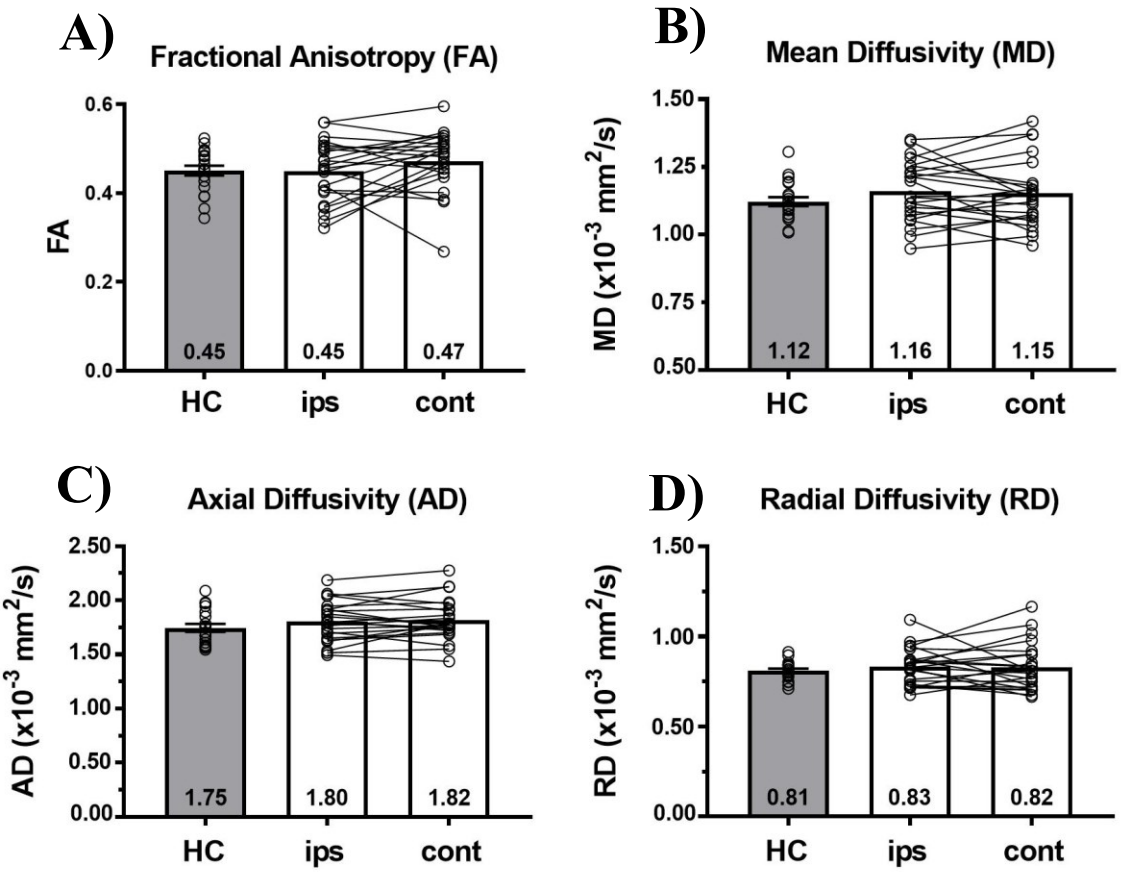

Figure 4.2: Preoperative nerve diffusivity. There are no preoperative differences between healthy controls (HC) and affected ipsilateral (ips) trigeminal nerve in TN patients across FA (**A**), MD (**B**), AD (**C**), or RD (**D**). There are also no differences in FA, MD, AD, or RD within TN patients between ipsilateral and unaffected contralateral (cont) nerves.

4.3.5 Perioperative CNV Diffusivity Change for All TN Patients:

Perioperative ipsilateral CNV diffusivity change for the entire TN patient cohort is displayed in **Figure 4.3**. CNV FA (**A**) was reduced at the delayed 1-month postoperative point (0.41 ±

0.08; p= 0.029). CNV MD (**B**) was reduced immediately following surgical treatment at the 1-day postoperative timepoint (1.08 $x10^{-3}$ $mm^2/s \pm 0.10$ $x10^{-3}$ mm^2/s, $p = 0.002$), and remained reduced at 1-week (1.05 $x10^{-3}$ $mm^2/s \pm 0.13$ $x10^{-3}$ mm^2/s, $p < 0.001$) and 1-month evaluations (1.09 $x10^{-3}$ $mm^2/s \pm 0.10$ $x10^{-3}$ mm^2/s, $p < 0.001$). CNV AD (**C**) was reduced immediately following surgical treatment at the 1-day postoperative timepoint (1.80 $x10^{-3}$ $mm^2/s \pm 0.15$ $x10^{-3}$ mm^2/s, $p = 0.031$), and remained reduced at 1-week (1.59 $x10^{-3}$ $mm^2/s \pm 0.19$ $x10^{-3}$ mm^2/s, $p < 0.001$) and 1-month evaluations (1.62 $x10^{-3}$ $mm^2/s \pm 0.18$ $x10^{-3}$ mm^2/s, $p < 0.001$). RD (**D**) was reduced immediately following surgical treatment at the 1-day (0.79 $x10^{-3}$ $mm^2/s \pm 0.09$ $x10^{-3}$ mm^2/s, $p = 0.026$) and 1- week (0.78 $x10^{-3}$ $mm^2/s \pm 0.12$ $x10^{-3}$ mm^2/s, $p = 0.037$) timepoints, but reverted back to a preoperative level at the delayed 1-month evaluation (0.81 $x10^{-3}$ $mm^2/s \pm 0.11$ $x10^{-3}$ mm^2/s, $p = 0.37$).

4.3.6 Perioperative CNV Diffusivity Change by Surgical Treatment Type:

Perioperative ipsilateral CNV diffusivity change by surgical treatment type is displayed in **Figure 4.4**. TN patients undergoing MVD (n=16) or BC (n=7) display the same direction of change for ipsilateral CNV FA (**A**), MD (**B**), AD (**C**), and RD (**D**), matching the pattern seen across all TN patients in **Figure 4.3**.

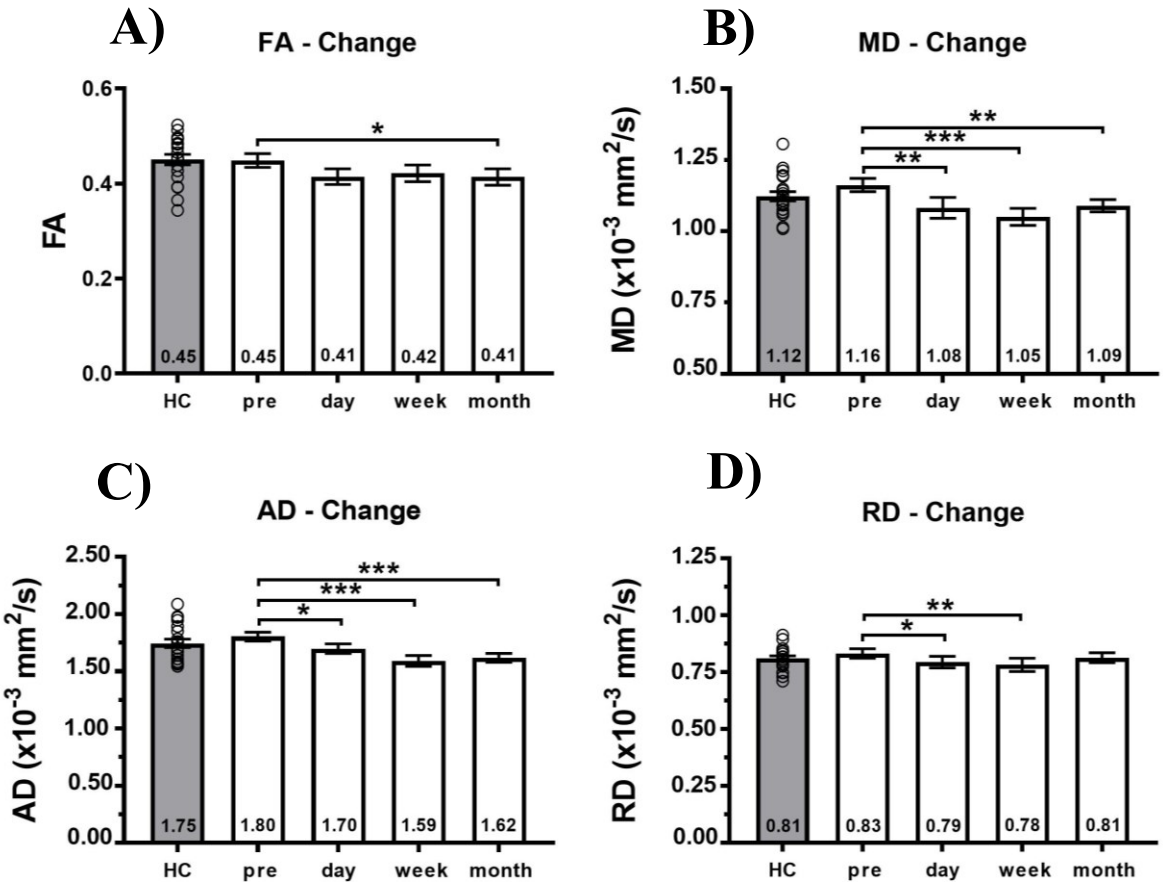

Figure 4.3: Perioperative ipsilateral CNV diffusivity change for the entire TN patient cohort. MD, AD, and RD are all reduced 1-day post-op, and nerve FA is reduced at 1-month post-op. MD and AD nerve change is maintained up to and including 1-month post-op, while RD has returned to baseline. Means +/ standard error of means are presented. Paired T-tests were used with threshold for statistical significance set at $P < 0.05$. $P < 0.05$ is indicated with *, $P < 0.01$ is indicated with **, and $P < 0.001$ is indicated with ***.

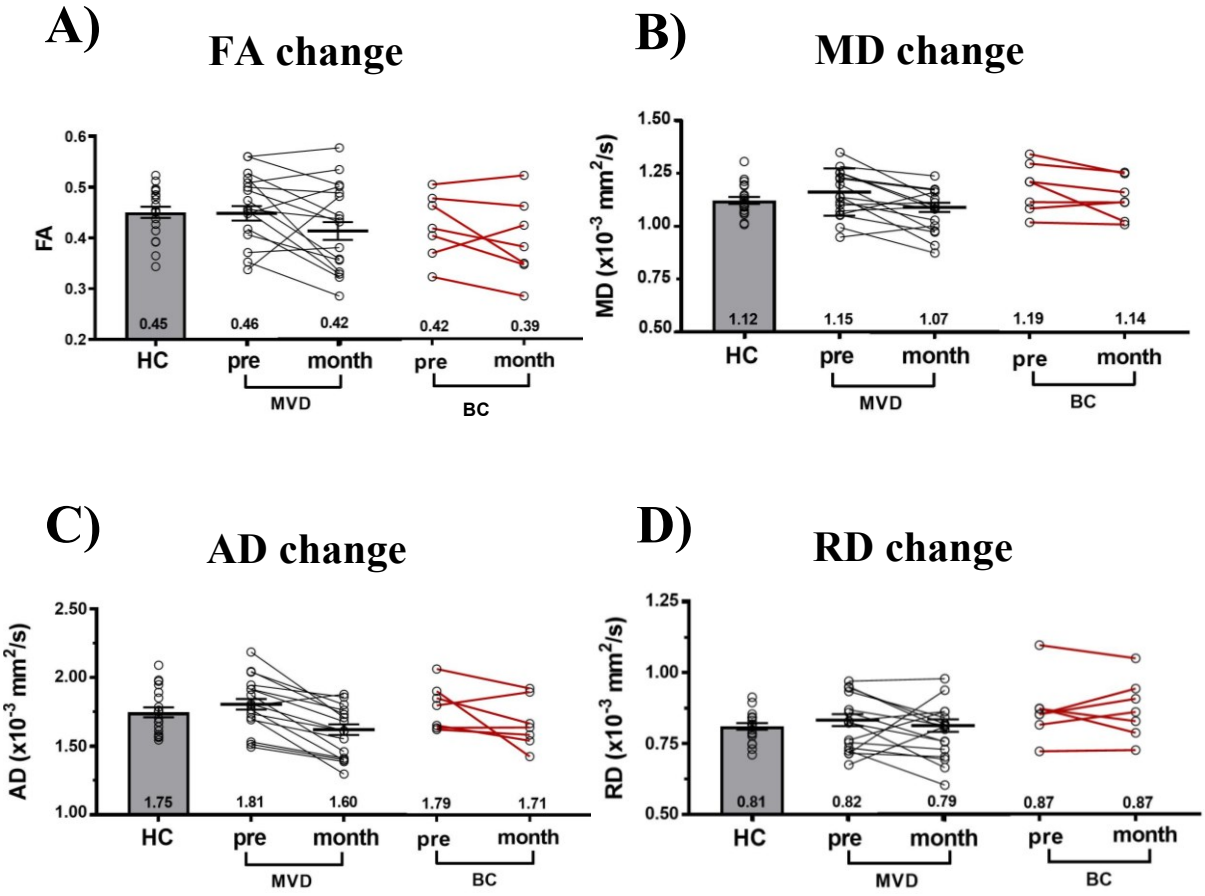

Figure 4.4: Comparison of perioperative nerve change between MVD and BC. Preoperative and 1-month postoperative ipsilateral CNV measurements for individual patients are displayed and are connected with a line illustrating time-dependent repeated measures. The left column (black lines) contains MVD patients, while the right column (red lines) contains BC patients. The mean +/- standard error of mean of the entire TN patient cohort is displayed in the MVD columns. The mean value for each surgical group timepoint is displayed on the x-axis. The pattern of perioperative ipsilateral CNV diffusion change between MVD and BC treatments groups does not differ.

4.3.7 Perioperative CNV Diffusivity Between Responders and Non-responders:

Perioperative ipsilateral CNV diffusivity of responders compared to non-responders to surgical treatment for TN is shown in **Figure 4.5**. Preoperatively (**left column**), there is no difference

between responders and non-responders in ipsilateral CNV FA (**A**—R = 0.45 ± 0.07; NR = 0.46 ± 0.08; p = 0.91), MD (**C**—R = 1.15 $x10^{-3}$ mm^2/s ± 0.11 $x10^{-3}$ mm^2/s; NR = 1.20 $x10^{-3}$ mm^2/s ± 0.12 $x10^{-3}$ mm^2/s; p = 0.19), AD (**E**—R = 1.77 $x10^{-3}$ mm^2/s ± 0.17 $x10^{-3}$ mm^2/s; NR = 1.88 $x10^{-3}$ mm^2/s ± 0.21 $x10^{-3}$ mm^2/s; p = 0.50), or RD (**G**—R = 0.82 $x10^{-3}$ mm^2/s ± 0.10 $x10^{-3}$ mm^2/s; NR = 0.84 $x10^{-3}$ mm^2/s ± 0.10 $x10^{-3}$ mm^2/s; p = 0.89). There is also no difference in the pre to 1-month postoperative trajectory of nerve diffusivity change for FA (**B**), MD (**D**), AD (**F**), or RD (**H**) between responders and non-responders.

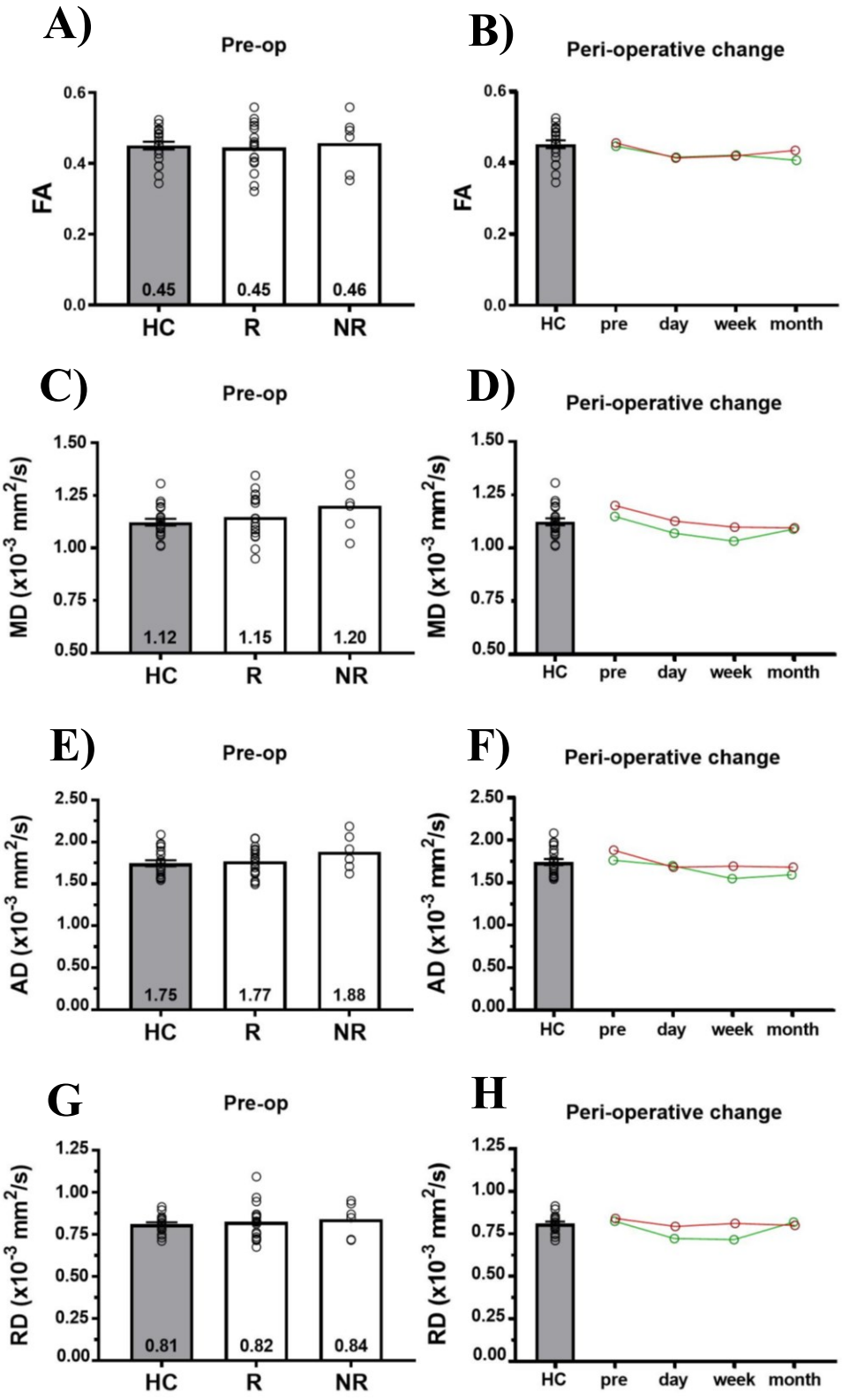

Figure 4.5: Perioperative nerve diffusivity change between responders and non-responders. There is no difference in preoperative nerve diffusivity between responders (R) and non-responders (NR) for FA, MD, AD, or RD (**left column**). There is no difference in the pre- to 1-month postoperative trajectory of nerve diffusivity between responders (green) and non-responders (red) (**right column**).

4.4 Discussion:

In this single-centre, prospective, longitudinal study, we utilized a novel high-resolution ($1.2x1.2x1.2mm^3$) FLAIR-DTI protocol—that was previously shown to be superior in a head-to-head comparison in healthy subjects against those previously used to study TN (224)—to evaluate pre and postoperative CNV microstructure in TN patients undergoing surgical treatment. In contrast to prior studies, we found that there were no preoperative CNV diffusivity differences between TN patients and HCs. However, we found that CNV diffusivity change occurs as early as 1-day following surgical treatment, with some of these diffusivity changes persisting through the 1-month postoperative period. Interestingly, these changes in nerve diffusivity occur regardless of surgical treatment type (i.e., MVD vs. BC) or surgical outcome (i.e., R vs. NR). Collectively, our findings suggest that CNV diffusivity—and by extension, whole nerve microstructure—may not be as impaired as once believed in TN, and further, that surgical outcome may be dependent on factors extending beyond CNV itself.

Overall, our patients demonstrated a 74% surgical response rate, in agreement with prior literature (98,102,115). All TN patients were taking antiepileptic medication, and while medication use was largely the same between responders and non-responders, a greater proportion of non-responders were also taking baclofen, perhaps reflecting more exhaustive attempts at medical management. In line with previous reports, non-responders were more likely to be female, younger at the time of surgery, and suffering from TN for nearly twice as long as responders (125). NVC was identified on preoperative MRI in 17 of 23 TN patients. At a group-wide level, there was no significant difference in NVC severity between responders and non-responders. However, it is worth noting that 50% of non-responders (3/6) but only

18% of responders (3/17) had absolutely no evidence of arterial NVC (i.e., NVC score 0), which may represent a relevant if not statistically significant difference. On reviewing these particular patients in greater detail, there were no obvious clinical or surgical factors that could explain response other than that all 3 non-responders with NVC score 0 were female. Interestingly, patient #23 was the only non-responder with the most severe NVC score of 3 (i.e., distortion); again, this patient was female, and experienced pain recurrence within one year despite technically successful (i.e., confirmed on postoperative imaging) MVD. Taken together, our data are consistent with the notion that some female patients with a diagnosis of TN—whether in association with NVC or not—may have a particularly treatment-resistant manifestation of the disease, perhaps explained by a distinct, though as yet unknown, pathophysiology (85).

We found no difference in CNV diffusivity between ipsilateral TN patients and HCs, or between ipsilateral and contralateral CNV within TN patients. Our findings contradict the majority of the work produced by studies of DTI in TN thus far, which have repeatedly shown that ipsilateral REZ FA is reduced and MD is increased in patients with TN (as well as increased AD and RD occasionally) (53–55,57–62,64,86,185,186). Despite this contradiction, confidence in the validity of the present study's findings is high. First, these other studies utilize low-resolution whole-brain DTI protocols which were shown to be inferior to the FLAIR-DTI protocol employed here (Chapter 3) (224). As such, CNV MD in our study—for both TN and HCs—was ~1.1×10^{-3} mm^2/s, closely approximating that which is expected in adult white matter (~0.8×10^{-3} mm^2/s) (141). In contrast, MD values in the unaffected CNV of TN patients or HCs in other TN studies have ranged widely from $1.2–4.3 \times 10^{-3}$ mm^2/s which is up to 5x higher than physiologic expectations (54,57,58,61,63,184,186,189,193). It is also worthwhile pointing out

that the theoretical maximum diffusivity of free water at 37C (i.e., body temperature) is $3x10^{-3}$ mm^2/s; therefore, values above this are physiologically impossible (141). Described in detail in Chapter 3, CNV diffusivity measures obtained using these low-resolution DTI protocols are subject to severe partial volume effects with surrounding CSF (224). As a result, atrophic or smaller volume nerves—a well-established feature in TN patients (56,175–179)—display artificially reduced FA, which may simply be a surrogate measure of nerve volume (224,232). The correlation between ipsilateral CNV FA and volume has indeed been observed before in some of these TN studies (54,59). Finally, studies in TN using higher-resolution DTI protocols ($1.2x1.2x1.6$ mm^3 and $1.2x1.2x2$ mm^3) in lieu of low-resolution whole-brain DTI protocols have found FA and MD to be normal in patients with TN, further supporting our findings in the current study (57,59).

Normal ipsilateral CNV diffusivity in TN does not align with demyelination or axon loss. However, our findings do not necessarily contradict histological reports in TN given that demyelination, dysmyelination, and neuron loss was found specifically at locations of vascular compression (51,52). We, as well as previous DTI studies in TN, have evaluated the entire nerve segment or cross-section at the REZ rather than the exact site of vascular compression (53–55,57–62,64,86,185,186). Pain is typically felt in a small region of the face and physical contact between CNV and compressive blood vessels—i.e., NVC believed to cause TN—only occurs between small adjacent regions. Therefore, it may be more likely that nerve segment diffusion metrics (i.e., nerve microstructure) are only affected at the exact site of vascular compression (51,52) or only within nerve bundles corresponding to painful face regions (20). Therefore, higher-resolution nerve DTI protocols facilitating more detailed cross-sectional

evaluations of nerve diffusion and microstructure—especially in relation to adjacent compressive vessels—are an important avenue for further research.

This study is the first evaluation (to our knowledge) of postoperative nerve DTI change 1-day after surgery, and one of only a few evaluating less than 1-month after surgery (184,188,190). We found that ipsilateral CNV MD, AD, and RD are all reduced as early as 1-day post-op, suggesting that surgical treatment has an immediate microstructural effect on the entire CNV segment. This makes sense considering patients often wake up from surgery experiencing significant pain relief (98,102), and further, because all surgical interventions directly manipulate CNV. MD and AD reductions are persistent up to and including our most delayed timepoint, 1-month post-op, suggesting that at least some of the initial changes to nerve microstructure associated with surgery extend beyond the immediate postoperative period. Interestingly, CNV FA on the other hand remains unchanged until 1-month post-op where it is also reduced, suggesting that delayed effects on nerve microstructure may also occur with surgical treatment. Our findings agree with Chen *et al.* who reported that MD and RD decrease 2-weeks post rhizotomy surgery, while FA and AD were unchanged (184). Given that remyelination of cranial nerves takes weeks to initiate and even longer to complete, we speculate that the early microstructural changes observed within the 1-month post-op period likely reflect physical damage and subsequent nerve inflammation resulting from surgery rather than remyelination (103,184).

We also found that patients undergoing either MVD or BC procedures display the same postoperative nerve diffusion change, suggesting that these procedures may have similar effects on nerve microstructure in the early postoperative period. While MVD is hypothesized to permit nerve healing and remyelination in the long term, this physiological process takes too

long to occur to explain the immediate pain relief achieved with this procedure (48,103). It is possible, therefore, that injury from physical manipulation of the nerve is more likely to be responsible for the immediate pain relief after MVD, and therefore could explain why MVD and BC appear to induce similar postoperative nerve diffusion change (39,40).

CNV microstructure does not differ between responders and non-responders preoperatively. To date, no studies (including this one) have identified preoperative differences in raw CNV diffusivity between responders and non-responders to surgical treatment for TN when evaluating entire nerve segment or cross-section diffusivity metrics. Simply put, either there are no preoperative differences in nerve microstructure between responders and non-responders or differences are restricted to smaller nerve sections, and are therefore, 'blurred out' when evaluating larger nerve regions. Perhaps the most interesting finding of this study is that postoperative CNV diffusivity change also does not differ between responders and non-responders through the entire 1-month postoperative period. This finding aligns with Chen *et al*., although that study did not perform serial evaluations (184). Our finding also contradicts Desouza *et al.* who found divergent CNV diffusivity change between responders and non-responders at 5.8 months post-op (62). Desouza *et al.* evaluated a different time course than that evaluated in the present study, and therefore, may be evaluating different microstructural processes (i.e., change in whole-nerve myelination level). Clearly, longer-term follow-up of patients in the present study will be required to look for more durable and long-lasting microstructural changes in CNV after surgery.

Taken collectively, the findings of our study suggest that restorative (MVD) and destructive (BC) surgical procedures may have similar effects on CNV in the immediate (up to 1-month) postoperative period. Furthermore, given that both responders and non-responders display the

same changes to nerve diffusion (and presumably nerve microstructure), factors beyond the nerve microstructure may be involved in the process of surgical response, which likely depends on more than simply a nerve-centric mechanism. Indeed, structural changes in more rostral locations along the trigeminal pathway within brainstem and thalamus locations may well be involved in treatment response(236,237), and are further explored in Chapter 5.

This study is not without limitations. First, while we have included a similar number of subjects as other DTI studies in TN, a larger sample size would have provided additional statistical power to distinguish smaller magnitude differences between groups of interest. Given the strong overlap in CNV diffusion metrics between TN patients and HCs, we suspect these results are unlikely to change; however, responder versus non-responder comparisons may show differences if more patients were to be added. Additionally, binarizing surgical response as *responder* or *non-responder* is admittedly an oversimplification. That said, the method of defining surgical response used in this study has also been used in numerous prior publications (219,236–238). Finally, because of logistical challenges including postoperative illness, scheduling difficulties, and patient travel considerations, not all 23 TN patients were able to have 1-day (n=13) and 1-week (n=18) postoperative imaging collected, and therefore all TN patients do not appear in every timepoint, potentially impacting the trajectories of change in CNV diffusivity metrics which we observed.

4.5 Conclusion:

This study is, to date, the most comprehensive serial perioperative evaluation of CNV microstructure in patients undergoing surgical treatment for TN, and the only one to use a

custom high-resolution FLAIR-DTI acquisition sequence. We found that preoperative whole-nerve segment diffusion in TN patients does not differ from HCs in agreement with other TN studies utilizing high-resolution DTI protocols. We also demonstrated for the first time 1-day, 1-week, and 1-month postoperative changes in CNV diffusivity, which suggests that both immediate and delayed microstructural nerve changes occur regardless of surgical approach (MVD or BC). Finally, responders and non-responders display similar changes to nerve microstructure up to 1-month post-op, suggesting that durable surgical response may involve extra-nerve factors. All in all, the findings of our study strongly suggest that higher-resolution nerve-specific protocols should be used to study nerve diffusion in patients with TN, and furthermore, that more proximal locations along the trigeminal pathway (e.g., brainstem or thalamus) or higher-order brain regions ought to be assessed and related to surgical outcome in TN.

CHAPTER 5: The Thalamus in Trigeminal Neuralgia: Structural and Metabolic Abnormalities, and Influence on Surgical Response

Modified with permission from (236): Danyluk H, Andrews J, Kesarwani R, Seres P, Broad R, Wheatley BM, Sankar TS. The thalamus in trigeminal neuralgia : structural and metabolic abnormalities , and influence on surgical response. BMC Neurol [Internet]. 2021;21(290):1–14. Available from: https://doi.org/10.1186/s12883-021-02323-4

5.1 Introduction:

Given the strong association between TN and NVC at the REZ of CNV as well as nerve atrophy (54,175,239), several studies have used MRI to examine CNV structure more closely in patients with TN. Crude nerve measures such as the severity of NVC, as well as clinical/demographic features such as TN pain character or female sex appear to prognosticate surgical outcome (124,240). More sophisticated nerve measures provided with DTI have previously revealed CNV microstructural abnormalities suggestive of de/dysmyelination or axon loss in TN (54,61,63,67,186), though, these preoperative DTI measures do not distinguish responders from non-responders to surgical treatment (Chapter 4). Overall, there is an incomplete understanding of the mechanisms underlying the failure of many TN patients to respond adequately to technically successful surgery. Identifying these mechanisms is important because such patients frequently undergo multiple repeat surgical interventions, with persistently diminished quality of life.

Proximal to CNV, the trigeminal sensory system includes second-order neurons in brainstem nuclei receiving afferents from CNV which project—via the ventral trigeminothalamic tract—

to third-order neurons residing in the contralateral VPM thalamus, that in turn project to the somatosensory cortex. Preliminary attempts to examine the brainstem with MRI in TN suggest that microstructural abnormalities exist upstream of CNV as well (86,241), though DTI in the brainstem is technically challenging and susceptible to error (193). Despite the well-known structural and functional alterations of the thalamus in chronic pain (195), and its role in the trigeminal sensory system, very few TN studies have directly examined the thalamus or its relationship to treatment outcome (198–201). Recently, we retrospectively identified preoperative enlargement of the thalamus contralateral to the painful side of the face in patients with TN (Chapter 6) (238), though, whether thalamic volume is related to surgical outcome per se remains uncertain.

Accordingly, the motivation for this study was to further investigate the role of the thalamus in TN, as this structure is positioned proximal to CNV along the trigeminal pathway and may be involved in surgical outcome. We hypothesized that TN patients will exhibit characteristic structural and metabolic abnormalities in the thalamus, and further, that these abnormalities will be associated with surgical outcome. To test our hypothesis, we used structural MRI and ^{1}H-magnetic MRS to evaluate the thalamus in TN patients prior to surgery (the same TN patient cohort appearing in Chapter 4), to identify longitudinal changes in thalamus structure and metabolism occurring in the early postoperative period, and to examine the relationship of these features to durable postoperative pain relief.

5.2 Methods:

5.2.1 Study participants:

This was a prospective, longitudinal study of patients undergoing surgical treatment for TN at a single centre between 2017 and 2020, approved by the Health Research Ethics Board—Health Panel of the University of Alberta. Potential study patients were identified in clinic by any one of three neurosurgeons (authors TS, BMW, RB) and provided informed consent. *Inclusion criteria:* medically-refractory classical or idiopathic TN defined using ICHD-III criteria (1); scheduled for surgical treatment by MVD or BC. *Exclusion criteria:* confirmed multiple sclerosis or other lesional causes of TN; diagnosed psychiatric illness; history of any prior non-TN neurosurgical procedures. Additionally, 20 HC subjects matched to the TN group in mean age and sex distribution, and without chronic pain or psychiatric conditions, were recruited.

5.2.2 Data acquisition:

TN patients underwent MRI scanning within 1-month prior to surgery (*preoperative* time-point) and at 5-12 days following surgery (1-week *pos-operative* time-point). HC subjects underwent a single MRI scanning session. Scanning was carried out on a 3T Siemens Prisma Magnetom MRI scanner (Erlangen, Germany) with 64-channel head radiofrequency coil. At every MRI acquisition, participants underwent: 3D T1-weighted structural scan (MPRAGE, field-of-view (FOV) = 250 x 250mm^2, 208 sagittal slices, 0.85mm isotropic, TR = 1800ms, TE = 2.37ms, TI = 900ms, 8° flip angle, 3:41 min), and 2-dimentional multivoxel MRS scan centered over the VPM thalamus (see below for details) in the coronal-orientation (point-resolved spectroscopy (PRESS), FOV = 160 x 160mm^2, 1 slice, interpolated voxel size = 5mm

x 5mm x 10mm, TR = 1700ms, TE = 35ms, 90° flip angle, 1024 repetitions, 2 averages, time = 14:37min). Participants also completed a pain questionnaire describing pain attack frequency, location, and severity measured with a 0-100mm VAS. All participants were followed for at least 12-months after surgery.

5.2.3 Clinical characteristics and outcome assessment:

The following demographic/clinical data were collected: sex; age; duration of TN since diagnosis; side-of-pain; preoperative pain severity (measured using VAS); first (virgin) or repeat surgical treatment for TN; surgery type (MVD or BC); and medications. Additionally, we determined NVC severity scores for each patient based on the scoring system of Sindou et al. (0: no neurovascular contact or venous contact alone; 1: arterial contact with no indentation of nerve root; 2: arterial contact with displacement and distortion of nerve root; 3: arterial contact with marked indentation in nerve root) (235). NVC severity scores were derived by a single observer (author TS) by examining routine high resolution clinical preoperative T2 weighted MRI scans, confirmed (in patients undergoing MVD) by intraoperative findings as indicated in operative reports. Note that, in our practice, patients who are found to have no compressive arterial NVC at the time of MVD also undergo internal neurolysis. Study participants were classified as responders or non-responders as follows: *responders* – 1) documented evidence of immediate and persistent pain relief for at least one-year after surgery (BNI facial pain score IIIa or better) (117); and 2) no offer of or repeat surgical TN treatment; *non-responders* – 1) inadequate initial pain relief from surgery or early pain recurrence within one year of surgery; or 2) offered or underwent repeat surgical treatment within one year.

5.2.4 MRI analysis:

Automated thalamus volumetry and shape analysis: T1-weighted MPRAGE images were used for thalamus volume and shape assessment. Image orientation depended on the analysis performed: 1) *native orientation* analysis—images remained unflipped, in their native orientation; 2) *ipsilateral orientation* analysis—images from patients with left-sided TN were left-right flipped with FMRIB's FSL toolbox such that the side-of-pain was on the right side of the image, while images from right-sided TN patients were not flipped (163). This permitted ipsilateral to contralateral side-of-pain comparisons. FMRIB's FSL brain tissue segmentation toolbox SIENAX was used to generate brain tissue (grey matter, white matter, cerebrospinal fluid) volumes and an estimate of intracranial volume (v-scaling factor) (242). Thalamus segmentations were derived using FSL-FIRST, part of the FSL toolkit (http://fsl.fmrib.ox.ac.uk/fsl/fslwiki/) (162). FIRST is a model-based segmentation tool that uses shape- and appearance-based models constructed from manually segmented images (164). Quality control was performed for each patient by two expert raters (authors HD and JA), who inspected all thalamus segmentations; evidence of mis-segmentation resulted in subject exclusion from volumetric analysis. Shape analysis was performed using the vertex analysis extension of the FSL-FIRST toolbox with the standard recommended parameters in the FSL user guide (https://fsl.fmrib.ox.ac.uk/fsl/fslwiki/FIRST/UserGuide) (164). Vertex-wise shape analysis was designed to assess between-group differences on a per-vertex basis using a multi-variate General Linear Model. Meshes of the thalamus were generated for each subject, and to normalize for inter-individual head size differences the meshes were reconstructed in MNI space. $P < 0.05$ was considered statistically significant after correction for multiple comparisons (FWER) using a cluster-based approach.

Metabolic assessment of the thalamus: MRS images were used for metabolic assessment of the thalamus. Native orientation raw RDA image files for every time-point were processed using LCModel version 6.3-1L (243). Individual ^{1}H spectra were generated for every interpolated voxel acquired. For every patient at every time point, an MRS voxel (5 x 5 x 10mm) was placed bilaterally to encompass the left and right VPM thalamus, with the epicenter of each voxel defined according to the following atlas-based coordinates: x = 13mm lateral to the mid-commissural point, y = 4mm anterior to the posterior commissure, and z = 1mm inferior to the mid-commissural point (244) (**Figure 5.1**). Absolute concentrations of Choline (Cho), N-Acetylaspartate (NAA), and creatine (Cr) obtained from ^{1}H spectra within each target voxel were combined to generate relative intra-voxel concentrations of Cho/Cr and NAA/Cr (using Cr as an internal reference), and subsequently used for all MRS analyses. All ^{1}H spectra were visually inspected for quality control.

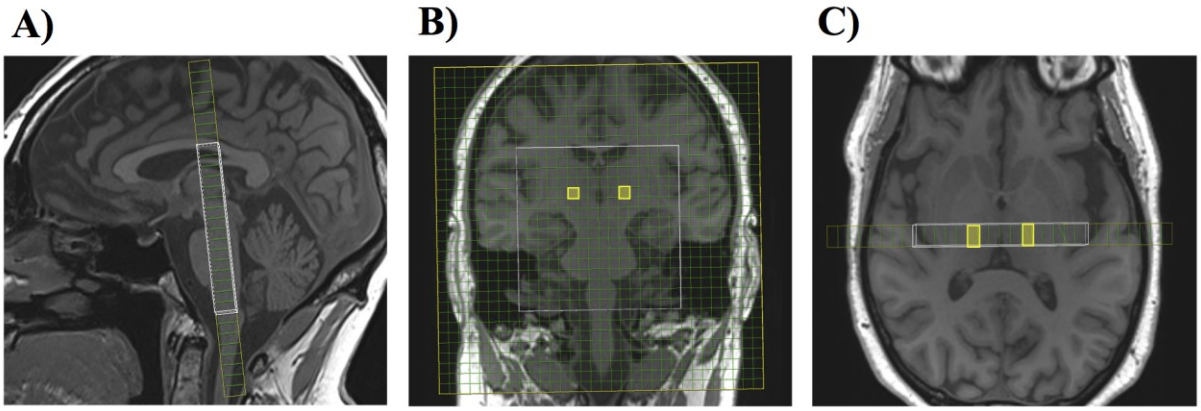

Figure 5.1: ^{1}H-MRS chemical shift image (CSI) slab placement and ventral posteromedial (VPM) thalamus voxel selection. CSI slab placement is shown in mid-sagittal (**A**), coronal (**B**), and axial (**C**) views, overlaid on T1-weighted MPRAGE images. Bilateral VPM thalamus voxel (indicated in yellow) is shown in coronal (**B**) and axial (**C**) views. This figure was produced from (236).

5.2.5 Statistical analysis:

Within-group left-versus-right, or ipsilateral-versus-contralateral, comparisons of thalamus volume and metabolite concentration were performed using Wilcoxon signed-rank tests. In left-versus-right comparisons, we also calculated inter-hemispheric percent differences in volume and metabolite concentrations, using the following formulas: 1) in left TN patients, %interhemispheric difference = (right – left) / left * 100; 2) in right TN patients, %interhemispheric difference = (left – right) / right * 100. For HC subjects, the selected formula depended on the desired between-group comparison (left-sided TN vs. left-HC, formula #1; right-sided TN vs. right-HC, formula #2). Between-group comparisons were performed using Mann-Whitney tests. Within-patient comparisons of preoperative versus 1-week postoperative thalamus metabolite concentrations were performed using Wilcoxon signed-rank tests. Clinical characteristics and demographic variables were compared using Mann-Whitney tests, as well as Chi-square or Fisher's exact test where appropriate. Statistical analyses were carried out with GraphPad Prism version 8 for Mac OS X (GraphPad Software, La Jolla California, USA). Statistical significance was set at $p < 0.050$ (2-tailed).

5.3 Results:

5.3.1 Study Participants:

Twenty-three TN patients and 20 HC were included in this study between 2017 and 2020 (**Table 5.1**). All 23 TN patients were included in the volumetric analysis, while only 19 TN

patients were included in the metabolite analysis because of inadequate spectral quality (n = 2) or failure to acquire MRS scans (n = 2).

5.3.2 Clinical characteristics and demographics:

All TN: Clinical and demographic features of all 23 TN patients and 20 HCs are presented in **Table 5.1**. TN and HC (14F/9M and 11F/9M, p = 0.70) groups were well matched in age (56.3 ± 10.4 years and 54.9 ± 9.4 years respectively, p = 0.65) and sex distribution.

Average TN duration was 5.3 ± 3.9 years, with right-sided TN being more common than left-sided TN (15R/8L). NVC was identified in 17/23 TN patients, and preoperative VAS was 77.6 ± 27.3 across the entire TN patient group. This study included virgin surgical procedures for 17/23 TN patients, with MVD most common (16 MVD, 7 BC). All TN patients were on antiepileptic medication at the time of surgery, including carbamazepine/oxcarbazepine (n = 21) and/or gabapentin/pregabalin (n = 12). Three TN patients were also on antidepressant/anxiolytic medication, six were on baclofen, one was taking opioids, and two others were taking cannabis oil.

By response to surgery: In total, there were 17 responders to surgery and 6 non-responders. Non-responders were exclusively female (6F/0M), while responders had a balanced sex distribution (8F/9M). Non-responders were younger than responders (47.4 ± 10.3 years and 58.6 ± 9.7 years respectively, p = 0.016), and showed a trend toward longer duration of TN compared to responders (8.8 ± 4.7 years versus 4.6 ± 3.3 years respectively, p = 0.061). NVC severity score was not statistically different between outcome groups (p = 0.64, Fisher's exact test), nor was frequency of surgery type (p = 0.32, Chi-square test). The proportion of patients taking baclofen was higher in non-responders than responders (p = 0.021), with no other

differences in medication use. Individual TN patient clinical profiles are presented in **Table 5.2**.

Table 5.1: Comparison of demographic and clinical characteristics between TN patients and healthy controls (HC), as well as within TN patients (responders vs. non-responders). Mann Whitney, and Chi-square or Fisher's-exact tests used where appropriate. Means ± standard deviations are presented. This table was produced from (236).

	Responders	**Non-Responders**	**P-value (2-tailed)**	**TN**	**HC**	**P-value (2-tailed)**
Total #	17	6	-	23	20	-
Sex (Female/Male)	8/9	6/0	0.048*	14/9	11/9	0.70
Age (years)	58.6 ± 9.7	47.4 ± 10.3	0.016*	56.3 ± 10.4	54.9 ± 9.4	0.65
Duration of TN (years)	4.6 ± 3.3	8.8 ± 4.7	0.061	5.3 ± 3.9	N/A	-
Side of pain (left/right)	6/11	2/4	>0.99	8/15	N/A	-
Pre-op VAS (mm)	80.7 ± 23.6	72.3 ± 37.2	0.53	78.5 ± 27.0	N/A	-
NVC (yes/no)	14/3	3/3	0.27	17/6	N/A	-
NVC score (0/1/2/3)	3/3/6/5	3/0/2/1	0.64	6/3/8/6	N/A	-
Virgin (yes/no)	14/3	3/3	0.28	17/6	N/A	-
Surgery type (MVD/BC)	13/4	3/3	0.32	16/7	N/A	-
Carbamazepine/ oxcarbazepine (yes/no)	15/2	6/0	>0.99	21/2	N/A	-
Gabapentin/pregabalin (yes/no)	7/10	5/1	0.16	12/11	N/A	-
Other antiepileptics (yes/no)	2/15	1/5	>0.99	3/20	N/A	-
Antidepressant (yes/no)	2/15	1/5	>0.99	3/20	N/A	-
Baclofen (yes/no)	2/15	4/2	0.021*	6/17	N/A	-
Opioid (yes/no)	0/17	1/5	0.26	1/22	N/A	-
Cannabis oil (yes/no)	1/16	1/5	0.46	2/21	N/A	-

NVC (yes/no): neurovascular compression; **NVC score** (0/1/2/3)(235): degree of neurovascular compression; **Virgin** (yes/no): first-time surgical treatment for TN; **MVD**: microvascular decompression; **BC**: balloon compression rhizotomy; **other antiepileptics**: lamotrigine, topiramate; **antidepressant**: amitriptyline, duloxetine.

Table 5.2: clinical characteristics of individual TN patients: This table was produced from (236).

	Sex	Age (years)	Side	Duration (years)	Pre-op VAS (mm)	Branch	NVC score	SX types	# prev. SX	Medications
Responders:										
1	M	57.5	R	6	66	3	2	MVD	0	carbamazepine
2	M	49.0	R	1	100	1/2/3	2	BC	3	oxcarbazepine, baclofen
3	M	45.1	L	9	98	1	2	MVD	0	carbamazepine, pregabalin
4	F	58.5	R	11	100	2/3	3	MVD	0	carbamazepine
5	M	63.9	R	8	82	1/2/3	2	MVD	0	carbamazepine
6	M	67.5	R	6	71	2/3	1	BC	1	carbamazepine
7	F	74.1	L	3	81	2	3	MVD	0	oxcarbazepine, pregabalin
8	F	65	R	1	93	3	1	MVD	0	gabapentin
9	F	60.3	L	6	36	2/3	3	MVD	1	gabapentin, amitriptyline
10	F	64.9	L	7	100	2/3	3	MVD	0	carbamazepine, gabapentin
11	F	60.4	L	7	86	2/3	2	MVD	0	carbamazepine, oxcarbazepine
12	F	60.4	R	15	80	2/3	0	BC	0	carbamazepine
13	M	41.8	R	2	89	1/2	2	MVD	0	carbamazepine, gabapentin, topiramate
14	F	68.5	L	1	100	3	1	MVD	0	carbamazepine
15	M	61.5	R	2.5	79	3	0	MVD/IN	0	carbamazepine
16	M	63.3	R	2.5	95	2/3	3	MVD	0	oxcarbazepine, lamotrigine, gabapentin
17	M	40.6	R	1	15	2/3	0	BC	0	carbamazepine, baclofen, duloxetine, cannabis oil
Non-Responders:										
18	F	37.3	L	6	63	2/3	0	MVD/IN	0	oxcarbazepine, baclofen
19	F	48.9	L	8	2	1/2/3	2	MVD	0	carbamazepine, gabapentin, baclofen

20	F	56.2	R	13	60	1/2/3	2	BC	1	carbamazepine, gabapentin, lamotrigine, baclofen, hydromorphone
21	F	55.5	R	3	100	1/2/3	0	BC	0	oxcarbazepine, gabapentin
22	F	57.5	R	13	100	1/2/3	0	BC	2	carbamazepine, gabapentin
23	F	36.3	R	3	89	2/3	3	MVD	0	carbamazepine, gabapentin, baclofen, amitriptyline, cannabis oil

M: male; **F**: female; **VAS**: visual analogue scale; **Branch**: affected trigeminal nerve branches; **NVC**: neurovascular compression; **SX**: surgical treatment; **MVD**: microvascular decompression; **BC**: balloon compression rhizotomy; **IN**: internal neurolysis

5.3.3 Thalamus structure:

Native orientation analysis: In HCs, the volume of the left thalamus was larger than the right (8209, 7895-9195 IQR and 7985, 7607-8974 IQR respectively; $p < 0.001$). There was no difference between left and right thalamus volume across all TN patients together (8077, 7590-8520 IQR and 8138, 7665-8506 IQR respectively; $p = 0.88$) (data not shown). The volume of the thalamus contralateral to the side-of-pain was larger in TN patients: in left TN patients (LTN) the right thalamus was larger than the left (8308, 8017-8633 IQR and 8111, 7641-8168 IQR respectively; $p = 0.008$); in right TN patients (RTN) the left thalamus was larger than the right (7895, 7485-8520 IQR and 8258, 7665-8858 IQR respectively; $p < 0.001$) (**Figure 5.2A**).

TN was associated with altered interhemispheric asymmetry of thalamic volume: left versus right thalamus interhemispheric % volume difference differed between HC and LTN patients (-3.1, -4.1 to -2.3 IQR; 3.9, 2.8-5.8 IQR; $p < 0.001$), while there was no difference between HC

and RTN patients (3.2, 2.4-4.3 IQR; 2.9, 2.3-4.0 IQR; p = 0.54) or between LTN and RTN (3.9, 2.8-5.8 IQR; 2.9, 2.3-4.0 IQR; p = 0.13) (**Figure 5.2B**).

Ipsilateral orientation analysis: After flipping the brains of left TN patients, we found no differences between average HC thalamus volume (8087, 7763-9084 IQR) and ipsilateral (ips) or contralateral (cont) thalamus volume of responders (ips: 8083, 7639-8348 IQR, p = 0.54; cont: 8365, 7944-8766 IQR, p = 0.48) or non-responders (ips: 7571, 6988-8461 IQR, p = 0.093; cont: 7810, 7239-8695 IQR, p = 0.32). Thalamus volume contralateral to the side-of-pain was larger than ipsilateral to the side-of-pain in both responders ($p < 0.001$) and non-responders ($p < 0.031$) (**Figure 5.3A**), though interhemispheric %volume difference did not differ between outcome groups (R: 2.9, 2.4-4.4 IQR; NR: 3.3, 2.8-4.6 IQR; p = 0.71) (**Figure 5.3B**). We did not observe any significant changes in thalamus volume between preoperative and 1-week postoperative time points in TN patients regardless of side-of-pain or surgical outcome (data not shown).

Intracranial volume: Intracranial volume as assessed using the v-scaling factor in FSL's SIENAX tool did not show any significant differences between any groups across all volumetric comparisons (data not shown).

Shape analysis: There were significant vertex-wise shape differences seen between the thalami of responders and non-responders (**Figure 5.4**). Non-responders showed significant contralateral thalamus volume reduction compared to responders in an axially-oriented band spanning the outer thalamic circumference made up of two clusters (peak p = 0.019).

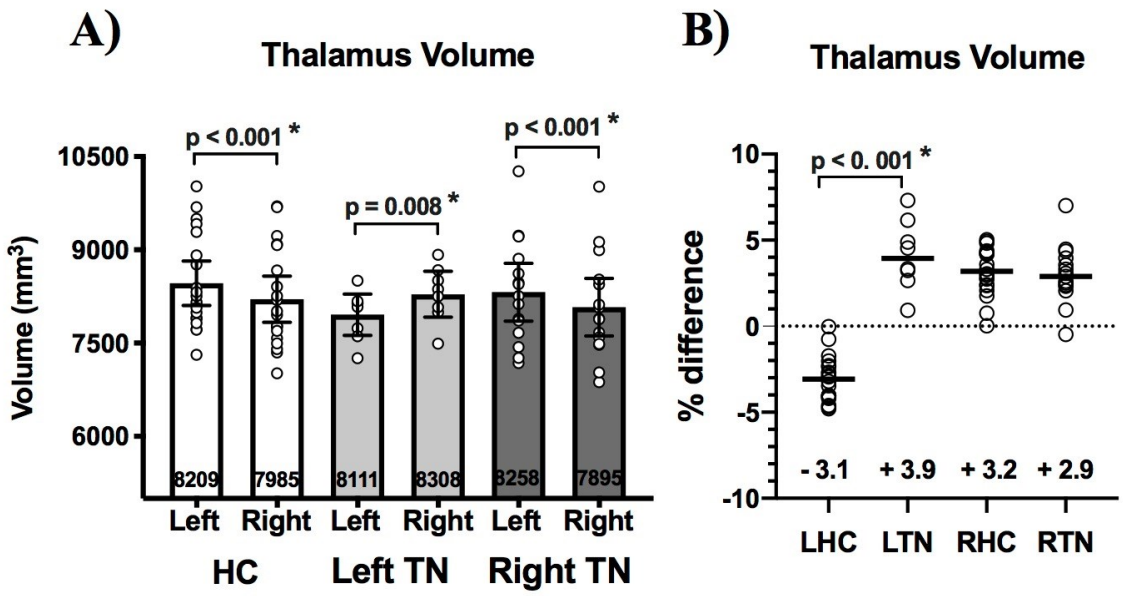

Figure 5.2: Preoperative thalamus volume in healthy controls (HC) and TN patients sorted by side-of-pain. (A) The left thalamus is larger than the right thalamus ($p < 0.001$) in healthy controls (HC). The contralateral thalamus is larger in TN patients regardless of the side-of-pain (left TN = LTN, right TN = RTN). **(B)** The left vs. right thalamus inter-hemispheric volume % difference differs ($p < 0.001$) between LTN and left-side healthy controls (LHC—see text for definition), while there is no difference in left vs. right thalamus inter-hemispheric % volume percentage difference between RTN and right-side healthy controls (RHC). Mann-Whitney tests were used to perform between-group comparisons, while Wilcoxon sign-rank tests were used to compare thalamus volumes within-groups. Statistical significance ($p < 0.05$) is indicated with *. Medians with interquartile ranges are displayed. This figure was produced from (236).

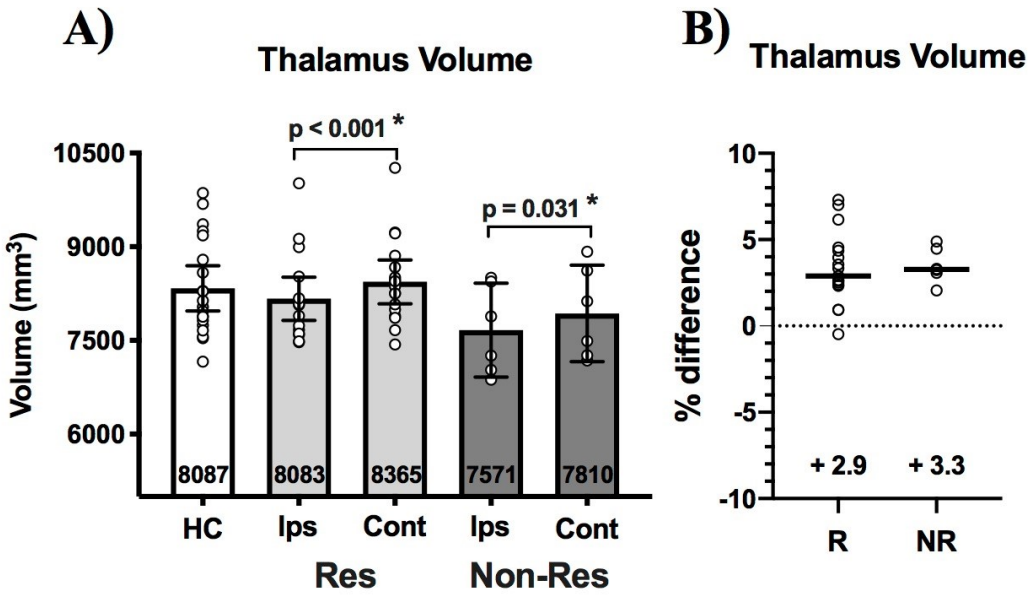

Figure 5.3: Preoperative thalamus volume in healthy controls (HC) and TN patients sorted by surgical outcome. There is no difference between HC thalamus volume (average of left and right thalamus) and ipsilateral or contralateral thalamus volume for either responders (Res—light grey bars) or non-responders (Non-Res—dark grey bars). **(A)** The contralateral thalamus is larger than the ipsilateral thalamus in both responders and non-responders. No differences were observed in thalamus volume between responders and non-responders, either ipsilaterally or contralaterally. **(B)** There is also no difference in left vs. right thalamus interhemispheric % volume difference between responders and non-responders. Mann-Whitney tests were used to perform between-group comparisons, while Wilcoxon sign-rank tests were used to compare thalamus volumes within-groups. Statistical significance ($p < 0.05$) is indicated with *. Medians with interquartile ranges are displayed. This figure was produced from (236).

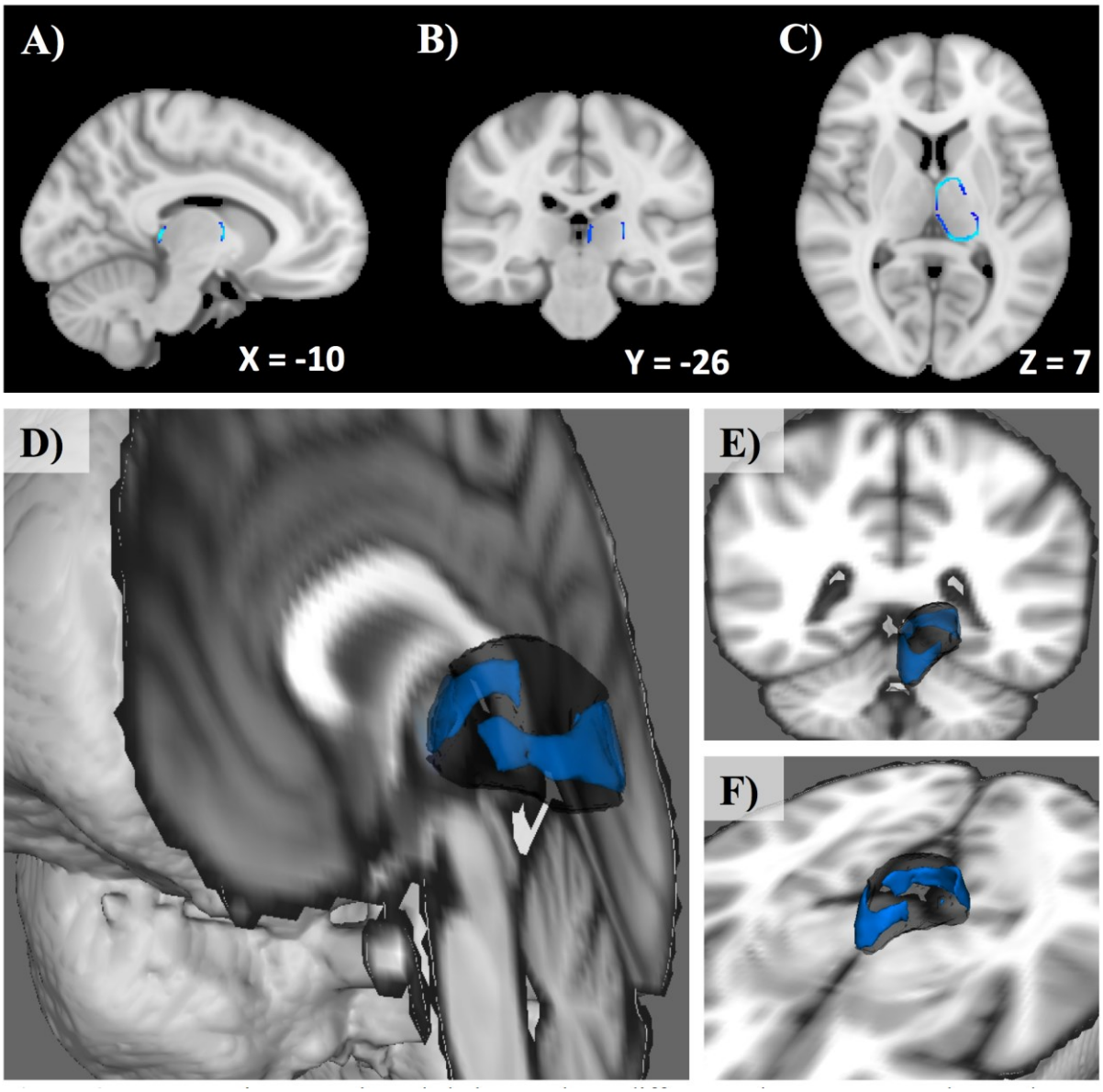

Figure 5.4: Preoperative contralateral thalamus shape differences between responders and non-responders to surgical treatment for TN. Results are overlaid on Montreal Neurological Institute (MNI) standard space and are displayed in sagittal- (**A**), coronal- (**B**), and axial-views (**C**). Contralateral thalamus volume loss is observed (blue, $p<0.05$) in non-responders compared to responders within an axially-oriented band spanning the outer thalamic circumference made up of two voxel clusters (peak p-value = 0.019), shown in 3-D renderings of the thalamus in **D-F**. MNI coordinates of cross-sectional slice are displayed in figures **A-C**. This figure was produced from (236).

5.3.4 Thalamus Metabolism:

Native orientation analysis: There was no preoperative difference in Cho/Cr between left and right VPM thalamus in HC, RTN, or LTN patients. Overall, across HC and TN patients, there was no difference in mean Cho/Cr (**Figure 5.5A**), nor any difference in %inter-hemispheric Cho/Cr difference between LHC and LTN patients (**Figure 5.5B**).

In HCs, there was a trend towards left greater than right VPM thalamus NAA/Cr (1.97, 1.88-2.28 IQR and 1.86, 1.63-2.04 IQR respectively; $p = 0.060$). There was no difference between left and right NAA/Cr in LTN or RTN patients. Left thalamus NAA/Cr was higher in HC compared to RTN patients ($p = 0.050$). Additionally, NAA/Cr of the left (ipsilateral) VPM thalamus in LTN patients was greater than the left (contralateral) and right (ipsilateral) VPM thalamus in RTN patients ($p = 0.029$ and $p = 0.010$ respectively). There were no other between-group differences (**Figure 5.5C and D**).

Ipsilateral orientation analysis: There were no differences between preoperative ipsilateral and contralateral VPM thalamus Cho/Cr in responders or non-responders. However, preoperative ipsilateral Cho/Cr in non-responders (0.88, 0.78-1.06 IQR) was reduced compared to HCs (1.02, 0.98-1.13 IQR; $p = 0.038$). There were no other between-group or within-group between-side thalamus Cho/Cr differences (**Figure 5.6A and B**).

There were no differences between ipsilateral and contralateral VPM thalamus NAA/Cr in responders or non-responders, and no other between-group or within-group between-side thalamus NAA/Cr differences (**Figure 5.6C and D**).

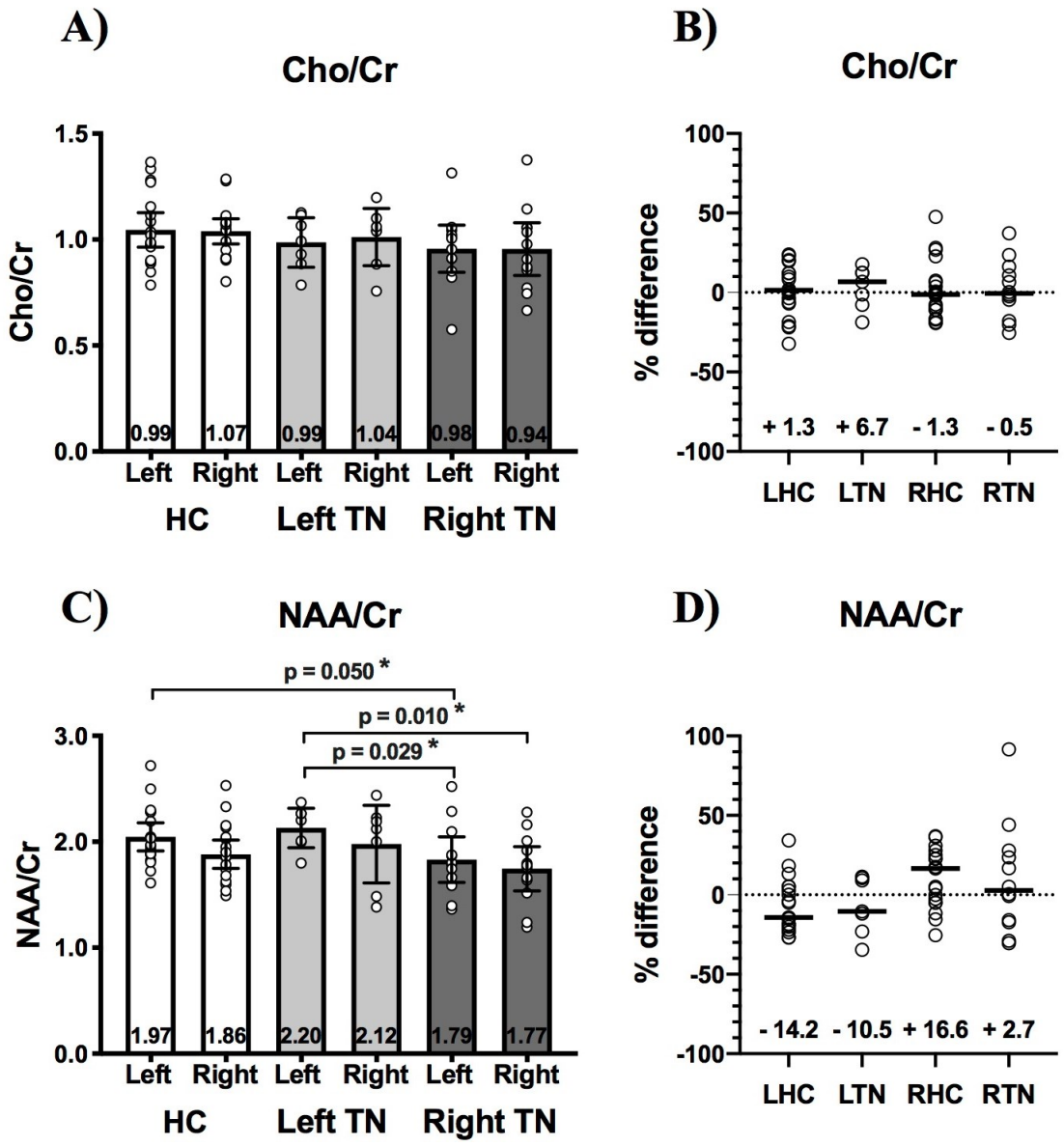

Figure 5.5: Preoperative thalamus Cho/Cr and NAA/Cr in healthy controls (HC) and TN patients sorted by side-of-pain. (**A)** There is no difference in Cho/Cr between the left and right thalamus within healthy controls (HC), left-sided TN patients (LTN), or right-sided TN patients (RTN). Additionally, there is no difference in thalamus Cho/Cr between any of these groups. (**C)** Left NAA/Cr is increased in HC compared to RTN ($p = 0.050$). NAA/Cr of the left thalamus is increased in LTN patients compared to both the left ($p = 0.029$) and right ($p = 0.010$) thalamus of RTN patients. Left vs. right interhemispheric % difference for Cho/Cr (**B**) or NAA/Cr (**D**) does not differ between left healthy controls (LHC) and LTN or right healthy controls (RHC) and RTN. Mann-Whitney tests were used to perform between-group comparisons, while Wilcoxon sign-rank tests were used to compare thalamus volumes within-groups. Statistical significance ($p < 0.05$) is indicated with *. Medians with interquartile ranges are displayed. This figure was produced from (236).

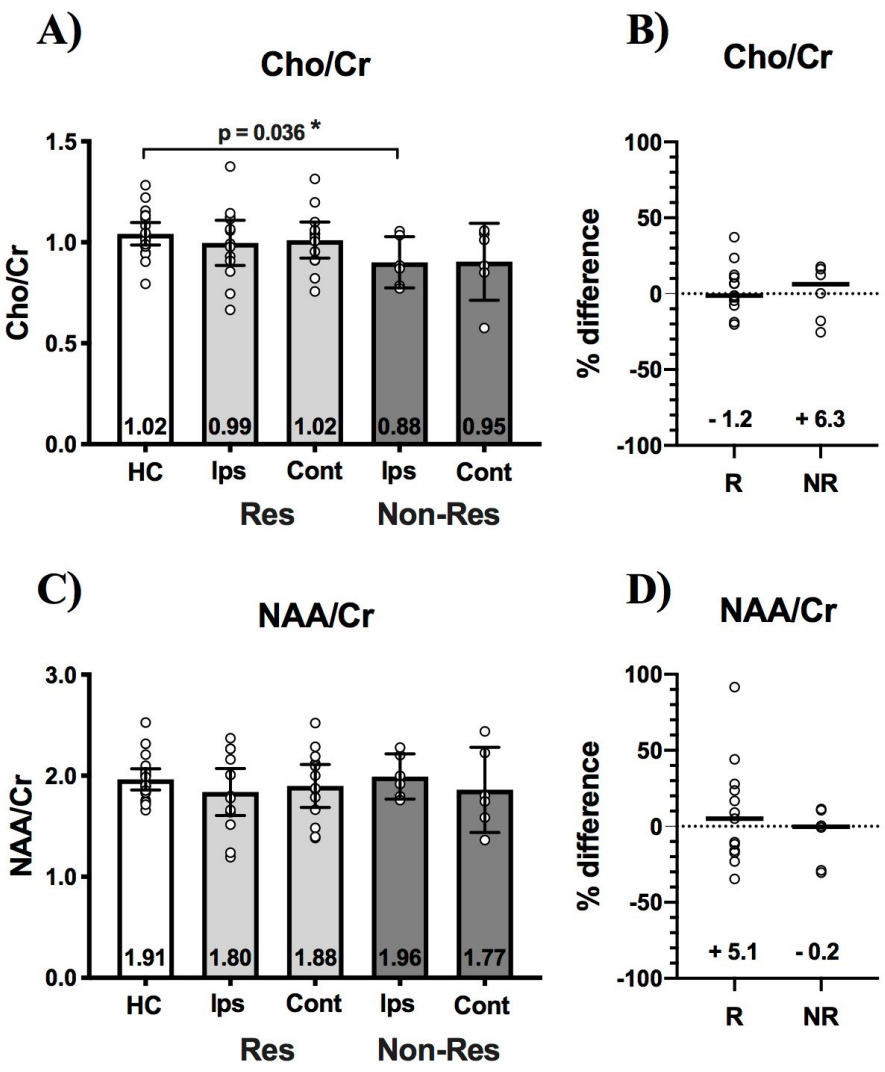

Figure 5.6: Preoperative thalamus Cho/Cr and NAA/Cr in healthy controls (HC) and TN patients sorted by surgical outcome. (A) Compared to healthy controls (HC), Cho/Cr in non-responders (Non-Res—dark grey bars) is reduced ipsilateral (Ips) to the side-of-pain ($p = 0.038$). There are no between-side differences in thalamus Cho/Cr for either responders (Res—light grey bars) or non-responders. **(C)** There are no between-group or within-group between-side (Ips vs. Cont) differences in thalamus NAA/Cr. Left vs. right interhemispheric % difference for Cho/Cr (**B**) or NAA/Cr (**D**) does not differ between responders (R) and non-responders (NR). Mann-Whitney tests were used to perform between-group comparisons, while Wilcoxon sign-rank tests were used to compare thalamus volumes within-groups. Statistical significance ($p < 0.05$) is indicated with *. Medians with interquartile ranges are displayed. This figure was produced from (236).

Postoperative metabolite change at 1-week: Preoperatively, average VPM thalamus Cho/Cr in HCs did not differ compared to preoperative contralateral Cho/Cr in either responders or non-responders (**Figure 5.7A**). Furthermore, preoperative contralateral Cho/Cr did not differ between responders and non-responders ($p = 0.32$). One week after surgery, Cho/Cr in non-responders was significantly lower than in responders (0.83, 0.67-0.97 IQR and 1.04, 0.93-1.17 IQR respectively; $p = 0.038$) and HCs ($p = 0.005$), and every single non-responder showed a reduction in Cho/Cr irrespective of surgical procedure type ($n = 3$ MVD and $n = 3$ BC). Conversely, responders showed no Cho/Cr change with surgery ($p = 0.57$). (**Figure 5.7A-C**).

Mirroring Cho/Cr, preoperative average VPM thalamus NAA/Cr in HCs did not differ compared to preoperative contralateral VPM thalamus NAA/Cr in responders or non-responders (**Figure 5.7D**). Furthermore, preoperative contralateral VPM thalamus NAA/Cr did not differ between responders and non-responders ($p = 0.77$). One week after surgery, NAA/Cr in non-responders was significantly lower than in responders (1.94, 1.83-2.41 IQR and 1.59, 1.37-1.79 IQR respectively; $p = 0.038$) and HCs ($p = 0.005$), and every single non-responder showed a reduction in NAA/Cr irrespective of surgical procedure type ($n = 3$ MVD and $n = 3$ BC). Conversely, responders showed no NAA/Cr change with surgery ($p = 0.20$). (**Figure 5.7D-F**).

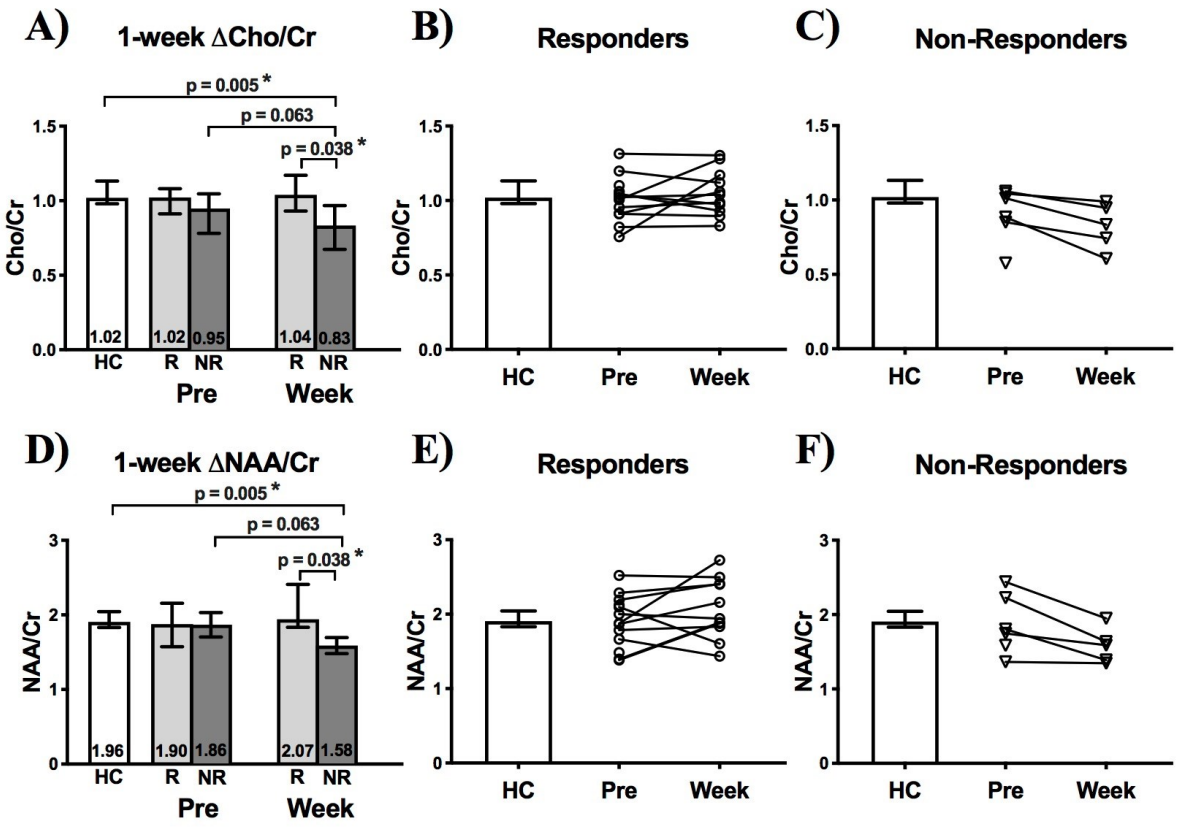

Figure 5.7: Perioperative contralateral thalamus Cho/Cr and NAA/Cr change in TN patients 1-week following surgical treatment. (A) A strong trend suggests that Cho/Cr decreases in non-responders (NR—dark grey bars) 1-week after surgery ($p = 0.063$), at which point Cho/Cr differs ($p = 0.038$) from responders (R—light grey bars). **(B)** Cho/Cr either increases or decreases in responders at the individual-subject level, while **(C)** all non-responders show a decrease in Cho/Cr. **(D)** A strong trend suggests that NAA/Cr decreases in non-responders 1-week after surgery ($p = 0.063$), at which point NAA/Cr differs ($p = 0.038$) from responders. **(E)** NAA/Cr either increases or decreases in responders at the individual-subject level, while **(F)** all non-responders show a decrease in NAA/Cr. Mann-Whitney tests were used to perform between-group comparisons, while Wilcoxon sign-rank tests were used to compare thalamus volumes within-groups. Statistical significance ($p < 0.05$) is indicated with *. Medians with interquartile ranges are displayed. This figure was produced from (236).

5.4 Discussion:

In this single-centre, prospective, longitudinal study, we identified several abnormalities of thalamic structure and metabolism in medically-refractory TN patients undergoing surgery. Preoperatively, TN patients showed increased thalamus volume contralateral to the painful side of the face, confirming the findings in Chapter 6 (238). Shape analysis showed characteristic areas of the contralateral thalamus that were larger in responders to surgery compared to non-responders who experienced early pain recurrence. Metabolically, right-sided TN patients showed reduced NAA/Cr concentration in the contralateral left VPM thalamus, but this was not observed for left-sided TN patients. Non-responders to surgery showed significantly reduced preoperative ipsilateral VPM thalamus Cho/Cr. Following surgery, we found novel evidence of metabolic changes in the VPM thalamus occurring as early as one-week after either MVD or BC. These changes—specifically a significant reduction in Cho/Cr and NAA/Cr—were observed only in non-responders, suggesting that surgery for TN has variable effects on thalamic metabolism which may impact long-term pain outcome.

Overall, our patients demonstrated a 74% surgical response rate, in agreement with prior literature, notwithstanding differences in how surgical outcome is measured between different studies (98). All TN patients were taking antiepileptic medication, and while medication use was largely the same between responders and non-responders, a greater proportion of non-responders were also taking baclofen, perhaps reflecting more exhaustive attempts at medical management. In line with previous reports, non-responders were more likely to be female, younger at the time of surgery, and had TN for nearly twice as long as responders (125). NVC was identified on preoperative MRI in 17 of 23 TN patients. At a group-wide level, there was no significant difference in NVC severity between responders and non-responders. However,

it is worth noting that 50% of non-responders (3/6) but only 18% of responders (3/17) had no evidence of arterial NVC (i.e., NVC score 0), which may represent a relevant if not statistically significant difference. On reviewing these particular patients in greater detail, there were no obvious clinical or surgical factors that could explain response other than that all 3 non-responders with NVC score 0 were female. Interestingly, patient #23 was the only non-responder with NVC score 3 (i.e., distortion); again, this patient was female, and experienced pain recurrence within one year despite technically successful (i.e., confirmed on postoperative imaging) MVD. Taken together, our data are consistent with the notion that some female patients with a diagnosis of TN—whether in association with true NVC or not—may have a particularly treatment-resistant manifestation of the disease, perhaps explained by a distinct, though as yet unknown, pathophysiology (85).

Despite the established role of the thalamus in chronic and neuropathic pain (195), and as a component of the trigeminal sensory system, there have been few in-depth investigations of thalamic structure in TN (198,201). We found no whole-thalamus volume differences between HCs and TN patients, aligning with the previous work of Gustin *et al.* (198). We did observe left-right volume asymmetry in HCs, which has been observed with many other subcortical structures (e.g., hippocampus), and may reflect normal functional and structural lateralization in the healthy brain. In line with our previous retrospective report (238), we also observed that the contralateral thalamus was larger across all TN patients, irrespective of the side-of-pain. Accordingly, it would appear that relative side (i.e., ipsilateral/contralateral) is the primary determinant of structural thalamic asymmetry in TN patients, possibly reflecting thalamic enlargement that is the result of sustained hyperactivity in the trigeminal system (216,245). These data also confirm that the trigeminal system is affected at least as far upstream as the

nuclei of third-order neurons residing in the contralateral thalamus. Prior to surgery, our data did not show clear evidence of differences in whole-thalamus volume between responders and non-responders, though more detailed vertex-wise shape analysis revealed a significant, circumferential band of contralateral thalamic volume loss in non-responders compared to responders. Given the small number of non-responders (n=6), our study was likely underpowered to show statistically significant reductions in whole thalamus volume. However, the robust shape differences we observed suggest that non-responders have a structurally different contralateral thalamus which may play a role in conferring treatment resistance. Given a reasonable degree of spatial overlap of this circumferential band with the VPM and medial dorsal nuclei, we speculate that volume loss may represent a form of trigeminal system injury—perhaps the result of prolonged chronic TN pain—which is more noticeable in non-responders, in whom it potentially dampens the effect of surgical interventions carried out at more peripheral locations (i.e., at the level of CNV). However, the lack of any significant difference in preoperative pain severity (measured using the VAS) between responders and non-responders, would suggest that focal thalamic volume loss of this nature does not seem to alter pain relay function in the trigeminal system per se.

Unlike thalamic volume, we did not observe robust evidence of inter-hemipsheric asymmetry in metabolite concentrations of either Cho/Cr or NAA/Cr in the VPM thalamus in HC or TN patients preoperatively. A trend suggests that NAA/Cr—an indicator of neuronal viability and number (152)—may be elevated in the left thalamus of HCs ($p = 0.060$), and may be further evidence of normal asymmetry between the left and right thalamus in humans. We did find that NAA/Cr was reduced in the contralateral left VPM thalamus in right-sided TN patients, perhaps reflecting reduced thalamic neuronal integrity associated with the chronic pain state. However,

we did not observe this in left-sided TN patients, perhaps due to the smaller number of LTN patients in our cohort (n=8). In line with our results, Wang *et al.* also found reductions in "posterior medial" and "posterior lateral" contralateral thalamus NAA/Cr in TN patients versus HC, and similarly found no difference in Cho/Cr—a marker of membrane turnover believed to indicate a heightened state of cellular proliferation or inflammation—between these groups (153,200). Of note, Wang *et al.* did not limit their analysis to the VPM thalamus, using instead a multi-voxel MRS approach to examine several different thalamic subdivisions, though there is considerable spatial overlap between the VPM as we defined it and their "posterior medial" thalamus.

We found novel metabolic alterations in the thalamus which appear to be implicated in durable response to surgery for TN. First, we observed that non-responders had significantly lower preoperative Cho/Cr concentration compared to HCs in the VPM thalamus ipsilateral to the side-of-pain. At first glance, this finding seems counterintuitive, since the bulk of trigeminal afferents to the VPM carry sensory information from the contralateral side of the face. That being said, there is neuroanatomical evidence that the smaller, ipsilateral dorsal trigeminothalamic tract containing non-decussating fibers may be implicated in orofacial pain (30), and recent *in situ* tractography results show ipsilateral thalamo-cortical diffusivity abnormalities in TN (201). Our current observations add to these findings, and further link surgical response to bilateral, system-wide changes in the trigeminal system.

Our most interesting finding is that of very early (1-week) metabolic changes occurring following TN surgery. While thalamus volume remained constant over this time interval, both contralateral Cho/Cr and NAA/Cr showed divergent changes between responders and non-responders: all non-responders had 1-week decreases in both metabolites, while responders

maintained stable concentrations postoperatively. We speculate that these findings further suggest—in conjunction with shape analysis results—that there exists a degree of injury to the contralateral thalamus in patients with highly refractory and surgically resistant TN, which prevents it from responding appropriately to upstream surgical interventions.

Our study is limited by a relatively small sample size of 23 TN patients (19 in MRS analysis) and 20 HCs, and our findings will need to be replicated in larger TN datasets. However, our sample size is comparable to other prospective MRI-based studies of the thalamus in TN (198,200,201). Another possible limitation is the heterogeneity of the TN group, which included patients who underwent different types of surgical procedures (MVD and BC), and in some cases repeat surgery. That being said, we did not observe any difference in thalamic volume or metabolite concentrations between patients treated with different surgical approaches, or undergoing non-virgin surgical treatment, suggesting that the central role of the thalamus in treatment responsiveness—or resistance—may be independent of interventions carried out more peripherally in the trigeminal system. Furthermore, while group-level medication-class use was largely the same between responders and non-responders, we did not have access to data on exact medication dosage and duration of use—both of which could have influenced the thalamic structural and metabolic abnormalities we observed—and could not correct for these in our statistical analyses. Finally, we defined responders as patients who continued to have satisfactory pain relief at one-year following surgery, though it is certainly possible that some of these patients could have gone on to have significant pain recurrence at more delayed follow-up.

5.5 Conclusion:

Our findings confirm that trigeminal system abnormalities exist in TN patients as far upstream as the thalamus, evidenced by structural and metabolic alterations primarily—though not exclusively—in the thalamus contralateral to the side-of-pain. TN patients who respond inadequately to surgery exhibit baseline differences in thalamic shape, and differing trajectories of early postoperative change in thalamic metabolism, compared to responders. We conclude that the thalamus has a critical role to play in the pathophysiology of TN and its response to surgical treatment. The clinical implications of this finding at the individual subject level are an important topic for further research.

CHAPTER 6: Hippocampal and Trigeminal Nerve Volume Predict Outcome of Surgical Treatment for Trigeminal Neuralgia

Modified with permission from (238): Danyluk H, Lee EK, Wong S, Sajida S, Broad R, Wheatley M, et al. Hippocampal and trigeminal nerve volume predict outcome of surgical treatment for trigeminal neuralgia. Cephalalgia. 2020;40(6):586–96.

6.1 Introduction:

A substantial proportion of TN patients become refractory to medical treatment over time, and are treated with neurosurgical procedures targeting CNV directly, including MVD, PR, or SRS. Unfortunately, pain recurrence following technically successful surgery is common: even with MVD—the most efficacious surgical treatment for TN—early recurrence within 2 years of treatment occurs in approximately 25% of patients, with a 4% per year failure rate thereafter (98). The presence and degree of NVC on preoperative imaging has been shown to be a predictor of positive outcome following MVD for TN (124). However, NVC of CNV in non-lesional TN is absent in as many as 28.8% of patients (41). Furthermore, a non-trivial minority of classical TN patients with prominent NVC do not achieve long-term pain relief following technically successful MVD surgery (98). Predicting surgical response in patients undergoing TN surgery remains an unmet challenge. Solving this challenge could, in turn, improve our ability to counsel TN patients regarding prognosis following surgery, improve our ability to match patients with the best surgical treatment strategy, and ultimately, to identify factors which may improve the durability of pain relief after surgery.

Neuroimaging using MRI provides a non-invasive means of generating objective biomarkers of eventual response to surgery for TN, although to date, no neuroimaging metrics have consistently been able to predict postoperative pain relief. While CNV volume and CSA are consistently reduced on the affected side in patients with TN (56,175), the exact relationship between these simple nerve-based measures and surgical outcome has been conflicting (175–179). Studies have also identified microstructural alterations in CNV using DTI and suggest that these measures may be related to surgical outcome (62,189,193). However, methodological challenges outlined in detail in Chapters 3 and 4 question the validity of these studies' findings. In either case, quantitative DTI approaches are disadvantaged because their implementation requires a non-trivial degree of image processing expertise, and further, because DTI acquisitions are not typically part of the routine clinical workup for TN patients.

Surprisingly, all previous attempts at predicting long-term pain response from preoperative imaging alone have failed to consider the potential importance of several grey matter brain regions involved in TN and other chronic pain conditions (e.g., insula, cingulate, amygdala, and parahippocampal region, among others) (185,208,218,223). Despite having identified that brain changes occur with successful surgical treatment of TN and other chronic pain conditions (62,210), no studies to date have looked at how preoperative brain and CNV features may interact to influence surgical outcome (223).

Our central hypothesis is that TN patients who do not respond to surgical treatment can be characterized by distinct neuroanatomical features—manifest both in CNV and at the brain-wide level—which distinguish them from patients who experience long-term pain relief. In the present study, we aim to identify these neuroanatomical features by performing quantitative analysis of routinely acquired clinical MRI scans obtained in TN patients prior to surgery.

Specifically, we focused on differences between surgical responders and non-responders in CNV volume, as well as the volumes of three subcortical brain structures involved in trigeminal sensory relay (thalamus) or as potential contributors to limbic components of chronic pain (hippocampus, amygdala).

6.2 Methods:

6.2.1 Study participants and data-acquisition:

This was a single-centre, retrospective study of patients treated surgically for TN at the University of Alberta Hospital between 2005 and 2018, approved by the Research Ethics Board of the University of Alberta. All patients had medically-refractory classical or idiopathic TN as defined by ICHD-III criteria (1). Potential study participants were identified from an operative database, and were included if they had undergone MVD surgery performed by any one of 3 experienced neurosurgeons, had proof of successful technical completion of surgery according to operative notes, and underwent preoperative brain MRI scanning no more than 12-months prior to surgery. Patients with a history of multiple sclerosis or other lesional cause of TN (e.g., brain tumor), or who had undergone any previous non-TN neurosurgical procedures were excluded. Demographic and clinical data were obtained from physical and electronic patient charts. Patients were only included in the study once, even if they had undergone multiple TN procedures. In such cases, brain imaging collected prior to the first surgical procedure—if available—was used for analysis, and response following this same initial procedure was used to define treatment outcome. If preoperative imaging was not available for the first attempted surgical treatment, preoperative imaging collected from the earliest possible surgical treatment

thereafter was used for analysis, and response from this same procedure was used to define treatment outcome.

6.2.2 Clinical characteristics and outcome assessment:

The following demographic and clinical data were collected: sex, age at preoperative MRI, duration of TN, affected side, presence of NVC, first (virgin) surgical treatment, time-to-surgery, intracranial volume (ICV) and medications at time of preoperative MRI (divided by medication class, i.e., antiepileptic, antidepressant, opioid, baclofen). Duration of TN was defined as the amount of time between the date of initial TN diagnosis to the date of preoperative brain MRI acquisition, and time-to-surgery was defined as the amount of time between preoperative imaging and the date surgery was performed. Patients were classified as responders or non-responders according to the following criteria: *responders* – documented evidence of initial pain relief following surgery, no evidence of documented pain recurrence within one-year of surgery (BNI facial pain score IIIa or better), and no evidence of repeat (or offer of repeat) surgical treatment within one-year of surgery; *non-responders*–documented evidence of inadequate initial pain relief following surgery OR offered or received repeat surgical treatment within one year of initial surgery OR documented evidence of pain recurrence following initial pain relief during that one-year period.

6.2.3 Quantitative MRI Analysis:

6.2.3.1 Subcortical volumetric analysis:

Preoperative 1.5T T1-weighted MPRAGE or SPGR MRI scans (voxel size 1 x 1 x 1mm) without contrast were used for subcortical structural analysis. DICOM images for each patient

were obtained from institutional PACS (Picture Archiving and Communication System), converted to NIFTII format, and reoriented as follows: images from patients with left-sided TN were flipped in the axial plane with FMRIB's FSL toolbox (163), while images from patients with right-sided TN remained in native orientation. FMRIB's FSL (163) brain tissue segmentation tool SIENAX (242) was used to generate brain tissue (grey matter, white matter, cerebrospinal fluid) volumes and an estimate of ICV called the v-scaling factor. Bilateral hippocampus, amygdala, and thalamus volumes were determined using FSL-FIRST (164). Quality control was performed for each patient by two expert raters (authors HD and CE) who inspected all subcortical segmentations; evidence of mis-segmentation in any structure resulted in subject exclusion from all future analyses. Subcortical structure volumes were calculated for comparison in the following ways: ipsilateral and contralateral to the side-of-pain, and total structure volume (ipsilateral + contralateral).

6.2.3.2 Trigeminal nerve volume analysis:

Preoperative 1.5T T2-weighted CISS or FIESTA images (0.67 x 0.67 x 1mm) were used for CNV volume analysis. Manual segmentation of CNV from its emergence at the pons to its entry at Meckel's cave (i.e., the entire cisternal segment) was performed with the ITK-SNAP toolbox (231). CNV volume was computed from slice-by-slice tracing of the nerve in the axial plane by author EL using the *Polygon Mode* tool. Intra-rater reliability testing was assessed by resegmentation of CNV by the same rater in 10 random subjects 3-months following initial segmentation. Inter-rater reliability was assessed by resegmentation of CNV in 10 random subjects by a second trained rater (author SW). Intraclass correlation coefficients (ICC) were calculated using a two-way, mixed effects model, and measures are reported for average measure using absolute agreement. Nerve volumes were calculated for comparison in the

following ways: ipsilateral and contralateral to the side-of-pain, total nerve volume (ipsilateral + contralateral), and % difference ((ipsilateral – contralateral / ipsilateral) x 100).

6.2.4 Statistical Analysis:

Within-patient inter-side comparisons: within-patient comparisons of ipsilateral versus contralateral volumes were performed separately for nerve and subcortical structures using repeated-measures one-way analysis of covariance (ANCOVA) [IBM SPSS Statistics for Mac OS X, version 24, IBM Corp., Armonk, N.Y., USA]. Demographic variables that differed between treatment outcome groups were included as covariates (i.e., ICV and number of previous surgical procedures for TN).

Comparisons between treatment outcome groups: CNV volumes were compared between responder and non-responder groups using one-way ANCOVA. Subcortical structure volumes were compared between responders and non-responders using multivariate-ANCOVA [MANCOVA, IBM SPSS Statistics for Mac OS X, version 24, IBM Corp., Armonk, N.Y., USA]. The independent variables of interest were: hippocampus, amygdala, and thalamus volumes. The dependent outcome variable of interest was response versus non-response. Three separate MANCOVAs were performed, one for each of the following "sides": ipsilateral, contralateral, and total. Demographic and clinical variables that differed between outcome groups were included as covariates (i.e., ICV and number of previous surgical procedures for TN).

Significance levels and correction for multiple comparisons: for repeated-measures ANCOVA comparing ipsilateral vs contralateral nerve volumes, statistical significance was set at a threshold of $p < 0.05$. For repeated-measures ANCOVA comparing ipsilateral vs contralateral

subcortical structure volumes (hippocampus, amygdala, thalamus), statistical significance was set at a threshold of $p < 0.017$ (i.e., 0.05/3, Bonferroni correction for three comparisons). Bonferroni correction was applied for between-treatment outcome comparisons of subcortical structure volumes (using MANCOVA) to generate adjusted p-values. The threshold for statistical significance for this comparison was therefore $p < 0.05$.

Outcome prediction: The ability of preoperative CNV and subcortical structure volumes to classify response versus non-response was assessed using receiver-operator characteristic curve (ROC) analysis [GraphPad Prism version 7 for Mac OS X, GraphPad Software, La Jolla California, USA]; the combined ability of CNV and subcortical structure volume to predict outcome was assessed using binomial logistic regression analysis [IBM SPSS Statistics for Mac OS X, version 24, IBM Corp., Armonk, N.Y., USA].

6.3 Results:

6.3.1 Study participants:

We identified 359 TN patients treated with surgery between 2005 and 2018 as potential study subjects (**Figure 6.1**). Forty-two had suitable preoperative T1-weighted imaging without contrast. Five patients had a potential lesional cause of TN identified and were excluded (4 multiple sclerosis and 1 tumor). Thirty-seven classical or idiopathic TN patients underwent FIRST automated segmentation. Quality assurance identified gross mis-segmentations in 3 subjects, who were excluded from further analyses. In total, 34 TN patients proceeded to subcortical volume analysis. High-resolution T2-weighted imaging is typically the first MRI acquisition performed in TN patients referred for neurosurgical assessment; as a consequence,

3 of the 34 patients included in the subcortical analysis had outdated T2-weighted imaging acquired more than 12-months months prior to surgical intervention. Thus, only a 31 patient subgroup could also be included for CNV analysis (**Figure 6.1**).

6.3.2 Clinical characteristics and demographics:

Thirty-four TN patients were included in all subcortical volumetric analyses (**Table 6.1**). Twenty-three were responders and 11 were non-responders. Thirty-two patients had NVC identified, and therefore had classical TN, while NVC was not present in two remaining

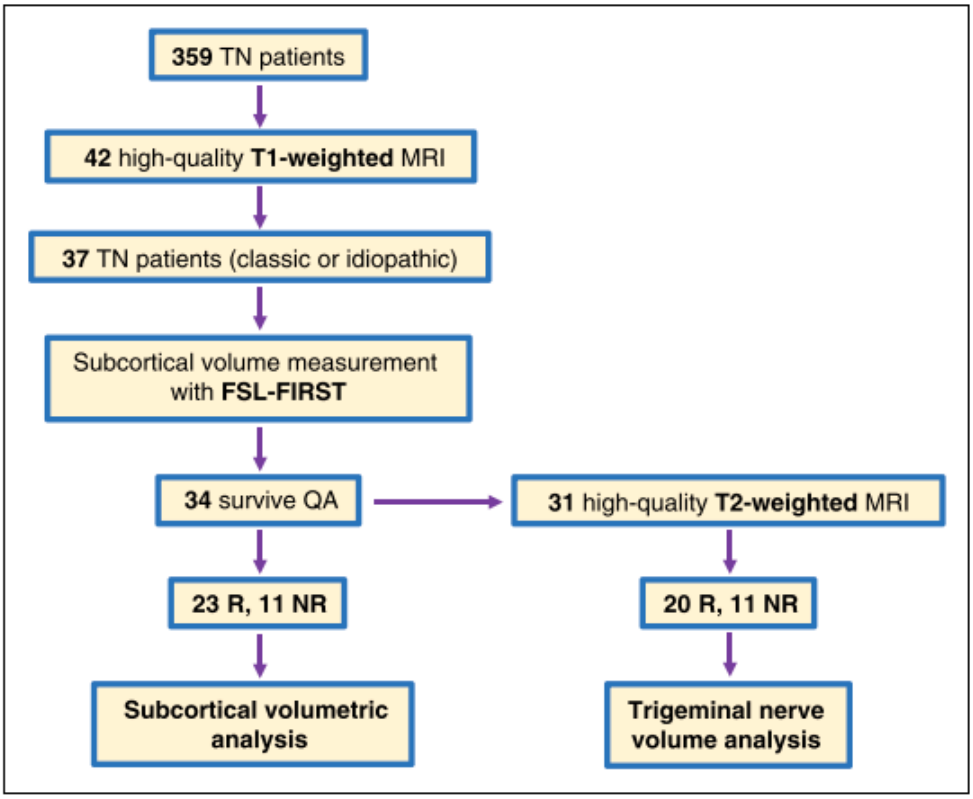

Figure 6.1: Patient selection for subcortical and CNV volumetric analysis. NR – non-responder; R – responder; QA – quality assurance. This figure was reproduced from (238) with permission from SAGE Journals.

idiopathic TN patients. Responder and non-responder groups did not differ in sex distribution, mean age at surgery, duration of TN, side-of-pain, NVC, time-to-surgery, and medication classes used at the time of preoperative MRI. ICV was found to be larger on average in non-responders ($p = 0.025$). Additionally, a greater proportion of non-responders had previously undergone surgical treatments for TN (n=4 instances of previous percutaneous rhizotomy in the non-responder group versus n=0 prior surgical treatments in responder group; $p = 0.007$). Accordingly, ICV and number of previous surgical treatments were added as cofactors in subsequent analyses (**Table 6.1**).

Table 6.1: Demographic and clinical Characteristics of TN patients included in subcortical volumetric analysis. Values represent mean ± standard deviation where appropriate. Student's T-test (with Welch's correction) used where appropriate. Fisher's exact test used for all categorical comparisons with the exception of sex (Pearson Chi-Squared). This table was reproduced from (238) with permission from SAGE Journals.

	Responders	Non-responders	*p*-value (two-tailed)
Outcome group	23	11	N/A
Sex (female/male)	12/11	6/5	>0.99
Age, years	52.59 ± 9.50	51.86 ± 16.7	0.90
Duration of TN, years	6.61 ± 5.07	5.55 ± 4.63	0.55
Affected side (left/right)	7/16	4/7	>0.99
Neurovascular compression (yes/no)	22/1	10/1	>0.99
Virgin surgical treatment (yes/no)	23/0	7/4	0.007*
Time to surgery, days	53.78 ± 72.0	42.09 ± 131	0.79
Intracranial volume (V-scaling factor)	1.39 ± 0.13	1.30 ± 0.09	0.025*
Antiepileptic (yes/no)	23/0	11/0	>0.99
Amitriptyline (yes/no)	1/22	2/9	0.24
Opioids (yes/no)	4/19	3/8	0.66
Baclofen (yes/no)	7/16	2/9	0.68

*Denotes statistical significance (*p*-value < 0.05).
Time to surgery: Amount of time between pre-operative MRI and surgical treatment.
V-scaling factor: Coefficient of enlargement used to scale individual whole brains to Montreal Neurological Institute standard template.
Antiepileptic: Antiepileptic medication class: Gabapentin, pregabalin, carbamazepine, oxcarbazepine.
Opioids: Opiate medication class: Hydromorphone, oxycodone, morphine.

6.3.3 CNV volume:

Intra-rater reliability for CNV volume was very good, with an average measures ICC 0.89 (95% confidence interval 0.54-0.97; $F(9,9) = 8.15$, $p = 0.002$). Inter-rater reliability for CNV volume was excellent, with average measures ICC 0.97 (95% confidence interval 0.86-0.99; $F(9,9) = 26.15$, $p < 0.001$). Across all patients, there was no difference in CNV volume ipsilateral and contralateral to the side-of-pain (37.14 ± 18.7 mm^3 and 39.11 ± 18.1 mm^3 respectively, $p = 0.46$), nor did ipsilateral and contralateral CNV volumes differ within responders or non-responders analyzed separately. Non-responders had significantly larger CNV volume contralateral to the side-of-pain compared to responders (53.3 ± 19.5 mm^3 and 31.3 ± 11.5 mm^3 respectively, $p = 0.009$), while there was no difference in ipsilateral and total CNV volume between outcome groups (46.2 ± 24.3 mm^3 and 32.1 ± 12.9 mm^3 respectively, $p = 0.83$; 99.6 ± 41.8 mm^3 and 63.4 ± 19.6 mm^3 respectively, $p = 0.11$) (**Figure 6.2**). There was no difference between responders and non-responders in % volume difference between ipsilateral and contralateral CNV.

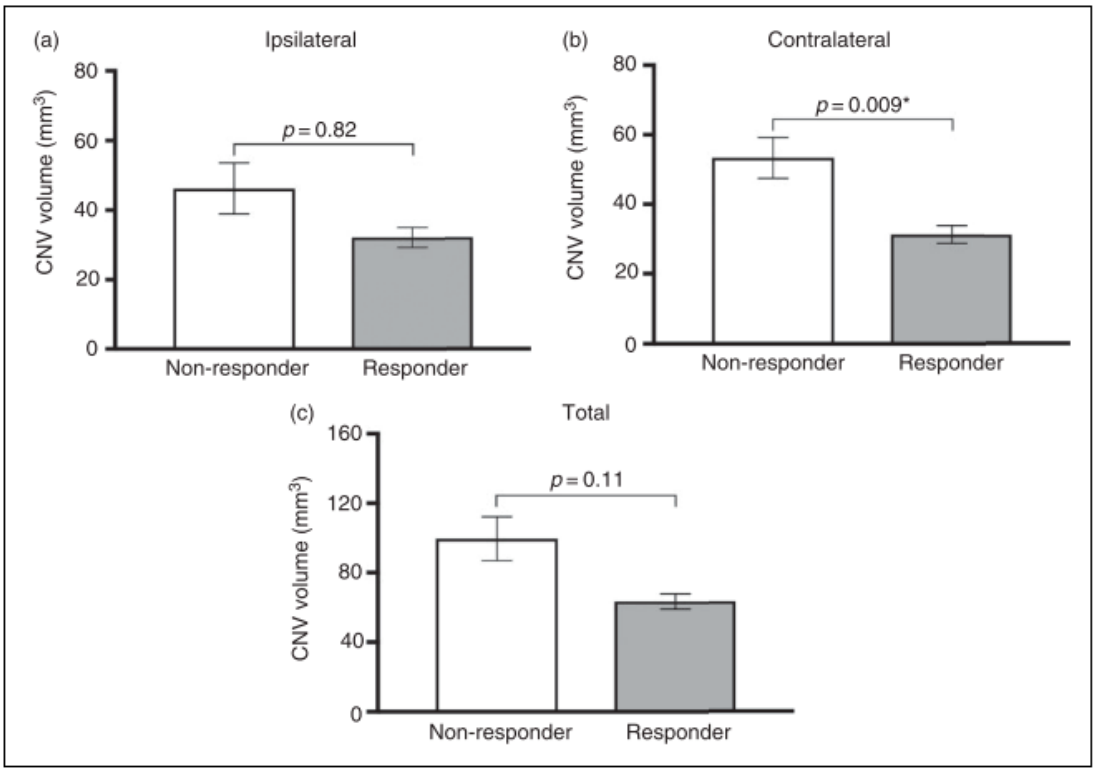

Figure 6.2: (A) Ipsilateral, (B) contralateral, and (C) total (ipsilateral + contralateral) CNV cisternal segment volume in responders and non-responders to surgical treatment for TN. Contralateral CNV volume is significantly larger in non-responders compared to responders ($p = 0.009$), while no difference in ipsilateral CNV volume or total CNV volume is observed. The influence of intracranial volume and number of previous surgical procedures was corrected using ANCOVA. Bars represent standard error of the mean. This figure was reproduced from (238) with permission from SAGE Journals.

6.3.4 Subcortical structure volumes:

Across all TN patients, thalamus volume was larger contralateral to the side-of-pain than ipsilateral (7915 ± 633 mm^3 and 7702 ± 568 mm^3 respectively; $p < 0.001$), while no between-side volume differences were observed for hippocampus (3592 ± 373 mm^3 and 3634 ± 367 mm^3 respectively; $p = 0.47$) or amygdala (1411 ± 239 mm^3 and 1352 ± 229 mm^3 respectively;

p = 0.08) (**Figure 6.3**). Contralateral hippocampus volume was larger in non-responders than responders (3830 ± 206 mm^3 and 3479 ± 385 mm^3 respectively; p = 0.032), as was ipsilateral

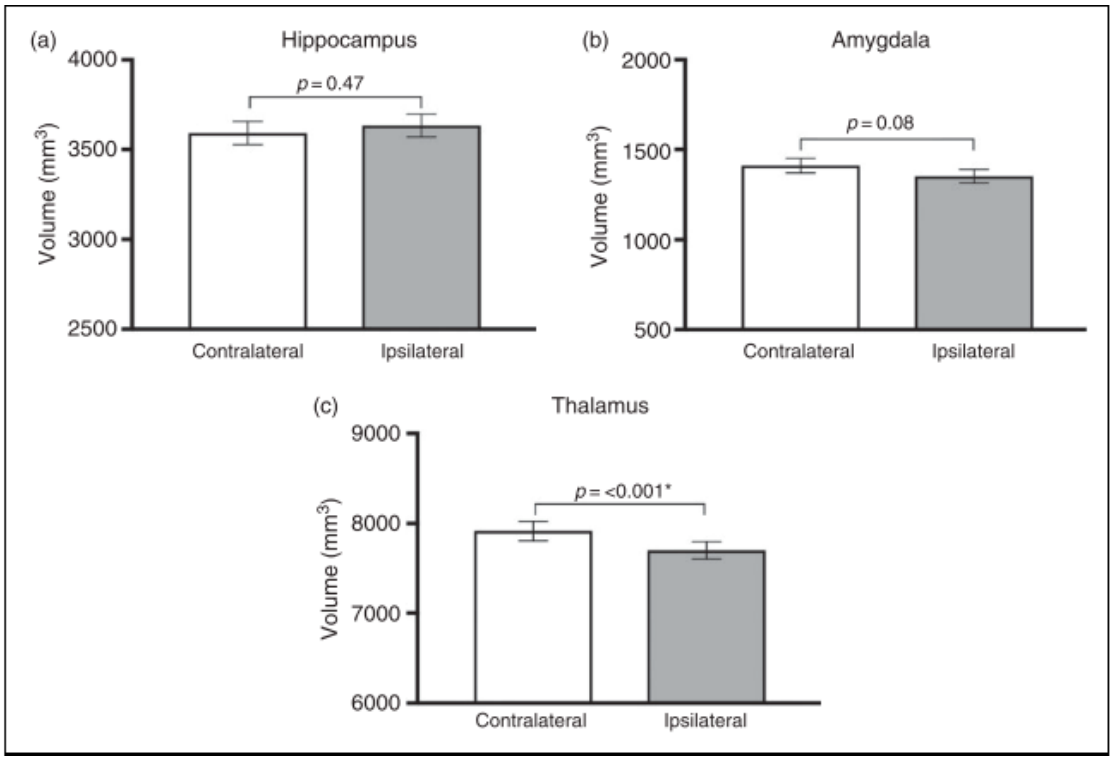

Figure 6.3: Volumes of subcortical structures of interest for entire TN patient cohort. (A) Hippocampus, (B) amygdala, (C) thalamus. Thalamus volume is larger contralateral to the side-of-pain than ipsilateral (p < 0.001), while there are no between-side volume differences observed for hippocampus or amygdala. The influence of intracranial volume and number of previous surgical procedures was corrected using repeated-measures ANCOVA. Error bars show standard error of the mean. This figure was reproduced from (238) with permission from SAGE Journals.

hippocampus volume (3821 ± 274 mm^3 and 3545 ± 378 mm^3 respectively; p = 0.012) and total hippocampus volume (7651 ± 388 mm^3 and 7024 ± 668 mm^3 respectively; p = 0.008) (**Figure 6.4**). There were no volume differences identified between non-responders and responders for ipsilateral amygdala (1372 ± 240 mm^3 and 1342 ± 228 mm^3 respectively; p = 0.91), contralateral amygdala (1499 ± 212 mm^3 and 1369 ± 244 mm^3 respectively; p = 0.43), and

total amygdala (2872 ± 410 mm^3 and 2712 ± 435 mm^3 respectively; p = 0.68), as well as ipsilateral thalamus (7863 ± 536 mm^3 and 7625 ± 578 mm^3 respectively; p = 0.49), contralateral thalamus (8140 ± 549 mm^3 and 7807 ± 654 mm^3 respectively; p = 0.38), and total thalamus (16003 ± 1074 mm^3 and 15432 ± 1213 mm^3 respectively; p = 0.42).

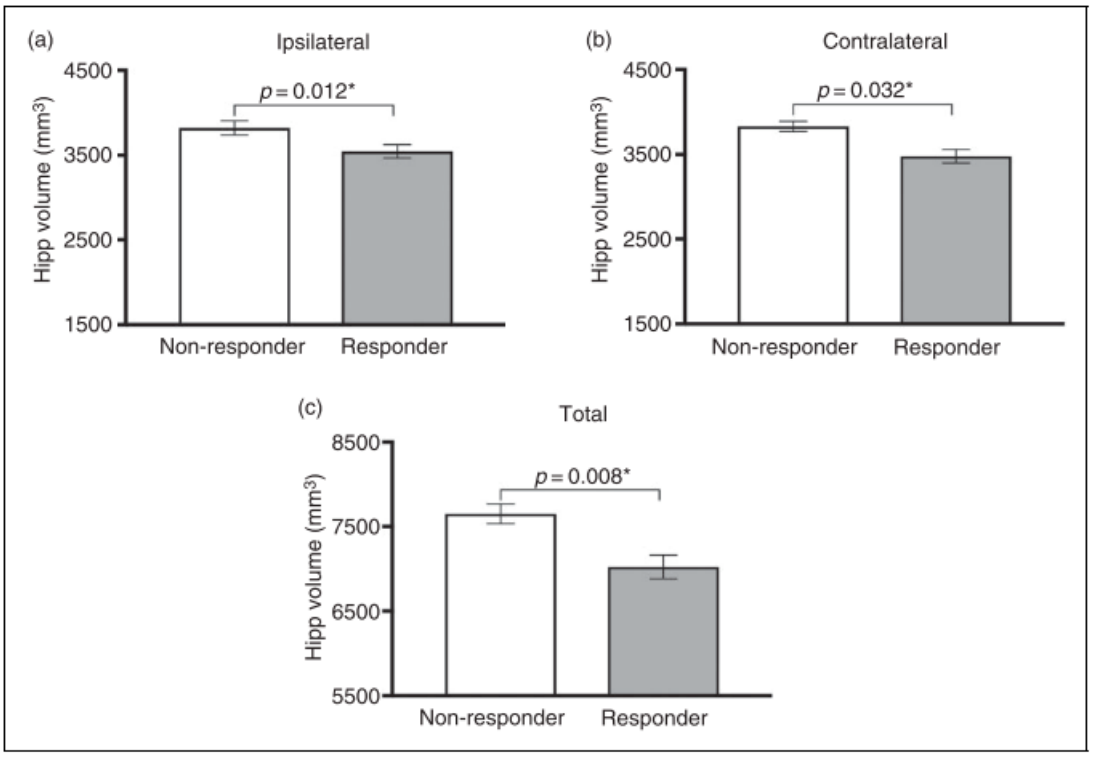

Figure 6.4: Hippocampal volumes in responders and non-responders to surgical treatment for TN. Hippocampal volume is larger in non-responders compared to responders (**A**) ipsilateral (p = 0.012) and (**B**) contralateral to the side of pain (p = 0.032). (**C**) Total hippocampal volume is also larger in non-responders than responders (p = 0.008). The influence of intracranial volume and number of previous surgical procedures was corrected using MANCOVA. Error bars show standard error of the mean. This figure was reproduced from (238) with permission from SAGE Journals.

6.3.5 Predicting surgical outcome from contralateral CNV and hippocampus volumes:

Receiver-operator characteristic curve analysis: We performed ROC curve analysis to determine the ability of contralateral CNV volume and contralateral hippocampus volume to segregate surgical outcome groups (**Figure 6.5**), since these represented the structures with the most significant volumetric differences between responders and non-responders. The ROC curve generated for contralateral CNV volume and surgical outcome has an area under the curve of 0.868 ($p < 0.001$). The optimal operating CNV volume threshold for this model is 33.37 mm^3, with 91% sensitivity and 75% specificity, correctly classifying outcome in 81% of cases (**Figure 6.5A and B**). The ROC curve generated for contralateral hippocampus volume and surgical outcome has an area under the curve of 0.787 ($p = 0.008$). The optimal operating contralateral hippocampus threshold volume is 3709 mm^3, with 91% sensitivity and 78% specificity, correctly classifying outcome in 82% of cases (**Figure 6.5C and D**).

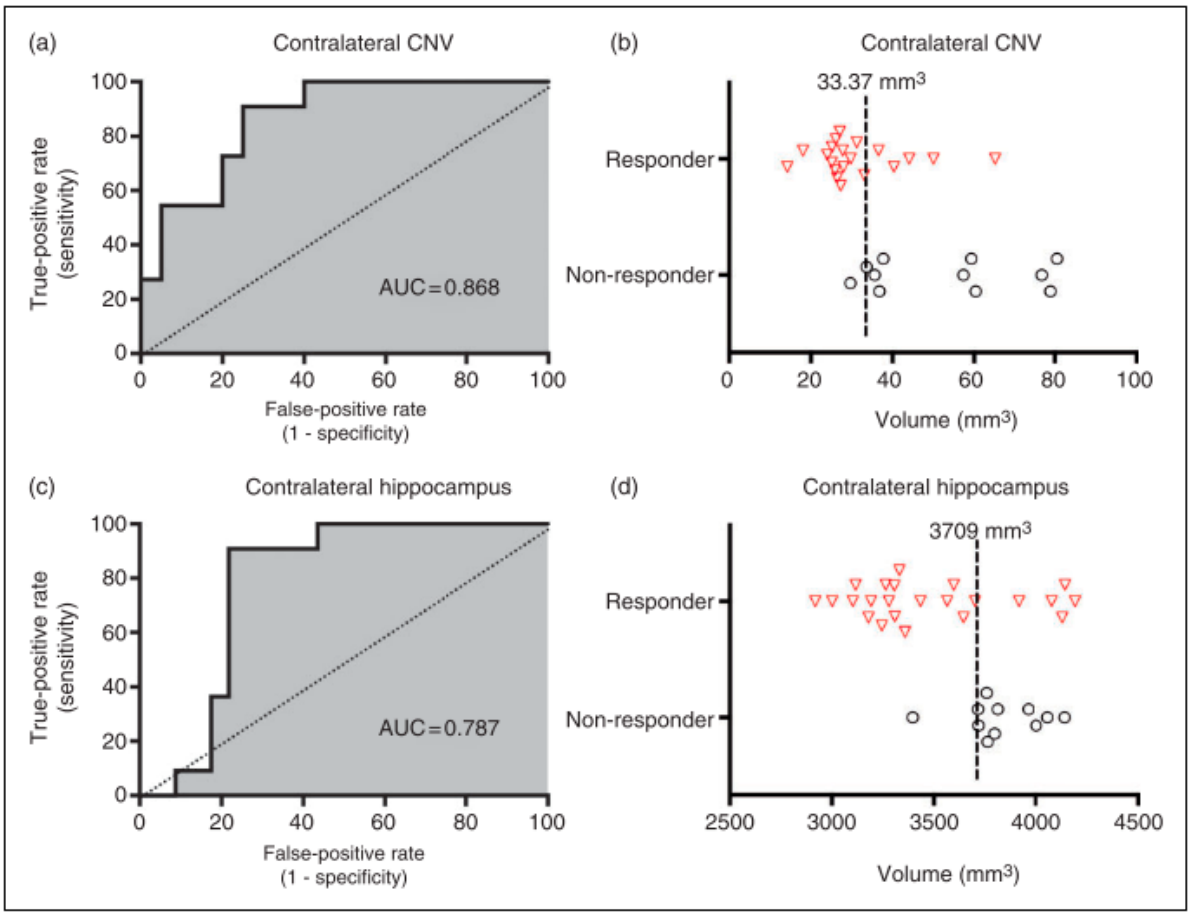

Figure 6.5: Receiver-operator (ROC) curve analysis of surgical treatment outcome in relation to contralateral CNV volume or contralateral hippocampus volume. (A) ROC curve for contralateral CNV volume and surgical outcome has area under the curve (AUC) of 0.868 ($p<0.001$) (**A**). The optimal operating threshold CNV volume of 33.37 mm^3 has 91% sensitivity and 75% specificity for response. **(B)** Contralateral CNV volumes for each individual responder and non-responder to surgical treatment are displayed with optimal operating threshold volume overlaid. **(C)** ROC curve generated for contralateral hippocampal volume and surgical outcome has AUC of 0.787 ($p=0.008$). The optimal operating threshold for hippocampus volume of 3709 mm^3 has 91% sensitivity and 78% specificity for response. **(D)** Contralateral hippocampal volumes for each individual responder and non-responder are displayed with optimal operating threshold volume overlaid. This figure was reproduced from (238) with permission from SAGE Journals.

Binomial logistic regression analysis: A binomial logistic regression model generated for surgical outcome using contralateral CNV and contralateral hippocampus volume as predictors was statistically significant ($X^2(2) = 19.9$, $p < 0.001$), and able to reliably classify patients as responders and non-responders (**Table 6.2**). The model explained 65.1% (Nagelkerke R^2) of variance in clinical outcome, and correctly classified 83.9% of cases (**Table 6.2**). Within the model, both contralateral hippocampus and contralateral CNV volumes made significant contributions to classification ($p = 0.044$ and $p = 0.009$ respectively).

Table 6.2: Binomial logistic regression analysis of surgical outcome using preoperative contralateral hippocampus and contralateral CNV volume as predictor variables. The logistic regression model for hippocampus and CNV volume was statistically significant ($X^2(2) = 19.9$, $p < 0.001$), indicating that contralateral hippocampus and contralateral CNV volumes reliably classified patients as responders and non-responders. The model explained 65.1% (Nagelkerke R^2) of variance in clinical outcome, and correctly classified 83.9 % of cases. Within the model, both contralateral hippocampus and CNV volumes made significant contributions to classification ($p = 0.044$ and $p = 0.009$ respectively). This table was reproduced from (238) with permission from SAGE Journals.

Group	Correct prediction	Incorrect prediction	Percentage correct
Non-responders	9	2	81.8
Responders	17	3	85.0
Total	26	5	83.9

6.4 Discussion:

We performed a single-centre, retrospective assessment of 34 TN patients (32 classic TN and two idiopathic TN) undergoing MVD surgery for TN and found that non-responders have larger average hippocampus and average contralateral CNV volume than responders. Furthermore, contralateral hippocampus and contralateral CNV volume were both good individual predictors of surgical outcome, correctly classifying 82% and 81% of cases respectively. We found that predictive capacity improved to 84% when these predictors were considered together in the same binomial logistic regression model, suggesting that both nerve and brain features may contribute to resistance to surgical treatment in TN. To our knowledge, ours is the first study where preoperative brain and CNV structure—obtained from standard preoperative clinical MRI scans—have been shown to relate to the outcome of surgical treatment for TN.

Our patients demonstrated a 68% surgical response-rate, which is in agreement with previously reported literature, notwithstanding differences in how surgical outcome is measured across various studies (98). Previous work has found that CNV volume ipsilateral to the painful side-of-the-face is typically reduced compared to the unaffected nerve in patients with TN as well as compared to healthy controls (56,175). This has been attributed to volume loss secondary to NVC of CNV ipsilateral to the side-of-pain (175,176). We did not find differences between ipsilateral and contralateral CNV volume across all patients. It is possible that our comparatively small sample size limited power to detect small inter-side nerve volume differences, or that NVC in our cohort was relatively non-severe. However, contralateral volume enlargement of the thalamus within TN patients was observed, suggesting that upstream neurons residing within the contralateral VPM thalamus are affected in TN, likely reflecting alterations in the trigeminal sensory system.

Very few studies to date have investigated the relationship between CNV volume and surgical outcomes, which was a primary focus in the present study. Previously published studies also appear to disagree on the exact nature of nerve-outcome relationships: while Cheng et al. (179) and Leal et al. (175) found that worse MVD outcome was associated with larger CNV volume and CSA ipsilateral to the side-of-pain, Duan et al. (176) found the opposite CSA relationship. We found no association between ipsilateral CNV volume and surgical outcomes. Rather, we identified larger average contralateral CNV volume in non-responders to surgical treatment and identified a threshold contralateral CNV volume which correctly predicted surgical outcome in 81% of cases within our cohort. Cisternal CNV volume reflects size differences across the entire cisternal nerve extent (unlike CSA); it is, therefore, well suited for capturing widespread nerve changes. Additionally, the measurement of cisternal CNV volume is less dependent on user input compared to CSA, which is measured on only a single MRI slice that needs to be selected by the observer. Our findings suggest that while initial CNV injury—say, due to NVC—may well initiate a sequence of events ultimately leading to the development of TN, delayed bilateral nerve-wide changes occurring in patients with longstanding TN might confer treatment resistance, and thus be more useful in predicting surgical outcome.

While a variety of grey matter brain structures have been implicated in TN and other chronic pain conditions (e.g., insula, cingulate, amygdala, parahippocampal region), exactly how cortical and subcortical brain regions may be altered in treatment resistant-TN has been understudied (185,208,218,223). We observed preoperative hippocampus volume to be larger in non-responders than responders, and found contralateral hippocampus volume specifically to be the best individual predictor of surgical outcome, correctly predicting response in 82% of cases. While the trigeminal sensory system is certainly central to the development and

maintenance of both acute and chronic pain in TN, affective limbic contributions have also been shown to be important in chronic pain experience (216,221). In humans, it has recently been shown that demyelinating lesions of the contralateral hippocampus constitute one of the most common supratentorial abnormalities in patients with TN due to multiple sclerosis (81). Additionally, a recent animal study identified a strong positive relationship between increased adult hippocampal neurogenesis and the maintenance of neuropathic pain (222). These findings are consistent with our observation that surgically-resistant TN patients have enlarged hippocampi, potentially owing to increased hippocampal activity related to the recollection and then integration of emotionally-significant stimuli with the experience of chronic pain (214,216,221). Specifically, why we found that hippocampus volume contralateral to the side-of-pain seems to be particularly important in treatment resistance remains an open question and warrants further investigation. The phenomenon of treatment resistance in chronic pain is unlikely to be driven by a single structure, despite our findings. Future network and connectivity examinations between responders and non-responders would complement this work nicely, as the hippocampus—and potentially other limbic structures as well—may represent a node within networks working together to influence pain (219).

There is no doubt that abnormalities within CNV, in particular demyelination associated with NVC, play a key role in the development and maintenance of TN in a substantial proportion of cases (67). We speculate that our novel finding of a relationship between hippocampal volume and treatment outcome in TN may suggest that, over time, hippocampal changes also occur which may relate to hyperactivity of the trigeminal system, and may in turn explain why nerve-centered surgical approaches are not definitive (98). In this vein, Wang et al.'s recent demonstration of a correlation between CNV and brain grey matter volume supports the

possibility of such a relationship (223). Indeed, the improved ability to predict surgical outcome when hippocampal and CNV metrics are considered together further underscores that both nerve and brain mechanisms may be important in TN, and in particular for the maintenance of the painful state.

This study is not without limitations. One must be cautious in making firm conclusions from observational retrospective study designs, and future longitudinal assessments are needed to generalize our findings beyond the particular patient cohort we have studied. Another limitation of this study is that patients were classified as responders and non-responders through chart review only, raising the possibility that we may have missed non-responders lost to patient follow-up, or at worst may have misclassified them as responders. Additionally, the non-responder group may contain patients who never achieved any pain relief from surgery, as well as those who did achieve initial pain relief but then experienced early pain-recurrence; it is possible that these distinct types of patients may exhibit different structural features of the brain or CNV. Therefore, it would be advantageous that future studies utilize quantitative measures of treatment response, which would also permit accurate descriptions of response and recurrence timelines. It is also important to note that preoperative MRIs were often collected well in advance of surgery, and, therefore, the brain-state we evaluated may differ from that at the time-of-surgery. Inter-scanner variability is another potential critique, as preoperative MRI scans were not necessarily collected on the same scanners. However, it has been demonstrated previously that FSL-FIRST (163,164) generates reliable subcortical structure volumes despite inter-scanner variation (156). Patients with right- or left-TN were both included in this study. As a result, brain-flipping was required in order to perform structural analysis in relation to the side-of-pain. We acknowledge brain-flipping as another potential limitation of our study

considering hemispheric-lateralization of pain processing has been demonstrated (246). While our approach may be susceptible to this particular confound, the proportion of left- and right-TN is equal between responders and non-responder groups, increasing confidence that hemispheric lateralization is not driving our findings. Finally, the small sample size is an obvious limitation, though we did use a hypothesis-driven approach, specifically evaluating CNV and three relevant subcortical structures selected *a priori*, with appropriate statistical thresholds and correction for multiple comparisons.

6.5 Conclusion:

We show that preoperative hippocampal and CNV volume, measured on standard clinical MRI scans, may predict early non-response to surgical treatment for TN. These findings suggest that pain-state maintenance and treatment resistance in medically-refractory TN may depend on the structural features of both CNV and structures involved in limbic contributions to chronic pain.

CHAPTER 7: General Discussion & Conclusions

7.1 Summary of Key Findings:

A summary of the key novel findings of this thesis are as follows:

- In Chapter 3, we developed a novel high-resolution nerve-specific FLAIR-DTI acquisition protocol to characterize CNV microstructure. We compared this protocol to other DTI acquisition protocols previously used in published studies of TN. FLAIR-DTI was quantitatively shown to be superior to any DTI protocol used to date to study TN through head-to-head comparison in healthy subjects, as CNV was more accurately delineated, and measures of nerve diffusivity were less contaminated by partial volume effects.
- In Chapter 3, we also found that the lower-resolution whole-brain DTI protocols previously used to study TN are subject to a critical error in which nerve segment FA in effect becomes a surrogate measure for nerve volume due to significant partial volume effects.
- In Chapter 4, we used our novel FLAIR-DTI protocol to study patients with TN and found, contrary to most previously published work, that there are no preoperative differences in CNV diffusivity metrics between TN patients and HCs.
- In Chapter 4, we also demonstrated that persistent nerve diffusion changes occur as early as 1-day after surgery which are similar regardless of surgery type (MVD, BC) or surgical outcome (responder, non-responder).

- In Chapter 5, we investigated structure and metabolism at a more proximal location within the trigeminal system (i.e., thalamus). We found that the contralateral thalamus is enlarged in patients with TN and that thalamus shape differences exist between surgical responders and non-responders preoperatively.
- In Chapter 5, we also found divergent metabolic changes in the VPM thalamus occurring at 1-week postoperatively in surgical responders compared to non-responders.
- In Chapter 6, we found that contralateral CNV volume is enlarged prior to surgical treatment in non-responders. This measure segregated treatment outcomes with good (81%) accuracy.
- In Chapter 6, we also found that the contralateral hippocampus is relatively enlarged in non-responders prior to surgery, which is the first example of preoperative brain structure being implicated in response to surgery for TN. Furthermore, contralateral hippocampus volume was able to distinguish surgical responders from non-responders with 82% accuracy, pointing to its potential utility as a clinical biomarker to inform prognostication and patient selection in TN surgery.

7.2 General Discussion & Future Directions:

CNV diffusion abnormalities that align with histological findings of demyelination in TN have been consistently demonstrated over the past decade. In an effort to more accurately characterize CNV microstructure so that these measures could be related to surgical outcome we developed a superior nerve-specific FLAIR-DTI protocol, less vulnerable to partial volume

effects. Surprisingly, through the development process we identified important shortcomings in DTI protocols currently used by other groups to study TN in which nerve FA is positively correlated with segment volume due to significant partial volume effects. Therefore, people with smaller CNV volume display artificially reduced CNV FA, which may be a serious problem for between group comparisons considering that ipsilateral CNV atrophy has been observed especially in classical TN.

Indeed, when using our specialized FLAIR-DTI protocol, we could not replicate previous findings of abnormal ipsilateral CNV diffusivity in patients with TN. Collectively, the nerve DTI findings of this thesis suggest that a re-examination of the relationship between CNV diffusivity metrics, the TN pain state, and response to surgery in TN, may be in order. While histology has shown that demyelination and axon loss are present in TN patients, these histological studies in general evaluated nerve structure with spatially limited biopsies of CNV at the exact site of vascular compression and not across the entire cisternal nerve segment (51,52). Moving forward, we would propose that higher-resolution evaluations of CNV diffusivity should break up the whole nerve segment into smaller sub-segments so that DTI too may focus on the specific site of vascular compression where microstructural abnormalities are expected to be maximal. At least in patients with classical TN, at this location nerve sub-segment diffusion will likely reflect true demyelination, and perhaps, may be related to surgical outcome.

Perhaps predictably given that surgical treatment for TN produces an immediate analgesic effect (with the exception of SRS), CNV diffusion changes are identifiable at the earliest timepoint tested: in this thesis, such changes were found 1-day after surgical treatment. These changes are the same regardless of surgical treatment type (MVD, BC) suggesting that the

immediate pain relief experienced by patients undergoing MVD may be due to similar mechanisms as pain relief achieved through destructive procedures. Interestingly, responders and non-responders also display the same CNV diffusion changes in the 1-month postoperative period suggesting that surgical treatment generally has the same effect on CNV microstructure in both responders and non-responders. It would be of significant interest to evaluate delayed postoperative timepoints to assess CNV microstructure long-term, and, more specifically, if responders and non-responders ever go on to diverge from one another, especially at the time of delayed pain recurrence. Additionally, the degree to which CNV microstructural changes correlate with facial sensory changes occurring after TN surgery—and how such changes influence long-term pain relief—is also an important question for future work.

Our finding that early CNV microstructure change occurring after surgery may be unrelated to long-term pain relief suggests that change in more proximal regions along the trigeminal pathway may be more influential in determining durable surgical outcome. Specifically, divergent contralateral VPM thalamus metabolism changes are observed between responders and non-responders, suggesting that while surgical treatment appears to have the same general effect on cisternal segment CNV microstructure, more proximal regions along the trigeminal system are, in fact, responding differently to the same surgical disruptions. Furthermore, preoperative thalamus shape differences observed between responders and non-responders suggest that thalamus structure may predispose some patients to poor surgical response. It would be of keen interest to evaluate thalamus metabolism and structure over the long-term in parallel with studies of CNV DTI to assess different positions along the trigeminal pathway and to investigate how these features relate to durable pain relief.

Even though CNV diffusivity does not distinguish surgical responders from non-responders, contralateral nerve cisternal segment volume appears to be a marker of surgical outcome. We also found that preoperative brain structures that are not part of the trigeminal system differ between responders and non-responders. Specifically, enlarged hippocampus volume in non-responders suggests that limbic system differences may also be involved in influencing surgical outcome. While this is not necessarily surprising given that limbic system changes have previously been associated with pain severity and recollection, as well as chronification of pain, our data in chapter 6 represent the first time that brain structure has been implicated in surgical outcome in TN. Future studies should expand on these limbic system findings, and specifically, ought to investigate the functional activity of, and connectivity between, various limbic system regions to identify and characterize treatment resistance pain networks in non-responders (207,216). Long-term assessments of limbic system structure and function should also be performed to determine if limbic system abnormalities are reversible with surgical treatment. If they are not, then perhaps in those patients for whom limbic system changes have taken place already, surgical treatments targeting the nerve directly may be less capable of inducing durable pain relief; in such cases, the potential benefits of these conventional treatments may not outweigh the surgical risk, which may need to be factored into patient selection.

All in all, the majority of TN patients respond favorably to the available surgical treatments for TN that target CNV directly. In these patients, manipulation of the nerve appears sufficient to induce durable relief. However, in non-responders it appears that while surgical treatment induces similar nerve changes as those seen in responders, more rostral regions along the trigeminal system such as the VPM thalamus may respond differently to these same surgical treatments. Furthermore, our finding of structural limbic system differences in non-responders

strengthen the notion that perhaps surgical treatment resistance in TN reflects brain structural and functional alterations which may need to be targeted directly in order to overcome a predilection to non-response in some TN patients.

7.3 Limitations:

There are a number of limitations to the studies presented in this thesis that are considered in the following section.

7.3.1 Small Sample Size:

This thesis is limited by relatively small sample sizes for individual studies: Chapter 3: N = 5HC; Chapter 4: N = 23TN (6NR) and 20HC; Chapter 5: N = 23TN (6NR) and 20HC; and Chapter 6: N = 34TN (11NR). To some extent, we mitigated sample size concerns by employing conservative, hypothesis driven methods focused on specific brain or nerve features, instead of unconstrained, data-driven, voxel-wise approaches. In Chapter 3, the powerful within-subject design negated the need for more than 5 healthy subjects. Additionally, the sample size of our prospective studies of CNV DTI (Chapter 4) and thalamus structure and metabolism (Chapter 5) closely match others in the literature that utilize the same imaging modalities (62,191,198–200). Admittedly though, our responder and non-responder groups were imbalanced and small (Chapters 4, 5, 6), limiting the statistical power available to detect smaller magnitude differences between these groups. Therefore, the findings of this thesis will need to be replicated using larger TN datasets.

7.3.2 Lack of Validation:

Because of sample size limitations, we were not able to withhold a cohort of study subjects from the initial analyses (Chapters 4, 5, 6). This approach would have allowed key brain and nerve features distinguishing responders from non-responders to be tested on a different patient cohort to validate initial study findings. Future studies utilizing new patient cohorts will be of particular importance in confirming the validity of the findings contained in this thesis.

7.3.3 Binarization of Surgical Outcome:

Another limitation of this thesis is the simplistic binarization of surgical outcome as *responder* or *non-responder*. In reality, the TN patient population is heterogenous, and therefore, so too is their response to surgical treatment (e.g., medication requirements, duration of pain relief, overall satisfaction with surgery, etc.). For example, non-responder groups may contain patients who never achieved any pain relief from surgery, as well as those who did achieve initial pain relief but then experienced early pain recurrence (Chapter 4, **Figure 4.1**); it is possible that these distinct types of patients may exhibit different structural features of the brain or CNV. Additionally, because of the retrospective nature of Chapter 6 specifically, some patients were classified as responders and non-responders through chart review only, increasingly the likelihood that some of these patients may have been misclassified.

7.5 Conclusion:

This thesis focused on identifying structural and metabolic MRI-based features of non-response to surgical treatment for TN to better understand treatment response. We identified many novel pre and perioperative features distinguishing surgical responders from non-responders. This thesis could not replicate previous CNV findings in TN when using a superior CNV-specific

DTI protocol, and instead found no differences in CNV microstructure in patients with TN, which questions the validity of previous findings as well as the role of whole segment CNV microstructure in TN. The majority of MRI features related to treatment outcome were instead produced from various brain regions that are rostral components of the trigeminal system or emotion-related structures. Collectively, the novel findings of this thesis suggest that despite TN being largely conceptualized as a nerve disease, understanding the role and structure of specific pain-relevant brain regions may explain the limitations of conventional nerve-based surgical treatments for TN patients.

References:

1. Olesen J. Headache Classification Committee of the International Headache Society (IHS) The International Classification of Headache Disorders, 3rd edition. Cephalalgia. 2018;38(1):1–211.
2. Koopman JSHA, Dieleman JP, Huygen FJ, de Mos M, Martin CGM, Sturkenboom MCJM. Incidence of facial pain in the general population. Pain. 2009;147(1–3):122–7.
3. Hall GC, Carroll D, McQuay HJ. Primary care incidence and treatment of four neuropathic pain conditions: A descriptive study, 2002-2005. BMC Fam Pract. 2008;9(26).
4. Montano N, Conforti G, Di Bonaventura R, Meglio M, Fernandez E, Papacci F. Advances in diagnosis and treatment of trigeminal neuralgia. Ther Clin Risk Manag. 2015;11:289–99.
5. Maarbjerg S, Gozalov A, Olesen J, Bendtsen L. Trigeminal neuralgia-a prospective systematic study of clinical characteristics in 158 patients. Headache. 2014;54(10):1574–82.
6. Bender MT, Bettegowda C. Percutaneous Procedures for the Treatment of Trigeminal Neuralgia. Neurosurg Clin N Am [Internet]. 2016;27(3):277–95. Available from: http://linkinghub.elsevier.com/retrieve/pii/S1042368016000061
7. Putzki N, Pfriem A, Limmroth V, Yaldizli Ö, Tettenborn B, Diener HC, et al. Prevalence of migraine, tension-type headache and trigeminal neuralgia in multiple sclerosis. Eur J Neurol. 2009;16(2):262–7.
8. Singh AMK, Editor C, Egan RA. Trigeminal Neuralgia. Medscape [Internet]. 2014;15(1):1–9. Available from: http://emedicine.medscape.com/article/1145144-overview
9. Adams H, Pendleton C, Latimer K, Cohen-Gadol AA, Carson BS, Quinones-Hinojosa A. Harvey Cushing's case series of trigeminal neuralgia at the Johns Hopkins Hospital: A surgeon's quest to advance the treatment of the "suicide disease." Acta Neurochir (Wien). 2011;153(5):1043–50.
10. Wu T-H, Hu L-Y, Lu T, Chen P-M, Chen H-J, Shen C-C, et al. Risk of psychiatric disorders following trigeminal neuralgia: a nationwide population-based retrospective cohort study. J Headache Pain [Internet]. 2015;16:64. Available from: http://www.pubmedcentral.nih.gov/articlerender.fcgi?artid=4501948&tool=pmcentrez&rendertype=abstract
11. Prasad S, Galetta S. Trigeminal neuralgia historical notes and current concepts. Neurologist. 2009;15(2):87–94.
12. Burchiel KJ. A new classification for facial pain. Neurosurgery. 2003;53(5):1164–6; discussion 1166-1167.

13. Advances in diagnosis and treatment of trigeminal neuralgia. Ther Clin Risk Manag. 2015;2015(default):289–99.

14. Obermann M, Yoon MS, Ese D, Maschke M, Kaube H, Diener HC, et al. Impaired trigeminal nociceptive processing in patients with trigeminal neuralgia. Neurology. 2007;69(9):835–41.

15. Liu GT. The trigeminal nerve and its central connections. In: Miller NR, editor. Walsh and Hoyt's Clinical Neuro-Ophthalmology. sixth. Philadelphia: Lippincott Williams & Wilkins; 2005. p. 1233–74.

16. Malhotra A, Tu L, Kalra VB, Wu X, Mian A, Mangla R, et al. Neuroimaging of Meckel's cave in normal and disease conditions. Insights Imaging. 2018;9(4):499–510.

17. Mira KM, Elnaga IA, el-Sherif H. Nerve cells in the intracranial part of the trigeminal nerve of man and dog. Anatomical study of the fifth cranial nerve. J Neurosurg. 1971;34(5):643–6.

18. Kerr FWL. The divisional organization of afferent fibres of the trigeminal nerve. Brain. 1963;86(4):721–32.

19. Gudmundsson K, Rhoton AL, Rushton JG. Detailed anatomy of the intracranial portion of the trigeminal nerve. J Neurosurg. 1971;35(5):592–600.

20. Sindou M, Brinzeu A. Topography of the pain in classical trigeminal neuralgia: insights into somatotopic organization. Brain. 2020 Feb 1;143(2):531–40.

21. Guberinic A, Souverein V, Volkers R, van Cappellen van Walsum AM, Vissers KCP, Mollink J, et al. Mapping the trigeminal root entry zone and its pontine fibre distribution patterns. Cephalalgia. 2020;40(14):1645–56.

22. Darian-Smith I. The trigeminal system. In: Iggo A, editor. Handbook of Sensory Physiology. Berlin: Springer-Verlag; 1973. p. 271–314.

23. Brown JA. the Trigeminal Complex. Neurosurg Clin N Am. 1997;8(1):1–10.

24. Dodd J, Kelly J. Trigeminal System. In: Kandel E, Schwartz J, Jessell T, editors. Principles of Neural Science. East Norwalk: Appleton & Lange; 1991. p. 701–10.

25. Corbin, Kendal B., Harrison F. Function of the MEsencephalic Root of Fifth Cranial Nerve. J neuroph. 1940;3:423–35.

26. Jerge CR. Organization and Function of the Trigeminal Mesencephalic Nucleus. J Neurophysiol. 1962;26:379–92.

27. Dallel R, Raboisson P, Auroy P, Woda A. The rostral part of the trlgeminal sensory complex is involved in orofacial nociception. Brain Res. 1988;448:7–19.

28. Olszewski J. On the anatomical and functional organization of the spinal trigeminal nucleus. J Comp Neurol. 1950;92(3):401–13.

29. Steindler DA. Trigeminocerebellar, Trigeminotectal, and Trigeminothalamic Projections : A Double Retrograde Axonal Tracing Study in the Mouse. J Comp

Neurol. 1985;237:155–75.

30. Henssen DJHA, Kurt E, Kozicz T, van Dongen R, Bartels RHMA, van Cappellen van Walsum AM. New insights in trigeminal anatomy: A double orofacial tract for nociceptive input. Front Neuroanat. 2016;10:1–14.

31. Penfield W, Rasmussen T. The Cerebral Cortex of Man: A Clinical Study of Localization of Function. New York: the Macmillan Company; 1950. 280 p.

32. Meda KS, Patel T, Joao BM, Malik R, Turner ML, Seifikar H, et al. Microcircuit Mechanisms through which Mediodorsal Thalamic Input to Anterior Cingulate Cortex Exacerbates Pain-Related Aversion. Neuron [Internet]. 2019;102(5):944-959.e3. Available from: https://doi.org/10.1016/j.neuron.2019.03.042

33. Craig AD, Bushnell MC, Zhang ET, Blomqvlstt A. A thalamic nucleus specific for pain and temperature sensation. Nature. 1994;372(December):770–3.

34. Patel SK, Liu JK. Overview and History of Trigeminal Neuralgia. Neurosurg Clin N Am. 2016;265–76.

35. Fothergill J. On a Painful Affliction of the Face. Med Obs Inq. 1773;5:129–42.

36. Bell C. On the nerves of the face; second part. Philos Trans R Soc London. 1829;119:317–30.

37. Dandy W. Concerning the Cause of Trigeminal Neuralgia. Am J Surg. 1934;24:447–55.

38. Barker FG, Jannetta PJ, Bissonette DJ, Larkins M V., Jho HD. The long-term outcome of microvascular decompression for trigmeminal neuralgia. N Engl J Med. 1996;334(17):1077–83.

39. TAARNHØJ P. Decompression of the trigeminal root. J Neurosurg. 1954;11(3):299–305.

40. Gardner J, Pinto P. The Taarnhoj Operation: Relief of Trigeminal Neuralgia Without Numbness. Cleve Clin Q. 1953;20(2):364–7.

41. Lee A, McCartney S, Burbidge C, Raslan AM, Burchiel KJ. Trigeminal neuralgia occurs and recurs in the absence of neurovascular compression. J Neurosurg [Internet]. 2014;120(5):1048–54. Available from: http://thejns.org/doi/abs/10.3171/2014.1.JNS131410

42. Jannetta PJ. Arterial Compression of the Trigeminal Nerve at the Pons in Patients with Trigeminal Neuralgia*. J Neurosurg [Internet]. 1967;107(1):216–37. Available from: http://thejns.org/doi/abs/10.3171/JNS-07/07/0216

43. Jo KW, Kong D-S, Hong K-S, Lee J a, Park K. Long-term prognostic factors for microvascular decompression for trigeminal neuralgia. J Clin Neurosci [Internet]. 2013;20(3):440–5. Available from: http://www.ncbi.nlm.nih.gov/pubmed/23312560

44. Wilcox SL, Gustin SM, Eykman EN, Fowler G, Peck CC, Murray GM, et al. Trigeminal nerve anatomy in neuropathic and non-neuropathic orofacial pain patients.

J Pain [Internet]. 2013;14(8):865–72. Available from: http://dx.doi.org/10.1016/j.jpain.2013.02.014

45. Magown P, Ko AL, Burchiel KJ. The Spectrum of Trigeminal Neuralgia Without Neurovascular Compression. Neurosurgery. 2019;0(0):2019.

46. Maarbjerg S, Wolfram F, Gozalov A, Olesen J, Bendtsen L. Significance of neurovascular contact in classical trigeminal neuralgia. Brain. 2015;(2014):311–9.

47. Nave K-A, Werner HB. Myelination of the Nervous System: Mechanisms and Functions. Annu Rev Cell Dev Biol [Internet]. 2014;30:503–33. Available from: http://www.annualreviews.org/doi/abs/10.1146/annurev-cellbio-100913-013101

48. Young KM, Psachoulia K, Tripathi RB, Dunn SJ, Cossell L, Attwell D, et al. Oligodendrocyte dynamics in the healthy adult CNS: Evidence for myelin remodeling. Neuron [Internet]. 2013;77(5):873–85. Available from: http://dx.doi.org/10.1016/j.neuron.2013.01.006

49. Peker S, Kurtkaya Ö, Üzün I, Pamir MN. Microanatomy of the central myelin-peripheral myelin transition zone of the trigeminal nerve. Neurosurgery. 2006;59(2):354–8.

50. Møller AR. Vascular compression of cranial nerves: II: Pathophysiology. Neurol Res. 1999;21(5):439–43.

51. Love S, Hilton D a, Coakham HB. Central demyelination of the Vth nerve root in trigeminal neuralgia associated with vascular compression. Brain Pathol [Internet]. 1998;8(1):1–11; discussion 11-2. Available from: http://www.ncbi.nlm.nih.gov/pubmed/9458161

52. Hilton D, Love S, Gradidge T, Coakham H. Pathological Findings Associated with Trigeminal Neuralgia Caused by Vascular Compression. Neurosurgery. 1994;35(2):299–303.

53. Herweh C, Kress B, Rasche D, Tronnier V, Troger J, Sartor K, et al. Loss of anisotropy in trigeminal neuralgia revealed by diffusion tensor imaging. Neurology. 2007;68(10):776–8.

54. Leal PRL, Amedee Roch J, Hermier M, Souza MAN, Cristino-Filho G, Sindou M. Structural abnormalities of the trigeminal root revealed by diffusion tensor imaging in patients with trigeminal neuralgia caused by neurovascular compression: A prospective, double-blind, controlled study. Pain [Internet]. 2011;152(10):2357–64. Available from: http://dx.doi.org/10.1016/j.pain.2011.06.029

55. Lin W, Zhu W ping, Chen Y li, Han G can, Rong Y, Zhou Y rong, et al. Large-diameter compression arteries as a possible facilitating factor for trigeminal neuralgia: analysis of axial and radial diffusivity. Acta Neurochir (Wien). 2016;158(3):521–6.

56. Erbay SH, Bhadelia R a, O'Callaghan M, Gupta P, Riesenburger R, Krackov W, et al. Nerve atrophy in severe trigeminal neuralgia: noninvasive confirmation at MR imaging--initial experience. Radiology [Internet]. 2006;238(2):689–92. Available from: http://www.ncbi.nlm.nih.gov/pubmed/16436823

57. Lutz J, Linn J, Mehrkens JH, Thon N, Stahl R, Seelos K, et al. Trigeminal neuralgia due to neurovascular compression: high-spatial-resolution diffusion-tensor imaging reveals microstructural neural changes. Radiology. 2011;258(2):524–30.

58. Lutz J, Thon N, Stahl R, Lummel N, Tonn J-C, Linn J, et al. Microstructural alterations in trigeminal neuralgia determined by diffusion tensor imaging are independent of symptom duration, severity, and type of neurovascular conflict. J Neurosurg [Internet]. 2015;124(March):1–8. Available from: http://thejns.org/doi/10.3171/2015.2.JNS142587

59. Fujiwara S, Sasaki M, Wada T, Kudo K, Hirooka R, Ishigaki D, et al. High-resolution Diffusion Tensor Imaging for the Detection of Diffusion Abnormalities in the Trigeminal Nerves of Patients with Trigeminal Neuralgia Caused by Neurovascular Compression. J Neuroimaging. 2011;21(2):102–8.

60. Trebbastoni A, D'Antonio F, Biasiotta A, Fiorelli M, De Lena C. Diffusion tensor imaging (DTI) study of a trigeminal neuralgia due to large venous angioma. Neurol Sci. 2013;34(3):397–9.

61. Liu Y, Li J, Butzkueven H, Duan Y, Zhang M, Shu N, et al. Microstructural abnormalities in the trigeminal nerves of patients with trigeminal neuralgia revealed by multiple diffusion metrics. Eur J Radiol [Internet]. 2013;82(5):783–6. Available from: http://dx.doi.org/10.1016/j.ejrad.2012.11.027

62. DeSouza DD, Davis KD, Hodaie M. Reversal of insular and microstructural nerve abnormalities following effective surgical treatment for trigeminal neuralgia. Pain [Internet]. 2015;156(6):1112–23. Available from: http://www.ncbi.nlm.nih.gov/pubmed/25782366

63. Desouza DD, Hodaie M, Davis KD. Abnormal trigeminal nerve microstructure and brain white matter in idiopathic trigeminal neuralgia. Pain [Internet]. 2014;155(1):37–44. Available from: http://dx.doi.org/10.1016/j.pain.2013.08.029

64. Neetu S, Sunil K, Ashish A, Jayantee K, Kant MU. Microstructural abnormalities of the trigeminal nerve by diffusion-tensor imaging in trigeminal neuralgia without neurovascular compression. Neuroradiol J. 2016;29(1):13–8.

65. DeSouza DD, Hodaie M, Davis KD. Structural Magnetic Resonance Imaging Can Identify Trigeminal System Abnormalities in Classical Trigeminal Neuralgia. Front Neuroanat [Internet]. 2016;10(October). Available from: http://journal.frontiersin.org/article/10.3389/fnana.2016.00095/full

66. Devor M, Amir R, Rappaport ZH. Pathophysiology of trigeminal neuralgia: the ignition hypothesis. Clin J Pain. 2002;18(1):4–13.

67. Devor M, Govrin-Lippmann R, Rappaport ZH. Mechanism of trigeminal neuralgia: an ultrastructural analysis of trigeminal root specimens obtained during microvascular decompression surgery. J Neurosurg [Internet]. 2002;96(3):532–43. Available from: http://thejns.org/doi/10.3171/jns.2002.96.3.0532

68. Burchiel KJ. Abnormal impulse generation in focally demyelinated trigeminal roots. J

Neurosurg [Internet]. 1980;53(5):674–83. Available from: http://www.ncbi.nlm.nih.gov/pubmed/7431076

69. Lisney SJW, Devor M. Afterdischarge and interactions among fibers in damaged peripheral nerve in the rat. Brain Res. 1987;415(1):122–36.

70. Love S, Gradidge T, Coakham HB. Trigeminal neuralgia due to multiple sclerosis: Ultrastructural findings in trigeminal rhizotomy specimens. Neuropathol Appl Neurobiol. 2001;27(3):238–44.

71. Amir R, Devor M. Chemically mediated cross-excitation in rat dorsal root ganglia. J Neurosci. 1996;16(15):4733–41.

72. Miller JP, Acar F, Hamilton BE, Burchiel KJ. Radiographic evaluation of trigeminal neurovascular compression in patients with and without trigeminal neuralgia: Clinical article. J Neurosurg. 2009;110(4):627–32.

73. Adamczyk M, Bulski T, Sowińska J. Trigeminal nerve-artery contact in people without trigeminal neuralgia-MR study. Med J [Internet]. 2007;13 Suppl 1(Suppl 1):38–43. Available from: http://www.ncbi.nlm.nih.gov/pubmed/17507883

74. Kakizawa Y, Seguchi T, Kodama K, Ogiwara T, Sasaki T, Goto T, et al. Anatomical study of the trigeminal and facial cranial nerves with the aid of 3.0-tesla magnetic resonance imaging. J Neurosurg. 2008;108(3):483–90.

75. Lin W, Chen YL, Zhang QW. Vascular compression of the trigeminal nerve in asymptomatic individuals: A voxel-wise analysis of axial and radial diffusivity. Acta Neurochir (Wien). 2014;156(3):577–80.

76. Farassati F, Yang AD, Lee PWK. Anatomical observations during microvascular decompression for idiopathic trigeminal neuralgia (with correlations between topography of pain and site of the neurovascular conflict). Prospective study in a series of 579 patients. Acta Neurochir (Wien). 2002;144(1):1–13.

77. Toda K. Etiology of Trigeminal Neuralgia. Oral Sci Int [Internet]. 2007;4(1):10–8. Available from: http://www.sciencedirect.com/science/article/pii/S1348864307800073

78. Ogleznev KY, Grigoryan YA, Slavin K V. Parapontine epidermoid tumours presenting as trigeminal neuralgias: Anatomical findings and operative results. Acta Neurochir (Wien). 1991;110(3–4):116–9.

79. Noory N, Smilkov EA, Frederiksen JL, Heinskou TB, Andersen ASS, Bendtsen L, et al. Neurovascular contact plays no role in trigeminal neuralgia secondary to multiple sclerosis. Cephalalgia. 2021;41(5):593–603.

80. Love S, Coakham HB. Trigeminal neuralgia: Pathology and pathogenesis. Brain. 2001;124(12):2347–60.

81. Fröhlich K, Winder K, Linker RA, Engelhorn T, Dörfler A, Lee DH, et al. Supratentorial lesions contribute to trigeminal neuralgia in multiple sclerosis. Cephalalgia. 2018;38(7):1326–34.

82. Chen DQ, DeSouza DD, Hayes DJ, Davis KD, O'Connor P, Hodaie M. Diffusivity signatures characterize trigeminal neuralgia associated with multiple sclerosis. Mult Scler [Internet]. 2015;1–13. Available from: http://www.ncbi.nlm.nih.gov/pubmed/25921052

83. Ahrendsen JT, MacKlin W. Signaling mechanisms regulating myelination in the central nervous system. Neurosci Bull. 2013;29(2):199–215.

84. Zakrzewska JM, Wu J, Brathwaite TSL. A Systematic Review of the Management of Trigeminal Neuralgia in Patients with Multiple Sclerosis. World Neurosurg [Internet]. 2018;111:291–306. Available from: https://doi.org/10.1016/j.wneu.2017.12.147

85. Magown P, Ko AL, Burchiel KJ. The Spectrum of Trigeminal Neuralgia Without Neurovascular Compression. Neurosurgery. 2019;85(43):553–9.

86. Tohyama S, Hung PSP, Cheng JC, Zhang JY, Halawani A, Mikulis DJ, et al. Trigeminal neuralgia associated with a solitary pontine lesion: clinical and neuroimaging definition of a new syndrome. Pain. 2020;161(5):916–25.

87. Bendtsen L, Zakrzewska JM, Abbott J, Braschinsky M, Di Stefano G, Donnet A, et al. European Academy of Neurology guideline on trigeminal neuralgia. Eur J Neurol. 2019;26(6):831–49.

88. Attal N, Cruccu G, Baron R, Haanpaa M, Hansson P, Jensen TS, et al. EFNS guidelines on the pharmacological treatment of neuropathic pain: 2010 revision. Eur J Neurol. 2010;17(9):1113–23.

89. Matwychuk MJ. Diagnostic Challenges of Neuropathic Tooth Pain. J Can Dent Assoc (Tor). 2004;70(8):542–6.

90. Jackson EM, Bussard GM, Hoard MA, Edlich RF. Trigeminal neuralgia: A diagnostic challenge. Am J Emerg Med. 1999;17(6):597–600.

91. Türp JC, Gobetti JP. Trigeminal neuralgia versus atypical facial pain: review of the literature and case report. Oral Surg Oral Med Oral Pathol Oral Radiol Endod. 1996;81(4):424–32.

92. Gronseth G, Cruccu G, Alksne J, Argoff C, Brainin M, Burchiel K, et al. Practice Parameter: The diagnostic evaluation and treatment of trigeminal neuralgia (an evidence-based review). Neurology. 2008;71:1183–90.

93. Pellock JM. Carbamazepine Side Effects in Children and Adults. Epilepsia. 1987;28:S64–70.

94. Heinskou T, Maarbjerg S, Rochat P, Wolfram F, Jensen RH, Bendtsen L. Trigeminal neuralgia – A coherent cross-specialty management program. J Headache Pain [Internet]. 2015;16(1–8). Available from: http://dx.doi.org/10.1186/s10194-015-0550-4

95. Brown JA. Percutaneous balloon compression for trigeminal neuralgia. Clin Neurosurg. 2009;56:73–8.

96. Little AS, Shetter AG, Shetter ME, Bay C, Rogers CL. Long-term pain response and quality of life in patients with typical trigeminal neuralgia treated with gamma knife stereotactic radiosurgery. Neurosurgery. 2008;63(5):915–23.

97. Gardner J. Response to Trigeminal Neuralgia to "Decompression" of Sensory Root. J Am Med Assoc. 1959;170(15):85–8.

98. Burchiel KIMJ, Clarke H, Haglund M, Loeser J. Long-term efficacy of microvascular decompression in trigeminal neuralgia. J Neurosurg. 1988;69:35–8.

99. TAARNHØJ P. Decompression of the posterior trigeminal root in trigeminal neuralgia. A 30-year follow-up review. J Neurosurg. 1981;57:14–7.

100. Brînzeu A, Drogba L, Sindou M. Reliability of MRI for predicting characteristics of neurovascular conflicts in trigeminal neuralgia: implications for surgical decision making. J Neurosurg [Internet]. 2018;1:1–11. Available from: http://thejns.org/doi/10.3171/2017.8.JNS171222

101. Hoz SS, Al-Sharshahi ZF, Dolachee AA, Chotai S, Salih H, Albanaa SA, et al. Transposition of Vessels for Microvascular Decompression of Posterior Fossa Cranial Nerves: Review of Literature and Intraoperative Decision-Making Scheme. World Neurosurg [Internet]. 2021;145:64–72. Available from: https://doi.org/10.1016/j.wneu.2020.08.173

102. Wang DD, Raygor KP, Cage TA, Ward MM, Westcott S, Barbaro NM, et al. Prospective comparison of long-term pain relief rates after first-time microvascular decompression and stereotactic radiosurgery for trigeminal neuralgia. J Neurosurg [Internet]. 2018;128(1):68–77. Available from: http://thejns.org/doi/10.3171/2016.9.JNS16149

103. Cottee LJ, Daniel C, Loh WS, Harrison BM, Burke W. Remyelination and recovery of conduction in cat optic nerve after demyelination by pressure. Exp Neurol. 2003;184(2):865–77.

104. Ko AL, Ozpinar A, Lee A, Raslan AM, McCartney S, Burchiel KJ. Long-term efficacy and safety of internal neurolysis for trigeminal neuralgia without neurovascular compression. J Neurosurg [Internet]. 2015;122(5):1048–57. Available from: http://www.ncbi.nlm.nih.gov/pubmed/25679283

105. Skirving DJ, Dan NG. A 20-year review of percutaneous balloon compression of the trigeminal ganglion. J Neurosurg. 2001;94(6):913–7.

106. Obermann M. Treatment options in trigeminal neuralgia. Ther Adv Neurol Disord. 2010;3(2):107–15.

107. Mullen S, Lichtor T. Percutaneous microcompression of the gasserian ganglion for trigeminal neuralgia. J Neurosurg. 1983;59:1007–12.

108. Asplund P, Linderoth B, Ling G, Winter J, Bergenheim AT. One hundred eleven Percutaneous Balloon Compressions for Trigeminal Neuralgia in a Cohort of66 Patients with Multiple Sclerosis. Oper Neurosurg. 2019;0(0):1–8.

109. Brown J, Hoeflinger B, Long P, Gunning W, Rhoades R, Bennett-Clarke C, et al. Axon and Ganglion Cell Injury in Rabbits after Percutaneous Trigeminal Balloon Compression. Neurosurgery. 2019;38(5):993–1004.

110. Muhammad G, Hussain I, Zadran KK, Bhatti SN. MICROVASCULAR DECOMPRESSION FOR TRIGEMINAL NEURALGIA Shahbaz Ali Khan , Baynazir Khan , Abdul Aziz Khan , Ehtisham Ahmed Khan Afridi , Shakir. j ayub med coll abbottabad. 2015;27(3):539–42.

111. Kanpolat Y, Savas A, Bekar A, Berk C. Percutaneous controlled radiofrequency trigeminal rhizotomy for the treatment of idiopathic trigeminal neuralgia: 25-year experience with 1600 patients. Neurosurgery. 2001;48(3):524–34.

112. Tuleasca C, Régis J, Sahgal A, De Salles A, Hayashi M, Ma L, et al. Stereotactic radiosurgery for trigeminal neuralgia: A systematic review. J Neurosurg. 2019;130(3):733–57.

113. Leksell L. The stereotaxic method and radiosurgery of the brain. Acta Chir Scand. 1951;102:316–9.

114. Pokhrel D, Sood S, McClinton C, Saleh H, Badkul R, Jiang H, et al. Linac-based stereotactic radiosurgery (SRS) in the treatment of refractory trigeminal neuralgia: Detailed description of SRS procedure and reported clinical outcomes. J Appl Clin Med Phys [Internet]. 2017;18(2):136–43. Available from: http://doi.wiley.com/10.1002/acm2.12057

115. Raygor KP, Wang DD, Ward MM, Barbaro NM, Chang EF. Long-term pain outcomes for recurrent idiopathic trigeminal neuralgia after stereotactic radiosurgery: a prospective comparison of first-time microvascular decompression and repeat stereotactic radiosurgery Kunal. Journal of Neurosurgery. 2018. p. 1–9.

116. Pollock BE. Radiosurgery for trigeminal neuralgia: is sensory disturbance required for pain relief? J Neurosurg. 2006;105:103–6.

117. Han PP, Shetter AG, Smith KA, Fiedler JA, Rogers CL, Speiser B, et al. Gamma Knife radiosurgery for trigeminal neuralgia: Experience at the Barrow Neurological Institute. Int J Radiat Oncol Biol Phys. 2000;47:1013–9.

118. Wong DL, Baker CM. Pain in Children: Comparison of Assessment Scales. Pediatr Nurs. 1988;14(1):9–17.

119. Hawker GA, Mian S, Kendzerska T, French M. Measures of adult pain: Visual Analog Scale for Pain (VAS Pain), Numeric Rating Scale for Pain (NRS Pain), McGill Pain Questionnaire (MPQ), Short-Form McGill Pain Questionnaire (SF-MPQ), Chronic Pain Grade Scale (CPGS), Short Form-36 Bodily Pain Scale (SF. Arthritis Care Res. 2011;63(SUPPL. 11):240–52.

120. Heller GZ, Manuguerra M, Chow R. How to analyze the Visual Analogue Scale: Myths, truths and clinical relevance. Scand J Pain [Internet]. 2016;13(2016):67–75. Available from: http://dx.doi.org/10.1016/j.sjpain.2016.06.012

121. Khatri A, Kalra N. Clinical Study A Comparison of Two Pain Scales in the

Assessment of Dental Pain in East Delhi Children. Int Sch Res Netw ISRN Dent. 2012;2012:1–4.

122. Aziato L, Dedey F, Marfo K, Asamani JA, Clegg-Lamptey JNA. Validation of three pain scales among adult postoperative patients in Ghana. BMC Nurs [Internet]. 2015;14(1):1–9. Available from: http://dx.doi.org/10.1186/s12912-015-0094-6

123. Fillingim RB. Individual differences in pain: Understanding the mosaic that makes pain personal. Pain. 2017;158(4):S11–8.

124. Zhang H, Lei D, You C, Mao BY, Wu B, Fang Y. The long-term outcome predictors of pure microvascular decompression for primary trigeminal neuralgia. World Neurosurg. 2013;79(5–6):756–62.

125. Heinskou TB, Rochat P, Maarbjerg S, Wolfram F, Brennum J, Olesen J, et al. Prognostic factors for outcome of microvascular decompression in trigeminal neuralgia: A prospective systematic study using independent assessors. Cephalalgia. 2019;39(2):197–208.

126. Hardaway FA, Gustafsson HC, Holste K, Burchiel KJ, Raslan AM. A novel scoring system as a preoperative predictor for pain-free survival after microsurgery for trigeminal neuralgia. J Neurosurg. 2020;132(1):217–24.

127. Panczykowski DM, Jani RH, Hughes MA, Sekula RF. Development and Evaluation of a Preoperative Trigeminal Neuralgia Scoring System to Predict Long-Term Outcome Following Microvascular Decompression. Neurosurgery. 2020;87(1):71–9.

128. Ishaque AH, Xie H, Danyluk H, Wheatley BM, Broad R, Kong L, et al. Comparison of Prognostic Scoring Systems to Predict Durable Pain Relief After Microvascular Decompression for Trigeminal Neuralgia. World Neurosurg [Internet]. 2022;157:e432–40. Available from: https://doi.org/10.1016/j.wneu.2021.10.111

129. Symms M, Jäger HR, Schmierer K, Yousry TA. A review of structural magnetic resonance neuroimaging. J Neurol Neurosurg Psychiatry [Internet]. 2004;75(9):1235–44. Available from: http://jnnp.bmj.com/content/75/9/1235.abstract

130. Dale B, Brown M, Semelka R. MRI : Basic Principles and Applications. fifth. New York: John Wiley & Sons, Incorperated; 2015. 247 p.

131. Larmor J. LXIII. On the Theory of Magnetic Influence on Spectra; and on the Radiation From Moving Ions. Philos Mag. 1897;271(44):503–12.

132. Gruber B, Froeling M, Leiner T, Klomp DWJ. RF coils: A practical guide for nonphysicists. J Magn Reson Imaging [Internet]. 2018; Available from: http://doi.wiley.com/10.1002/jmri.26187

133. Van Geuns RJM, Wielopolski PA, De Bruin HG, Rensing BJ, Van Ooijen PMA, Hulshoff M, et al. Basic principles of magnetic resonance imaging. Prog Cardiovasc Dis. 1999;42(2):149–56.

134. Brant-Zawadzki M, Gillan G, Nitz W. MP RAGE: a three-dimensional, T1-weighted, gradient-echo sequence--initial experience in the brain. Radiology. 1992;182(3):769–

75.

135. Saranathan M, Worters PW, Rettmann DW, Winegar B, Becker J. Physics for clinicians: Fluid-attenuated inversion recovery (FLAIR) and double inversion recovery (DIR) Imaging. J Magn Reson Imaging [Internet]. 2017;1–11. Available from: http://doi.wiley.com/10.1002/jmri.25737%0Ahttp://www.ncbi.nlm.nih.gov/pubmed/28419602

136. Baliyan V, Das CJ, Sharma R, Gupta AK. Diffusion weighted imaging: Technique and applications. World J Radiol [Internet]. 2016;8(9):785. Available from: http://www.wjgnet.com/1949-8470/full/v8/i9/785.htm

137. Basser PJ, Mattiello J, Lebihan D. MR Diffusion Tensor Spectroscopy and Imaging. Biophys J [Internet]. 1994;66(1):259–67. Available from: http://dx.doi.org/10.1016/S0006-3495(94)80775-1

138. Soares JM, Marques P, Alves V, Sousa N. A hitchhiker's guide to diffusion tensor imaging. Front Neurosci. 2013;7(March):1–14.

139. Jones DK. Diffusion MRI : theory, methods, and applications. New York: Oxford University Press; 2011. 767 p.

140. Le Bihan D, Mangin J-F, Poupon C, Clark CA, Pappata S, Molko N, et al. Diffusion Tensor Imaging: Concepts and Applications. J Magn Reson Imaging. 2001;13:534–46.

141. Beaulieu C. The basis of anisotropic water diffusion in the nervous system - A technical review. NMR Biomed. 2002;15(7–8):435–55.

142. Song S, Sun S, Ju W, Lin S, Cross AH, Neufeld AH. Diffusion tensor imaging detects and differentiates axon and myelin degeneration in mouse optic nerve after retinal ischemia. Neuroimage. 2003;20:1714–22.

143. Song S, Sun S, Ramsbottom MJ, Chang C, Russell J, Cross AH. Dysmyelination Revealed through MRI as Increased Radial (but Unchanged Axial) Diffusion of Water. Neuroimage. 2002;1436:1429–36.

144. Basser PJ, Pajevic S, Pierpaoli C, Duda J, Aldroubi A. In Vivo Fiber Tractography Using DT-MRI Data. Magn Reson Med. 2000;44:625–32.

145. Lazar M, Weinstein DM, Tsuruda JS, Hasan KM, Arfanakis K, Meyerand ME, et al. White Matter Tractography Using Diffusion Tensor Deflection. Hum Brain Mapp. 2003;18:306–21.

146. Sarwar T, Ramamohanarao K, Zalesky A. Mapping connectomes with diffusion MRI: deterministic or probabilistic tractography? Magn Reson Med. 2019;81(2):1368–84.

147. Lebel C, Benner T, Beaulieu C. Six is enough? Comparison of diffusion parameters measured using six or more diffusion-encoding gradient directions with deterministic tractography. Magn Reson Med. 2012;68(2):474–83.

148. Shapey J, Vos SB, Vercauteren T, Bradford R, Saeed SR, Bisdas S, et al. Clinical applications for diffusion MRI and tractography of cranial nerves within the posterior

fossa: A systematic review. Front Neurosci. 2019;13(FEB).

149. Buonocore MH, Maddock RJ. Magnetic resonance spectroscopy of the brain: A review of physical principles and technical methods. Rev Neurosci. 2015;26(6):609–32.

150. Cichocka M, Kozub J, Karcz P, Urbanik A. Regional Differences in the Concentrations of Metabolites in the Brain of Healthy Children: A Proton Magnetic Resonance Spectroscopy (1HMRS) Study. Polish J Radiol [Internet]. 2016;81:473–7. Available from: http://www.polradiol.com/abstract/index/idArt/897750

151. Bracken BK, Jensen JE, Prescot AP, Cohen BM, Renshay PF, Ongur D. Brain metabolite concentrations across cortical regions in healthy adults. Brain Res. 2011;(1369):89–94.

152. Moffett JR, Ross B, Arun P, Madhavarao CN, Namboodiri AMA. N-Acetylaspartate in the CNS: From neurodiagnostics to neurobiology. Prog Neurobiol. 2007;81(2):89–131.

153. Tayebati SK, Amenta F. Choline-containing phospholipids: Relevance to brain functional pathways. Clin Chem Lab Med. 2013;51(3):513–21.

154. Attwell D, Nave K-A, Saab A, Kolodziejczyk K. Why do oligodendrocyte lineage cells express glutamate receptors? F1000 Biol Rep [Internet]. 2010;2(August):57. Available from: http://www.ncbi.nlm.nih.gov/pubmed/21173873%5Cnhttp://www.pubmedcentral.nih.gov/articlerender.fcgi?artid=PMC2990618%5Cnhttp://www.f1000.com/reports/b/2/57/

155. Despotovic I, Goossens B, Philips W. MRI Segmentation of the Human Brain : Challenges , Methods , and Applications. 2015;2015.

156. Nugent AC, Luckenbaugh DA, Wood SE, Bogers W, Zarate CA, Drevets WC. Automated subcortical segmentation using FIRST: Test-retest reliability, interscanner reliability, and comparison to manual segmentation. Hum Brain Mapp. 2013;34(9):2313–29.

157. Hsu YY, Schuff N, Du AT, Mark K, Zhu X, Hardin D, et al. Comparison of automated and manual MRI volumetry of hippocampus in normal aging and dementia. J Magn Reson Imaging. 2002;16(3):305–10.

158. Frisoni GB, Jack CR, Bocchetta M, Bauer C, Frederiksen KS, Liu Y, et al. The EADC-ADNI harmonized protocol for manual hippocampal segmentation on magnetic resonance: Evidence of validity. Alzheimer's Dement. 2015;11(2):111–25.

159. Power BD, Wilkes FA, Hunter-Dickson M, van Westen D, Santillo AF, Walterfang M, et al. Validation of a protocol for manual segmentation of the thalamus on magnetic resonance imaging scans. Psychiatry Res - Neuroimaging [Internet]. 2015;232(1):98–105. Available from: http://dx.doi.org/10.1016/j.pscychresns.2015.02.001

160. Meyer JR, Roychowdhury S, Russell EJ, Callahan C, Gitelman D, Mesulam MM. Location of the Central Sulcus via Cortical Thickness of the Precentral and Postcentral Gyri on MR. Am J Neuroradiol. 1996;17(9):1699–706.

161. Fischl B, Dale AM. Measuring the thickness of the human cerebral cortex from

magnetic resonance images. Proc Natl Acad Sci U S A. 2000;97(20):11050–5.

162. Jenkinson M, Beckmann CF, Behrens TEJ, Woolrich MW, Smith SM. FSL. Neuroimage [Internet]. 2012;62(2):782–90. Available from: http://www.ncbi.nlm.nih.gov/pubmed/21979382

163. Smith SM, Jenkinson M, Woolrich MW, Beckmann CF, Behrens TEJ, Johansen-Berg H, et al. Advances in functional and structural MR image analysis and implementation as FSL. Neuroimage. 2004;23(S1):208–19.

164. Patenaude B, Smith SM, Kennedy D, Jenkinson M. A Bayesian Model of Shape and Appearance for Subcortical Brain. Neuroimage [Internet]. 2011;56(3):2011. Available from: papers3://publication/uuid/84AEE6CC-45FE-4378-8D12-D3AEAD4F941F

165. Ashburner J, Friston KJ. Voxel-Based Morphometry—The Methods. Neuroimage [Internet]. 2000;11(6):805–21. Available from: http://linkinghub.elsevier.com/retrieve/pii/S1053811900905822

166. Manuscript A, Proximity I. NIH Public Access. 2011;4(164):1–35.

167. Smith SM, Jenkinson M, Johansen-Berg H, Rueckert D, Nichols TE, Mackay CE, et al. Tract-based spatial statistics: Voxelwise analysis of multi-subject diffusion data. Neuroimage. 2006;31(4):1487–505.

168. Smith SM, Johansen-Berg H, Jenkinson M, Rueckert D, Nichols TE, Klein JC, et al. Acquisition and voxelwise analysis of multi-subject diffusion data with tract-based spatial statistics. Nat Protoc. 2007;2(3):499–503.

169. Mechelli A, Price CJ, Friston KJ, Ashburner J. Voxel-based morphometry of the human brain: methods and applications. Curr Med Imaging Rev. 2005;1(2):105–13.

170. Tardif CL, Collins DL, Pike GB. Regional Impact of Field Strength on Voxel-Based Morphometry Results. 2010;957:943–57.

171. Leemans A, Jeurissen B, Sijbers J, Jones DK. ExploreDTI: a graphical toolbox for processing, analyzing, and visualizing diffusion MR data. 17th Annu Meet Intl Soc Mag Reson Med. 2009;3537.

172. Curran-Everett D. Multiple comparisons: Philosophies and illustrations. Am J Physiol - Regul Integr Comp Physiol. 2000;279(1 48-1):1–8.

173. Midway S, Robertson M, Flinn S, Kaller M. Comparing multiple comparisons: practical guidance for choosing the best multiple comparisons test. PeerJ. 2020;8:1–26.

174. Smith SM, Nichols TE. Threshold-free cluster enhancement: Addressing problems of smoothing, threshold dependence and localisation in cluster inference. Neuroimage [Internet]. 2009;44(1):83–98. Available from: http://dx.doi.org/10.1016/j.neuroimage.2008.03.061

175. Leal PRL, Barbeir C, Hermier M, Souza MA, Cristino-Filho G, Sindou M. Atrophic changes in the trigeminal nerves of patients with trigeminal neuralgia due to neurovascular compression and their association with the severity of compression and

clinical outcomes. J Neurosurg. 2014;120(June):1484–95.

176. Duan Y, Sweet J, Munyon C, Miller J. Degree of distal trigeminal nerve atrophy predicts outcome after microvascular decompression for Type 1a trigeminal neuralgia. J Neurosurg. 2015;123(December):1–7.

177. Urgosik D, Rulseh AM, Keller J, Svehlik V, Pingle JMVN, Horinek D. Trigeminal nerve asymmetry in classic trigeminal neuralgia - Evaluation by magnetic resonance imaging. Ces a Slov Neurol a Neurochir. 2014;77(5):582–5.

178. Hu Y-S, Lee C-C, Guo W-Y, Lin C-J, Yang H-C, Wu H-M, et al. Trigeminal Nerve Atrophy Predicts Pain Recurrence After Gamma Knife Stereotactic Radiosurgery for Classical Trigeminal Neuralgia. Neurosurgery [Internet]. 2018;0(0):1–8. Available from: https://academic.oup.com/neurosurgery/advance-article/doi/10.1093/neuros/nyy122/4967790

179. Cheng J, Meng J, Liu W, Zhang H, Hui X, Lei D. Nerve atrophy in trigeminal neuralgia due to neurovascular compression and its association with surgical outcomes after microvascular decompression. Acta Neurochir (Wien). 2017;159(9):1699–705.

180. Brînzeu A, Drogba L, Sindou M. Reliability of MRI for predicting characteristics of neurovascular conflicts in trigeminal neuralgia: Implications for surgical decision making. J Neurosurg. 2019;130(2):611–21.

181. Jung HH, Park CK, Jung NY, Kim M, Chang WS, Chang JW. Gamma knife radiosurgery for idiopathic trigeminal neuralgia: does the status of offending vessels influence pain control or side effects? World Neurosurg. 2017;(August):687–93.

182. Lee C-C, Guo W-Y, Hu Y-S, Liu K-D, Yang H-C, Chung W-Y, et al. Trigeminal Nerve Atrophy Predicts Pain Recurrence After Gamma Knife Stereotactic Radiosurgery for Classical Trigeminal Neuralgia. Neurosurgery. 2018;84(4):927–34.

183. Barzaghi LR, Albano L, Scudieri C, Gigliotti CR, del Vecchio A, Mortini P. Factors affecting long-lasting pain relief after Gamma Knife radiosurgery for trigeminal neuralgia: a single institutional analysis and literature review. Neurosurg Rev. 2021;

184. Chen ST, Yang JT, Weng HH, Wang HL, Yeh MY, Tsai YH. Diffusion tensor imaging for assessment of microstructural changes associate with treatment outcome at one-year after radiofrequency Rhizotomy in trigeminal neuralgia. BMC Neurol. 2019;19(1):1–9.

185. DeSouza DD, Moayedi M, Chen DQ, Davis KD, Hodaie M. Sensorimotor and Pain Modulation Brain Abnormalities in Trigeminal Neuralgia: A Paroxysmal, Sensory-Triggered Neuropathic Pain. PLoS One. 2013;8(6).

186. Leal PRL, Roch J, Hermier M, Berthezene Y, Sindou M. Diffusion tensor imaging abnormalities of the trigeminal nerve root in patients with classical trigeminal neuralgia: a pre- and postoperative comparative study 4 years after microvascular decompression. Acta Neurochir (Wien). 2019;161(7):1415–25.

187. Chen F, Chen L, Li W, Li L, Xu X, Li W, et al. Pre-operative declining proportion of fractional anisotropy of trigeminal nerve is correlated with the outcome of micro-

vascular decompression surgery. 2016;1–8.

188. Lee YL, Chen ST, Yang JT, Weng HH, Wang HL, Tsai YH. Diffusivity parameters of diffusion tensor imaging and apparent diffusion coefficient as imaging markers for predicting the treatment response of patients with trigeminal neuralgia. J Neurosurg. 2020;132(6):1993–9.

189. Tohyama S, Hung PS, Zhong J, Hodaie M. Early postsurgical diffusivity metrics for prognostication of long-term pain relief after Gamma Knife radiosurgery for trigeminal neuralgia. J Neurosurg. 2018;131(August):539–48.

190. Chen ST, Yang JT, Yeh MY, Weng HH, Chen CF, Tsai YH. Using diffusion tensor imaging to evaluate microstructural changes and outcomes after radiofrequency rhizotomy of trigeminal nerves in patients with trigeminal neuralgia. PLoS One. 2016;11(12):1–10.

191. Hodaie M, Chen DQ, Quan J, Laperriere N. Tractography delineates microstructural changes in the trigeminal nerve after focal radiosurgery for trigeminal neuralgia. PLoS One. 2012;7(3):1–8.

192. Lee CC, Chong ST, Chen CJ, Hung SC, Yang HC, Lin CJ, et al. The timing of stereotactic radiosurgery for medically refractory trigeminal neuralgia: the evidence from diffusion tractography images. Acta Neurochir (Wien). 2018;160(5):977–86.

193. Hung PSP, Chen DQ, Davis KD, Zhong J, Hodaie M. Predicting pain relief: Use of pre-surgical trigeminal nerve diffusion metrics in trigeminal neuralgia. NeuroImage Clin. 2017;15(January):710–8.

194. Leal PRL. Fraction of anisotropy and apparent diffusion coefficient as diagnostic tools in trigeminal neuralgia. Acta Neurochir (Wien). 2019;161(7):1403–5.

195. Vartiainen N, Perchet C, Magnin M, Creac'h C, Convers P, Nighoghossian N, et al. Thalamic pain: Anatomical and physiological indices of prediction. Brain. 2016;139(3):708–22.

196. Lim M, Jassar H, Kim DJ, Nascimento TD, DaSilva AF. Differential alteration of fMRI signal variability in the ascending trigeminal somatosensory and pain modulatory pathways in migraine. J Headache Pain. 2021;22(1):1–15.

197. Tsai YH, Yuan R, Patel D, Chandrasekaran S, Weng HH, Yang JT, et al. Altered structure and functional connection in patients with classical trigeminal neuralgia. Hum Brain Mapp. 2018;39(2):609–21.

198. Gustin SM, Peck CC, Wilcox SL, Nash PG, Murray GM, Henderson LA. Different pain, different brain: thalamic anatomy in neuropathic and non-neuropathic chronic pain syndromes. J Neurosci [Internet]. 2011;31(16):5956–64. Available from: http://www.ncbi.nlm.nih.gov/pubmed/21508220

199. Gu T, Ma X-X, Xu Y-H, Xiu J-J, Li C-F. Metabolite concentration ratios in thalami of patients with migraine and trigeminal neuralgia measured with 1H-MRS. Neurol Res. 2008;30(3):229–33.

200. Wang Y, Li D, Bao F, Ma S, Guo C, Jin C, et al. Thalamic metabolic alterations with cognitive dysfunction in idiopathic trigeminal neuralgia: A multivoxel spectroscopy study. Neuroradiology. 2014;56(8):685–93.

201. Rutland JW, Huang K-H, Gill CM, Villavisanis DF, Alper J, Verma G, et al. First application of 7-T ultra–high field diffusion tensor imaging to detect altered microstructure of thalamic-somatosensory anatomy in trigeminal neuralgia. J Neurosurg. 2019;1–9.

202. Wang Y, Cao DY, Remeniuk B, Krimmel S, Seminowicz DA, Zhang M. Altered brain structure and function associated with sensory and affective components of classic trigeminal neuralgia. Pain. 2017;158(8):1561–70.

203. Wang Y, Zhang X, Guan Q, Wan L, Yi Y, Liu CF. Altered regional homogeneity of spontaneous brain activity in idiopathic trigeminal neuralgia. Neuropsychiatr Dis Treat. 2015;11:2659–66.

204. (Bud) Craig AD. How do you feel — now? The anterior insula and human awareness. Nat Rev Neurosci [Internet]. 2009;10(1):59–70. Available from: papers3://publication/uuid/2CB3E0C6-D12A-4CD4-976C-4EB906C77CF1%5Cnhttp://www.nature.com/doifinder/10.1038/nrn2555

205. Kong J, White NS, Kwong KK, Vangel MG, Rosman IS, Gracely RH, et al. Using fMRI to dissociate sensory encoding from cognitive evaluation of heat pain intensity. Hum Brain Mapp. 2006;27(9):715–21.

206. Davis KD, Moayedi M. Central mechanisms of pain revealed through functional and structural MRI. J Neuroimmune Pharmacol. 2013;8(3):518–34.

207. Zhang Y, Mao Z, Pan L, Ling Z, Liu X, Zhang J, et al. Dysregulation of Pain- and Emotion-Related Networks in Trigeminal Neuralgia. Front Hum Neurosci [Internet]. 2018;12(March):1–10. Available from: http://journal.frontiersin.org/article/10.3389/fnhum.2018.00107/full

208. Rodriguez-Raecke R, Niemeier A, Ihle K, Ruether W, May A. Brain Gray Matter Decrease in Chronic Pain Is the Consequence and Not the Cause of Pain. J Neurosci [Internet]. 2009;29(44):13746–50. Available from: http://www.jneurosci.org/content/29/44/13746%5Cnhttp://www.jneurosci.org/content/29/44/13746.full.pdf%5Cnhttp://www.jneurosci.org/content/29/44/13746.short%5Cnhttp://www.ncbi.nlm.nih.gov/pubmed/19889986

209. Wang Y, Cao DY, Remeniuk B, Krimmel S, Seminowicz DA, Zhang M. Altered brain structure and function associated with sensory and affective components of classic trigeminal neuralgia. Pain. 2017;158(8):1561–70.

210. Rodriguez-Raecke R, Niemeier A, Ihle K, Ruether W, May A. Structural Brain Changes in Chronic Pain Reflect Probably Neither Damage Nor Atrophy. PLoS One. 2013;8(2).

211. D.D. DS, K.D. D, M. H. Reversal of insular and microstructural nerve abnormalities following effective surgical treatment for trigeminal neuralgia. Pain [Internet].

2015;156(6):1112–23. Available from: http://www.embase.com/search/results?subaction=viewrecord&from=export&id=L614482631%0Ahttp://dx.doi.org/10.1097/j.pain.0000000000000156%0Ahttp://sfx.library.uu.nl/utrecht?sid=EMBASE&issn=18726623&id=doi:10.1097%2Fj.pain.0000000000000156&atitle=Reversal+of

212. Ghaziri J, Tucholka A, Girard G, Boucher O, Houde JC, Descoteaux M, et al. Subcortical structural connectivity of insular subregions. Sci Rep. 2018;8(1):1–12.

213. Weininger J, Roman E, Tierney P, Barry D, Gallagher H, Murphy P, et al. Papez's forgotten tract: 80 years of unreconciled findings concerning the thalamocingulate tract. Front Neuroanat. 2019;13(February):1–11.

214. Berger SE, Vachon-Presseau É, Abdullah TB, Baria AT, Schnitzer TJ, Apkarian AV. Hippocampal morphology mediates biased memories of chronic pain. Neuroimage. 2018;166(October 2017):86–98.

215. Shackman AJ, Salomons T V., Slagter HA, Fox AS, Winter JJ, Davidson RJ. The integration of negative affect, pain and cognitive control in the cingulate cortex. Nat Rev Neurosci. 2011;12(3):154–67.

216. Hashmi JA, Baliki MN, Huang L, Baria AT, Torbey S, Hermann KM, et al. Shape shifting pain: Chronification of back pain shifts brain representation from nociceptive to emotional circuits. Brain. 2013;136(9):2751–68.

217. Wager TD, Atlas LY, Lindquist M a, Roy M, Woo C-W, Kross E. An fMRI-based neurologic signature of physical pain. N Engl J Med [Internet]. 2013;368(15):1388–97. Available from: http://www.pubmedcentral.nih.gov/articlerender.fcgi?artid=3691100&tool=pmcentrez&rendertype=abstract

218. Obermann M, Rodriguez-Raecke R, Naegel S, Holle D, Mueller D, Yoon MS, et al. Gray matter volume reduction reflects chronic pain in trigeminal neuralgia. Neuroimage. 2013;74(February):352–8.

219. Danyluk H, Lang S, Monchi O, Sankar T. Pre-operative Limbic System Functional Connectivity Distinguishes Responders From Non-responders to Surgical Treatment for Trigeminal Neuralgia. 2021;12(October):1–10.

220. Yen CP, Kung SS, Su YF, Lin WC, Howng SL, Kwan AL. Stereotactic bilateral anterior cingulotomy for intractable pain. J Clin Neurosci. 2005;12(8):886–90.

221. Shimo K, Ueno T, Younger J, Nishihara M, Inoue S, Ikemoto T, et al. Visualization of painful experiences believed to trigger the activation of affective and emotional brain regions in subjects with low back pain. PLoS One. 2011;6(11):2–7.

222. Apkarian AV, Mutso AA, Centeno MV, Kan L, Wu M, Levinstein M, et al. Role of adult hippocampal neurogenesis in persistent pain. Pain. 2016;157(2):418–28.

223. Wang Y, Yang Q, Cao D, Seminowicz D, Remeniuk B, Gao L, et al. Correlation between nerve atrophy, brain grey matter volume and pain severity in patients with primary trigeminal neuralgia. Cephalalgia. 2018;0(0):1–11.

224. Danyluk H, Sankar T, Beaulieu C. High spatial resolution nerve-specific DTI protocol outperforms whole-brain DTI protocol for imaging the trigeminal nerve in healthy individuals. NMR Biomed. 2021;34(2):e4427.

225. Jacquesson T, Frindel C, Kocevar G, Berhouma M, Jouanneau E, Attyé A, et al. Overcoming Challenges of Cranial Nerve Tractography: A Targeted Review. Clin Neurosurg. 2019;84(2):313–25.

226. Xie G, Zhang F, Leung L, Mooney MA, Epprecht L, Norton I, et al. Anatomical assessment of trigeminal nerve tractography using diffusion MRI: A comparison of acquisition b-values and single- and multi-fiber tracking strategies. NeuroImage Clin. 2020;25(September).

227. Kwong KK, Mckinstry RC, Chien D, Crawley AP, Pearlman D, Rosen BR, et al. CSF-Suppressed Quantitative Single-Shot Diffusion Imaging. 1991;c:157–63.

228. Concha L, Gross DW, Beaulieu C. Diffusion tensor tractography of the limbic system. Am J Neuroradiol. 2005;26(9):2267–74.

229. Wheeler-kingshott CAM, Parker GJM, Symms MR, Hickman SJ, Tofts PS, Miller DH, et al. ADC Mapping of the Human Optic Nerve : Increased Resolution , Coverage , and Reliability With CSF-Suppressed Zoom-EPI. Magn Reson Med. 2002;47:24–31.

230. Hodaie M, Quan J, Chen DQ. In vivo visualization of cranial nerve pathways in humans using diffusion-based tractography. Neurosurgery. 2010;66(4):788–95.

231. Yushkevich PA, Piven J, Hazlett HC, Smith RG, Ho S, Gee JC, et al. User-guided 3D active contour segmentation of anatomical structures: Significantly improved efficiency and reliability. Neuroimage. 2006;31(3):1116–28.

232. Vos SB, Jones DK, Viergever MA, Leemans A. Partial volume effect as a hidden covariate in DTI analyses. Neuroimage. 2011;55:1566–76.

233. Benes L, Shiratori K, Gurschi M, Sure U, Tirakotai W, Krischek B, et al. Is preoperative high-resolution magnetic resonance imaging accurate in predicting neurovascular compression in patients with trigeminal neuralgia? A single-blind study. Neurosurg Rev. 2005;28(2):131–6.

234. Hajnal J V., Oatridge A, Herlihy AH, Bydder GM. Reduction of CSF artifacts on FLAIR images by using adiabatic inversion pulses. Am J Neuroradiol. 2001;22(2):317–22.

235. Sindou M, Leston J, Decullier E, Chapuis F. Microvascular decompression for primary trigeminal neuralgia: Long-term effectiveness and prognostic factors in a series of 362 consecutive patients with clear-cut neurovascular conflicts who underwent pure decompression. J Neurosurg. 2007;107(6):1144–53.

236. Danyluk H, Andrews J, Kesarwani R, Seres P, Broad R, Wheatley BM. The thalamus in trigeminal neuralgia : structural and metabolic abnormalities , and influence on surgical response. BMC Neurol [Internet]. 2021;21(290):1–14. Available from: https://doi.org/10.1186/s12883-021-02323-4

237. Danyluk H, Ishaque A, Ta D, Yang YH, Wheatley BM, Kalra S, et al. MRI Texture Analysis Reveals Brain Abnormalities in Medically Refractory Trigeminal Neuralgia. Front Neurol. 2021;12(February):1–10.

238. Danyluk H, Lee EK, Wong S, Sajida S, Broad R, Wheatley M, et al. Hippocampal and trigeminal nerve volume predict outcome of surgical treatment for trigeminal neuralgia. Cephalalgia. 2020;40(6):586–96.

239. Guclu B, Sindou M, Meyronet D, Streichenberger N, Simon E, Mertens P. Cranial nerve vascular compression syndromes of the trigeminal, facial and vago-glossopharyngeal nerves: Comparative anatomical study of the central myelin portion and transitional zone; Correlations with incidences of corresponding hyperactive dysfunctio. Acta Neurochir (Wien). 2011;153(12):2365–75.

240. Holste K, Chan AY, Rolston JD, Englot DJ. Pain Outcomes Following Microvascular Decompression for Drug-Resistant Trigeminal Neuralgia: A Systematic Review and Meta-Analysis. Neurosurgery. 2019;86(2):182–90.

241. Willsey MS, Collins KL, Conrad EC, Chubb HA, Patil PG. Diffusion tensor imaging reveals microstructural differences between subtypes of trigeminal neuralgia. J Neurosurg. 2020;133(2):573–9.

242. Smith SM, Zhang Y, Jenkinson M, Chen J, Matthews PM, Federico A, et al. Accurate, robust and automated longitudinal and cross-sectional brain change analysis. Neuroimage. 2002;17(1):479–89.

243. Provencher SW. Automatic quantitation of localized in vivo 1H spectra with LCModel. NMR Biomed. 2001;14(4):260–4.

244. Schaltenbrand G, Wahren W, Hassler RG. Atlas for stereotaxy of the human brain. 2d, rev. a ed. Stuttgart : Thieme; 1977.

245. Schmidt-Wilcke T, Leinisch E, Gänßbauer S, Draganski B, Bogdahn U, Altmeppen J, et al. Affective components and intensity of pain correlate with structural differences in gray matter in chronic back pain patients. Pain. 2006;125(1–2):89–97.

246. Symonds LL, Gordon NS, Bixby JC, Mande MM. Right-Lateralized Pain Processing in the Human Cortex: An fMRI Study. J Neurophysiol. 2006;95(6):3823–30.